EJA

European Journal of Anatomy

Volume 25 - Number 1 January 2021

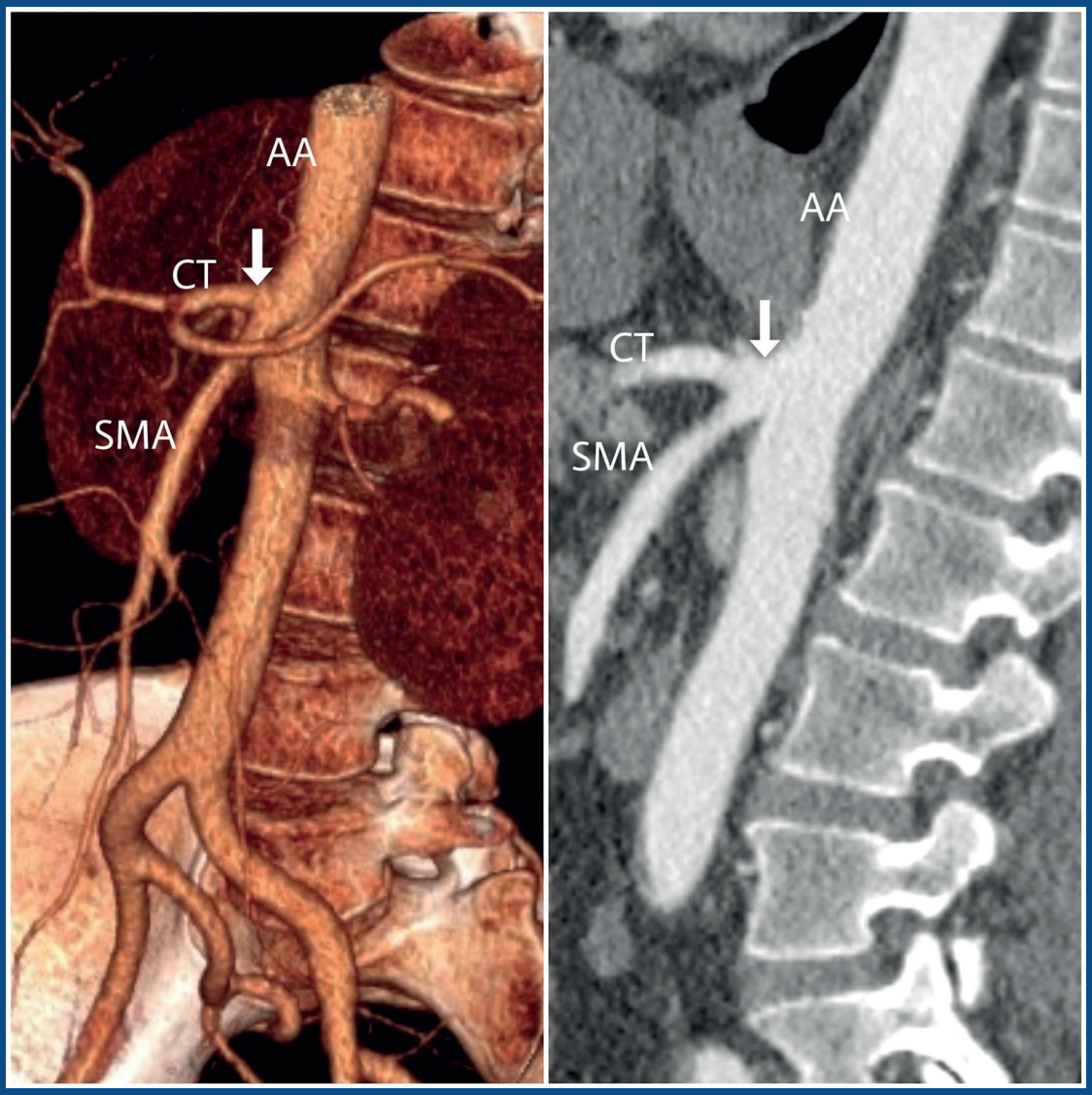

Indexed in:
EMBASE / Excerpta Medica
IBECS / Índice Bibliográfico Español en Ciencias de la Salud
REVICIEN / Red de Revistas Científicas Españolas (www. revicien.net)

Official Journal of the Spanish Society of Anatomy

EJA
European Journal of Anatomy

Volume 25 - Number 1 January 2021

CONTENTS

Onwards to A New Era

The European Journal of Anatomy (EJA) was launched in 1997 as the official Journal of the Spanish Association of Anatomy (SAE). It is a successor to the "Annals of Anatomy", a journal founded in 1952, which, due to financial difficulties, ceased publication after the 100th issue.

Initially EJA was not only dedicated to human morphology but also comparative and experimental anatomy. In addition, it also covered medical education and development. In this early period the journal was published in print with a modern design and its Editorial Board included foreign researchers. After publication of volume 4, the Journal decided to migrate to online publication.

This new era confronted the journal with pressing innovative challenges and possibilities.

The first and foremost aim is admission to the JCR index and Medline. Our applications are currently under review by the respective administrative bodies.

The second project is to open the Journal up to other international societies in Latin America. The "*Sociedad Mexicana de Anatomía*" (SMA) has already been accepted for integration in the EJA as an Associate Society with active participation in the Editorial Board.

The third objective is the modernisation of the management of the Journal. A change in publishers aims at improving the functionality and design of the Journal. The Journal will reduce the duration of revision through a prespecified format.

The fourth component is that, while the Journal will continue to cover morphological topics, it will expand to include new fields such as, for example, gene expression and anatomy, which is closely related to developmental biology. The range of anatomical topics will be extended to cover experimental studies based on lesion, regeneration and transplants, etc. of tissues or organs. Furthermore, technical studies in the field of microscopy with its wide span of optical, electron microscopy, confocal, laser, infrared, immunohistochemistry, molecular techniques (ISH) etc. will also be covered. Efforts will also be made to attract manuscripts from the neurosciences as well as facilitating the inclusion of manuscripts with 3D reconstructions or videos.

Finally, our most earnest objective is the publication of 12 volumes per year with more efficient operational and review processes and prompt publication following acceptance.

The Journal will continue to operate on a free-access, no-charge basis, regardless of the number of pages, color plates, videos or 3D reconstructions.

Furthermore, the Journal will continue with the publication of one supplement per year, under the supervision of a Guest Editor. The practice of inviting important researchers to submit manuscripts will also be maintained.

We will, thus, be providing an appropriate frame for scientific publications from a wide range of anatomical topics, from molecular to gross anatomy and a broad field of professions: not only medicine but also from the fields of biology, dentistry, veterinary, physiotherapy, nursing, pediatrics and generally all professions connected with health sciences.

Prof. Dr. Ricardo Vázquez. Past Editor-In-Chief
Prof. Dr. Jose Sañudo. Present and future Editor-In-Chief
Prof. Dr. Pedro Mestres. Vice-Editor-In-Chief

History of the Mexican Society of Anatomy

Diego Pineda Martínez [1], Francisco R. Barroso Villafuerte [2], Antonio Soto Paulino [1], Sebastián M. Arteaga Martínez [1], Lorena Valencia Caballero [1]

[1] Department of Innovation in Human Biological Material, School of Medicine, National Autonomous University of Mexico

[2] Department of Basic Science, School of Medicine, Health Science division, Anahuac University Mexico

SUMMARY

The Mexican Society of Anatomy (SMA) was founded in 1957. Since its creation it has been composed of the most prestigious morphologists in the country, who have achieved a solid and widely recognized society within and outside our borders.

Within a few years of its founding, the creation of the magazine entitled *Archivos Mexicanos de Anatomía* (*Mexican Archives of Anatomy*) was promoted, with quarterly publications that began in 1960, and whose last issue was in 2008 already in digital format.

Since its founding, the society has had 30 presidents whose main function has been to promote morphological sciences at national and international level, so during their biennial terms, according to the Statutes of the Society, they have been in charge of monthly meetings where the most current topics concerning morphological sciences are discussed, as well as the organization, together with their boards of directives, of 28 National Congresses of Anatomy, 23 National Meetings of Morphology, 12 National Student Morphology Competitions and 2 Regional Student Competitions.

Since 1961, as the statutes of the SMA point out, during each congress or meeting the "Andreas Vesalio Award" has been conferred, and since 2003 another distinction was added, called "Dedication of the Academic Year", as the highest awards and public recognition to the morphologist or institution that stands out for its contributions and dedication to this discipline. Finally, it is important to highlight the growth that the society has had: it started with the participation of 49 founding members and it currently has 101 numeral members, 1 honorary member, 7 corresponding members, 89 student members, with a total of 198 members.

INTRODUCTION

On the eve of the celebration of the sixty-fifth anniversary of the Mexican Society of Anatomy, the authors of this publication have given us the task of recapitulating the most important events that have made our society a space for dialogue, teaching, coexistence and exchange of experiences of lovers of morphological sciences, and that have therefore made them a very important part in their professional and personal life.

Since it is the only Society of Anatomy in Mexican territory and one of the most important

Corresponding author:
Lorena Valencia. National Autonomous University of Mexico, Faculty of Medicine, Department of Innovation in Human Biological Material, University avenue 3000, CP 04510, México city, Mexico. Phone: +52 1 5560707995. E-mail: drpineda@unam.mx

Submitted: November 16, 2020. **Accepted:** December 12, 2020

in Latin America, the purpose is to document and witness to the legacy they receive, and which the new generations of the different members of our society must take care of. With them it is with whom we want to share these historical facts, because by expressing their passion for morphology, they will have an interest in knowing who they were and who are the social and academic actors that have conducted the development of the society at different historical times.

FOUNDING OF THE SOCIETY

The SMA was founded in 1957, and since then activities have been carried out uninterrupted to this day (Sociedad Mexicana de Anatomía, 1960-1). These activities have always been framed in accordance with their statutes, which can be summarized as follows:

- Promoting the study of Human Anatomy and related sciences.
- Encouraging anatomical research.
- Consolidating the study of anatomical disciplines as the primary basis for medical science teaching.
- Fighting for the training of Career Masters in anatomical sciences.
- Advocating the selection of teachers from qualified professionals.
- Promoting scientific exchange and rapprochement with other societies or institutions.

Table 1. Statutes of the Mexican Society of Anatomy.

CHAPTER, TRANSIENT OR ANNEX	Objective	ITEMS
Chapter I	Denomination, headquarters and emblem	3
Chapter II	Purposes	1
Chapter III	Objectives	1
Chapter IV	Means of action	1
Chapter V	Members	1
Chapter VI	Requirements	1
Chapter VII	Attributions	4
Chapter VIII	Sanctions	1
Chapter IX	Government	1
Chapter X	Obligations	10
Chapter XI	Editorial Board	1
Chapter XII	Activities	1
Chapter XIII	Elections	5
Chapter XIV	Dues	1
Chapter XV	Legacy	1
Chapter XVI	Reforms	1
Chapter XVII	Advisory Council	5
Transitory I	Election of president and vice president	
Transitory II	Election of the Legacy secretary	
Transitory III	Election of the student representative	
Annex A	Internal regulation of the advisory council	6 chapters and 14 articles
Annex B	Rules of Procedure for National Anatomy Congresses and Meetings	12 chapters and 23 articles
Annex C	Andreas Vesalio Award	
Annex D	Academic year and dedication of the meeting or congress	
Annex E	Website	

The SMA has grouped in a single body all teachers and researchers of the morphological disciplines in Mexico, as well as the professionals whose activity favors them directly or indirectly.

STATUTES

Since its origins, the founding members established the statutes that govern us and dictate the objectives of our society, as well as the mechanisms of action to achieve them.

Similarly, these statutes clearly set out the rights and obligations of the different types of members that make up society (*Sociedad Mexicana de Anatomía*, 2020).

However, these statutes with just over half a century of life have been over the way in some respects by technological advancement and the current life of the world of academia and science, so in 2010 changes were revised and approved into new statutes: originally consisting of 15 chapters and 25 articles, the contents are now as follows: 17 chapters, 40 articles, 3 transients and 5 annexes, which we summarized in Table 1 (*Sociedad Mexicana de Anatomía*, 1960-1).

It is very important to mention that this society takes anatomy, embryology, histology and neuroanatomy as its fundamental pillars, and includes other disciplines such as anthropology, dentistry, biology, comparative anatomy, nursing, surgery, imaging, among many others.

FOUNDING MEMBERS

Since its creation, the Society has gathered the best-known morphologists in the country, who have managed to make it a solid and widely recognized society within and outside our borders. Among these 49 notable academics a number of outstanding names can be highlighted: Dr Fernando Quiroz Gutiérrez, Dr José Negrete Herrera, Dr Gregorio Benítez Padilla, Dr Salvador de Lara Galindo and Dr Luis López Antúnez, who through their works and contributions have managed to train many generations, as some of these books continue to be part of the mandatory literature in some educational institutions (see Table 2).

OFFICIAL EMBLEM

The original drawing of our emblem was made by Salvador Gómez Álvarez and became the official emblem of the Mexican Society of Anatomy since its foundation in 1957, being officialized in 1960 in the first issue of "Mexican Archives of Anatomy".

The official emblem is an ensemble that consists of the image of a stylized eagle. In the center of that image is the figure and the name of Andreas Vesalius, the father of modern anatomy. Forming the base of the emblem is the acronym: SMA corresponding to **Mexican Society of Anatomy.** This emblem reminds us of our foundation and perennial values of this great society (*Sociedad Mexicana de Anatomía*, 1960-1) (Fig. 1).

Fig. 1.- Original drawing taken from the first edition of the magazine "Mexican Archives of Anatomy" Mexico City January 1960.

FORMER PRESIDENTS OF OUR SOCIETY

The first president of the Mexican Society of Anatomy and founding member of the society was Dr Fernando Quiroz Gutiérrez (1957 to 1959), author of the book of Human Anatomy that remains the official text of many universities inside and outside Mexico. He has been followed by a good number of morphologists, who with the staff very high, have managed to consolidate our society and place it at the level it is now. We have a great debt to all of them, as well as to their collaborators, who integrated the respective boards that, with their quiet but fundamental work, made each of the activities of society a success and a step forward of Mexican

morphology. Since its founding, these have been the presidents (Sociedad Mexicana de Anatomía, 2020):

- 1957-1959 Fernando Quiroz Gutiérrez
- 1959-1961 Enrique Acosta Vidrio
- 1962-1963 Mario García Ramos
- 1964-1966 Fernando Quiroz Pavía
- 1967-1968 Salvador de Lara Galindo
- 1969-1972 Salvador Gómez Álvarez
- 1973-1974 Gildardo Espinosa de Luna
- 1975-1976 Alicia Álvarez Ramírez
- 1977-1978 Luis Cárdenas Ramírez
- 1979-1980 Manuel Granados Navarrete
- 1981-1982 Carlos Gilbert Rodríguez
- 1983-1984 Joaquín Reyes Téllez-Girón
- 1985-1986 Felipe Zaragoza Flores
- 1987-1988 Cassandra Núñez Tovar
- 1989-1990 Ismael Herrera Vázquez
- 1991-1992 Natalio González Rosales
- 1993-1994 Eugenio Alfredo Millán Dena
- 1995-1996 Luis Delgado Reyes
- 1997-1998 Armando Pérez Torres
- 1999-2000 Andrés Castell Rodríguez
- 2001-2002 Enrique Canchola Martínez
- 2003-2004 Patricia Herrera Saint Leu
- 2005-2006 Virgilio W. Escalante Silva
- 2007-2008 S. Manuel Arteaga Martínez
- 2009-2010 Manuel Ángeles Castellanos
- 2011-2012 Miguel Herrera Enríquez
- 2013-2014 María Isabel García Peláez
- 2015-2016 William Ortiz Briceño
- 2017-2018 Antonio Soto Paulino
- 2019-2020 Rodrigo E. Elizondo Omaña
- 2021-2022 Diego Pineda Martínez (Current)

CREATION OF "MEXICAN ANATOMY ARCHIVES"

For the first time in Mexico, a publication specializing in the different branches of anatomy was considered to the medical class. It appeared in 1960 and became the official journal of the Mexican Society of Anatomy with the title *Mexican Archives of Anatomy* (see Fig. 2). It pursued the objectives of enduring, growing, improving, consolidating bonds and friendships, providing the Mexican and foreign medical class with

Table 2. List of the founding members of the Mexican Society of Anatomy.

FOUNDING MEMBERS 1957	
1. Manuel Aceves Pérez	26. Joaquín López Cabal
2. Felipe Aceves Zubieta	27. Luis E. Martínez Ballesteros
3. Enrique Acosta Vidrio	28. César Martínez Garza
4. Nicolás Aguilar García	29. Sergio Arturo Mendoza
5. Emilio Banda Sousa	30. Roberto Morales Huerta
6. Benjamín Bandera	31. Enrique Morán Huerta
7. Carlos Barrera Rosales	32. José Negrete Herrera
8. Gregorio Benítez Padilla	33. Horacio Oliva Abarca
9. Eduardo Bravo García	34. Alberto Pérez García
10. Rogelio Camacho Becerril	35. Fernando Pino Quintal
11. Graciela Coria Illizaliturri	36. Fernando Quiroz Gutiérrez
12. Gonzalo Cosío	37. Fernando Quiroz Pavía
13. Salvador de Lara Galindo	38. Joaquín Rangel Villarreal
14. Francisco García Herrera	39. Luis Robles González
15. Mario García Ramos	40. Luis Román de la Rivera
16. Carlos Gilbert Rodríguez	41. Justo Ruiz López
17. Salvador Gómez Álvarez	42. Anuar Said Said
18. Tarquino González de la Garza	43. Carlos Sevilla Monroy
19. Guillermo Hidalgo Barroso	44. Leonardo Silva Espinosa
20. Gabriel Landetta Sigüenza	45. Carlos Talancón Zapata
21. Ignacio Larios	46. Eduardo Trujillo
22. Alberto Leal Ramírez	47. Felipe Vázquez Guzmán
23. Alfredo Lejarza	48. Roberto Villarreal Villareal
24. Raymundo Limón Díaz	49. Fernando Zetina García
25. Luis López Antúnez	

Fig. 2.- Images from the first 4 issues of Mexican Archives of Anatomy magazines.

another means of expression and dissemination, contributing to the uncontainable progress of science for the benefit of Mexico and Humanity.

The journal continued from 1960 to 1973 where it was discontinued for 5 years, resuming its regularity until 1988. Unfortunately, its last digital issue was in 2008 (see Table 3).

Below we cite the words written in the first issue of the journal, which reflect the spirit and impetus that made it grow for many years, and which should be an inspiration to revive:

"The urgent need for its emergence, coupled with our classic hardship, made the magazine's material presentation does not fit with much, all our aspirations: we want it better, with more issues, more pages available and a higher frequency. For this we need and ask for the collaboration of all the members of the Mexican Society of Anatomy, of all the scientists and philanthropists who want to help a noble and future cause". (Sociedad Mexicana de Anatomía, 1960-1).

NATIONAL CONGRESSES AND MEETINGS

Perhaps one of the greatest challenges that presidents have had along with their executive boards, but also one of the most enriching functions, is the organization of national conferences and meetings that have allowed the exchange of knowledge, new collaborations between different institutions and scientific discussions, among many others. Without a doubt it is the space that gives student members the opportunity to present their works and interact with the various authors and leaders of morphological sciences related to their bachelor's

Table 3. List of years of publication as well as volumes for each year of the journal of Mexican Archives of Anatomy.

Year of publication	Volume No.	Number of magazines
1960	1	4
1961	2	4
1963	3	4
1963-1964	4	4
1964	5	3
1965	6	3
1966	7	3
1967	7	3
1968	8	2
1969	9	2
1970	10	1
1970	11	2
1971	12	1
1972	13	2
1973	14	1
1978	15	2
1979	16	1
1980	17	1
1981	18	1
1982	19	1
1983	20	1
1984	21	1
1985	22	1
1986	23	1
1987	24	1
1988	25	1
1990	26	1
2003	27	1
2007	28	1
2008	29	1

degrees. It is a high motivation to sow in them a passion for morphological sciences and academy.

It is very important to mention that for several years the SMA has had exponential growth, especially concerning attendance at congresses and meetings, which by statutes have continued to be called "national", but which should actually be called "international", since in recent years there has been an average participation of 10 countries, in addition to being held in conjunction with the Pan-American and global congresses. (see Table 4).

Table 4. SMA Congresses and Meetings through 2020.

Biennium	President	National Meeting	National Congress	Other
1960	Enrique Acosta Vidrio			I International Congress of Anatomy
1961			I : D.F.	
1963	Mario García Ramos		II: San Luis Potosí, San Luis Potosí	
1966	Fernando Quiroz Pavía		III: D.F.	I Pan American Congress of Anatomy
1968	Salvador de Lara Galindo		IV: Toluca, Estado de México.	
1971	Salvador Gómez Alvarez		V: D.F.	
1974	Gildardo Espinosa de Luna		VI: Morelia, Michoacán.	
1975	Alicia Alvarez Ramirez	I: Tuxtla Gutiérrez, Chiapas.		
1976			VII: Veracruz, Veracruz	
1977	Luís Cárdenas Ramírez	II: Monterrey, Nuevo León.		
1978			VIII: Chapala, Jalisco.	Extraordinary National Meeting of Morphology
1979	Manuel Granados Navarrete	III: Querétaro, Querétaro		
1980				XI International Congress of Anatomy
1981	Carlos Gilbert Rodriguez	IV: Tijuana, Baja California.		
1982			IX: Matamoros, Tamaulipas.	
1983	Joaquín Reyes-Téllez G.	V: Puebla, Puebla.		
1984			X: Zacatecas, Zacatecas.	
1985	Felipe Zaragoza Flores	VI: Cuernavaca, Morelos.		
1986			XI: Merida, Yucatan.	
1987	Cassandra Núñez Tovar	VII: Toluca, Estado de México.		
1988			XII: Jalapa, Veracruz.	
1989	Ismael Herrera Vazquez	VIII: Oaxaca, Oaxaca.		
1990			XIII: Villa Hermosa, Tabasco.	
1991	Natalio González Rosales	IX: Morelia, Michoacán.		
1992			XIV: Pachuca, Hidalgo.	
1993	Alfredo Eugenio Millán Dena	X: Tlaxcala, Tlaxcala.		
1994			XV: Aguascalientes, Aguascalientes	

Biennium	President	National Meeting	National Congress	Other
1995	Luis Delgado Reyes	XI: Metepec		
1996			XVI: Oaxaca, Oaxaca.	
1997	Armando Pérez Torres	XII: Queretaro, Querétaro.		
1998			XVII: León, Guanajuato.	
1999	Andrés Castell Rodríguez	XIII: Acapulco, Guerrero.		
2000			XVIII: Ixtapa Zihuatanejo, Guerrero.	
2001	Enrique Canchola Martínez	XIV: Veracruz, Veracruz		
2002			XIX: Colima, Colima.	
2003	Patricia Herrera Saint-Leu	XV: Monterrey, Nuevo León.		
2004			XX: Guadalajara, Jalisco.	
2005	Virgilio W. Escalante Silva	XVI: Zacatecas, Zacatecas.		
2006			XXI: San Luis Potosí, San Luis Potosí.	
2007	Manuel Arteaga Martínez	XVII: Tuxtla Gutiérrez Chiapas.		
2008			XXII: Matamoros, Tamaulipas.	
2009	Manuel Angeles Castellanos	XVIII: Oaxaca, Oaxaca.		
2010			XXIII: Irapuato	
2011	Miguel A. Herrera Enríquez	XIX: Puebla, Puebla.		
2012			XXIV: Zacatecas, Zacatecas.	
2013	Ma. Isabel García Peláez	XX: Huatulco, Oaxaca		XVIII Pan American Congress of Anatomy
2014			XXV: Durango, Durango.	1st National Meeting of Neuromorphology
2015	William H. Ortiz Briceño	XXI: Campeche, Campeche.		
2016			XXVI: León, Guanajuato.	
2017	Antonio Soto Paulino	XXII: Acapulco, Guerrero.		
2018			XXVII: Monterrey, Nuevo León.	
2019	Rodrigo Elizondo Omaña	XXIII: Chihuahua, Chihuahua.		IV Unesco World Congress of Digital Anatomy
2020			XXVIII: (1st virtual congress)	

RECOGNITIONS GRANTED

Andreas Vesalio Award

This award is the highest award given by the SMA in each of its National Congresses or Meetings. It has the purpose, as indicated by the statutes of our society, to "publicly and in a special way signify the recognition and gratitude to the Professor or Institution who, in the teaching of Morphology in our national environment, marks an age greater than twenty-five years or that for its contribution, research and dedication to these disciplines, is a

creditor to this award". It was first awarded to Dr Fernando Quiroz Gutiérrez in September 1961 as part of the First National Congress of Anatomy.

This award consists of awarding a medal with the engraved image of Andreas Vesalius and has been granted to the morphologists listed in Table 5.

Table 5. Recipients of the Andreas Vesalio Award.

Recipients of the Andreas Vesalio Award
1961: First National Congress of Anatomy to **Fernando Quiroz Gutierrez**
1963: II National Congress of Anatomy to **Luis Martínez Ballesteros**
1974: VI National Congress of Anatomy to **Samuel Reyna Miranda**
2007: XVII National Meeting of Morphology to **the Morphological Sciences Department of the School of Medicine "Dr. Manuel Velasco Suárez" of the Autonomous University of Chiapas**
2008: XXII National Congress of Anatomy to **the Academic Department of Health Sciences and Technology of the Autonomous University of Tamaulipas**
2009: XVIII National Meeting of Morphology to **Biological Material Conservation Workshop of the School of Medicine and Surgery of the Autonomous University "Benito Juárez" of Oaxaca**
2010: XXIII National Congress of **Anatomy, (School of Medicine of Quetzalcoatl University of Irapuato)**
2011: IX National Meeting of Morphology **(School of Medicine of the Benemérita Universidad Autónoma de Puebla)**
2012: XXIV National Congress of Anatomy **(Alvaro Díaz Zarate**)
2013: X National Meeting of **Morphology (UNAM School of Medicine)**
2014: XXV National Congress of Anatomy **(Santiago Aja Guardiola)**
2015: XI National Meeting of Morphology **(Manuel Granados and Navarrete**)
2016: XXVI National Congress of Anatomy **(School of Medicine of the University of Guanajuato Campus León)**
2017: XII National Meeting of Morphology **(School of Medicine of the Autonomous University of Guerrero)**
2018: XXVII National Congress of Anatomy **(Manuel Arteaga Martínez)**
2019: XXIII National Meeting of Morphology **(Noel del Val Ochoa)**
2020: XXVII Virtual National Congress of Anatomy **(Not granted)**

Dedication of the academic year

With the beginning of the new century, the acting board of directors of the society proposed and its members accepted to award a new distinction "Dedication of the Academic Year". With this distinction the Society intends to give a well-deserved recognition and gratitude for the morphologist, or institution that, in Mexico, has distinguished itself by its contributions in teaching, research and dedication in the different morphological disciplines.

This distinction was first awarded in 2003 and has since been awarded each year, with some particular exceptions, being as follows (Sociedad Mexicana de Anatomía, 1960-2):

- Year 2003 - (Dr. Manuel Granados Navarrete)
- Year 2004 - (Dr. Alicia Álvarez Ramírez)
- Year 2005 - (Dr. Gregorio Benítez Padilla)
- Year 2006 - (Dr. Gildardo Espinosa de Luna)
- Year 2007- on the occasion of the celebration of the 50th Anniversary of the founding of our society, this year was designated as the Year of the Fiftieth Anniversary, intended to recognize in this way each and every member morphologist who have contributed to achieve what is now the Mexican Society of Anatomy.
- Year 2008 - (Dr. Luis López Antúnez)
- Year 2009 - (Dr. Carlos Gilbert Rodríguez)
- Year 2010 -(Dr. Amelia Sámano Bishop)
- Year 2011 - (Dr. Enrique Acosta Vidrio)
- Year 2012 - (Dr. Carlos Serrano Sánchez)
- Year 2013 - (XLVII Anniversary of the Pan American Association of Anatomy)
- Year 2014 - (María Elena Castillo Romero)
- Year 2015 - (Horacio Oliva Abarca)
- Year 2016 - (Salvador de Lara Galindo)
- Year 2017 - (Carlos Jesús Guzmán Cuervo)
- Year 2018 - (Dr. Santiago Aja Guardiola)
- Year 2019 - (Natalio González Rosales)
- Year 2020 – Not awarded due to the pandemic

CONCLUSIONS

For more than 60 years, the Mexican Society of Anatomy has been composed of leading national and international morphologists dedicated to the teaching and research of health and related sciences. Its common objective is to promote the updating of anatomy, neuroanatomy, histology and embryology, to encourage teachers and students to love these disciplines and thus integrate the new generations into national and international collaborative work, introducing them immediately to research and teaching. The history of our society has made it clear to us that the sum of efforts leads us to better professional and personal development. This is how we must have academic programs common to the needs of our time and services that offer the necessary means and tools for the transfer of information from our daily work, and thus bring together more members who have the same objective of disseminating the morphological sciences.

Finally, our vision in the future as part of the board of directors and members of the Mexican Society of Anatomy is to resume the edition of the journal *Mexican Archives of Anatomy*, and to be the official organ of the *European Journal* of *Anatomy,* allowing our members to publish in an indexed journal specialized in morphological sciences with the aim of giving opportunity to strengthen our own journal. This will strengthen ties with European, American and Latin American societies, giving us greater international projection.

During these months, the incorporation of our society into the International Federation of Associations of Anatomists (IFAA) will be formalized and we will promote the linkage with the Mexican Association of Faculties and Schools *of* Medicine (AMFEM) and the International Association of Medical Science Educators (IAMSE), seeking to be a consulting body to generate criteria or basic axes for the academic approval of programs studying morphological disciplines in the Schools and Faculties of Health Sciences in Mexico—this was one of the first objectives of our society since its foundation.

Given the high participation of international attendees that have registered in recent years in our congresses and meetings, originating in more than 10 countries, we consider it relevant to promote the discussion of changes in the statutes so that our congresses and meetings take character and are called “International”.

BIBLIOGRAPHIC REFERENCES

SOCIEDAD MEXICANA DE ANATOMÍA (1960-1) *Archivos mexicanos de anatomía*. Enero-marzo. Imprenta Aldina, México D.F. 1(1): 7-9.

SOCIEDAD MEXICANA DE ANATOMÍA (1960-2) A*rchivos mexicanos de anatomía.* Abril-junio. Imprenta Aldina, México D.F. 1(2): 57-68.

SOCIEDAD MEXICANA DE ANATOMÍA (2020) https://www.sociedadmexicanadeanatomia.com/quienes-somos

Gender and age-related differences in the morphometry of corpus callosum: MRI study

Maher T. Al-Hadidi[1], Heba M. Kalbouneh[2], Ashraf Ramzy[3], Aiman Al Sharei[3], Darwish H. Badran[2,3], Amjad Shatarat[2], Emad S. Tarawneh[4], Waleed S. Mahafza[4], Fadi A. Al-Hadidi[5], Azmy M. Hadidy[3]

[1] Department of Anatomy and Histology, Faculty of Medicine, Al-Balqa Applied University, Al Salt, Jordan

[2] Department of Anatomy and Histology, School of Medicine, The University of Jordan, Al Salt, Jordan

[3] Department of Basic Medical Sciences, School of Medicine, The Hashemite University, Zarqa, Jordan

[4] Department of Diagnostic Radiology and Nuclear Medicine, School of Medicine, The University of Jordan, Amman, Jordan

[5] Department of Special Surgery, School of Medicine, The University of Jordan, Amman, Jordan

SUMMARY

The aim of this study is to establish age and sex based-reference values of corpus callosum (CC) length and its distances to the fornix and anterior commissure. Brain MRIs of 214 subjects, who had normal MRI scans according to radiologists' reports, were reviewed retrospectively. Scans were obtained from April 2013 until April 2014 at Jordan University Hospital, Radiology Department (Amman, Jordan). The antero-posterior (longitudinal) dimensions of the CC (AB), the vertical distance between the anterior commissure and the most superior point of CC (CD), the distance between the genu and the fornix (AE), and the angle between AB (the longitudinal dimension of the CC) and AD (the distance from the genu to the anterior edge of the anterior commissure) (BAD) were measured and subjected to statistical analysis. Regardless of sex, CC length and other parameters (CD and AE) increased dramatically with age in children and adolescents (≤ 18years). A significant negative correlation was found between age and BAD angle in females only. We observed a continuous increase in CC length after childhood in both sexes, with a slower rate of growth in females. Sexual dimorphism was observed in AB and BAD angle in infants (≤ 2years) and AE in the adolescent group (12 to 18 years old). A local reference of CC length and its distances to nearby structures were established. Sexual dimorphisms of some CC parameters were more evident during the early years of life. Our data also indicated important sex differences in the development of the CC. Such knowledge is essential in evaluating the normal neurological development of the CC and the pathological conditions affecting it.

Keywords: Corpus callosum – Fornix – Anterior commissure – Sexual dimorphism – MRI

Corresponding author:
Darwish H. Badran. Department of Anatomy and Histology, School of Medicine, The University of Jordan, Amman 11942, Jordan. E-mail: dhbadran@ju.edu.jo

Submitted: February 20, 2020. **Accepted:** August 31, 2020

INTRODUCTION

The corpus callosum (CC) is the largest white matter structure in the human brain. It connects the right and left cerebral hemispheres in a mostly homotopic fashion. The CC lies in the midsagittal plane between the two hemispheres with the fornix and the third ventricle related to it inferiorly (Griffiths et al., 2009). The growth and shape of the CC are determined by several factors including age, prematurity, genetics, handedness, childhood neglect, and gender (Garel et al., 2011; Nosarti et al., 2004; Teicher et al., 2004; Westerhausen et al., 2004; Woldehawariat et al., 2014).

Neurologists can use CC dimensions and its relation to the nearby structures to compare with certain neurological and psychological disease entities (Luders et al., 2010; Woldehawariat et al., 2014). Most of the studies on the size and shape of CC were performed outside the Middle East and other countries to confirm the genetic and racial factors in anthropometry. In our study population, the mean CC length was similar to the data recorded from Iranian and Turkish populations (Mohammadi et al., 2011; Unlu et al., 2014), but was higher than the data from the Japanese (Takeda et al., 2003), indicating that ethnicity could play an important role in CC size (Mohammadi et al., 2011).

Alterations in the size and morphology of the CC are commonly documented in several psychiatric disorders. For example, alterations in the size and shape of the CC were reported in patients with schizophrenia and bipolar disorder (Downhill et al., 2000; Walterfang et al., 2009). Furthermore, schizophrenia patients had reduced CC total area and length when compared with controls (Unlu et al., 2014). Fractional anisotropy (a diffusion tensor imaging measure that reflects the degree to which white matter fibers are aligned in a specific direction) of the genu, splenium and total corpus callosum was significantly reduced in autism (Alexander et al., 2007). Additional studies provide preliminary evidence of impaired neural connectivity in the CC and other major fiber tracts in autism (Barnea-Goraly et al., 2004; Jou et al., 2011). A reduction in the CC area was also found to be associated with impulsivity, as well as suicidal behavior (Cyprien et al., 2011; Moeller et al., 2005). Thus, CC morphometric data may indirectly reflect underlying pathologic processes. In this study, our aim is to investigate the possible sex-related differences in the length of the CC, its morphometric relationship to nearby structures (the fornix and anterior commissure) and the postnatal developmental changes based on cross-sectional MRI data from healthy Jordanian children and adults.

MATERIAL AND METHODS

Cerebral MRIs from the midsagittal plane were collected from April 2013 until April 2014 at Jordan University Hospital, Radiology Department (Amman, Jordan). Informed consent was obtained from all study participants or their legal guardians, and ethical approval was obtained from the Academic Research Council of the Faculty of Medicine, University of Jordan, according to the ethical principles of the Declaration of Helsinki.

Two hundred and fourteen normal MRIs were obtained from 95 males and 119 females (mean age ± SD: 27.0±21.8 and 27.9±19.5 years, respectively). The subjects of the sample were selected from those referred for advanced evaluation of the brain by MRI and proved to be negative. Only normal MRI scans (according to the radiologists' reports) were included.

Exclusion criteria

For our study, the following exclusion criteria were used: a) intracranial lesions, masses or head injury on the MRI, b) demyelination and degenerative diseases (multiple sclerosis), c) history of neurosurgery, d) previous cerebrovascular accidents, e) history of neurological or psychiatric diseases (epilepsy, autism, depression, dementia, schizophrenia and bipolar disorder), and g) CC anomalies (hypoplasia, dysplasia, and complete agenesis). None of the participants had ever received psychopharmacotherapy.

Using 18 years as the beginning of adulthood, the subjects were divided into two main groups: group 1) children and adolescents (≤ 18 years), and group 2) adults (>18 years). To study the developmental sexual dimorphism of the CC**,** each of these two groups was further subdivided into

subgroups on the basis of age as follows: infancy (birth to 2 years old), early childhood (3-8 years old), middle childhood (9-11 years old), adolescence (12-18 years old), young adulthood (19-39 years old), middle adulthood (40-60 years old), and late adulthood (>60 years old).

Procedure

A Siemens Magnetic Vision Plus (1.5 Tesla) (Siemens, Erlangen, Germany) was used in T1 sequence (TR=600, TE=14) with a 512x512 matrix and 32 cm FOV. Twelve sagittal images scanning from right to left were performed in two minutes for each patient while in a supine position. The sagittal images were parallel to the axial plane of the CC. The obtained images were reconstructed at 5 mm slices with a verified inclination of less than 1° from the midline. The best image showing the CC was selected. The parameters were measured by Syngo Fast View software (Siemens Medical Solutions, Department SW, Erlangen, Germany) on the same slice image and recorded to the nearest millimeter. The distances were measured directly from the MRI screen and documented on printed images. The anteroposterior length of the corpus callosum (AB) was taken as the distance between the anterior edge of the genu and the posterior edge of the splenium. The distance from the anterior edge of genu to the anterior edge of the fornix (AE) was measured, and the anterior edge of its column was considered at the bifurcation above the anterior commissure. The maximum height (CD) of the CC was taken as the vertical distance from the anterior commissure to the dorsal edge of the CC. The angle (BAD) formed by the meeting of the longitudinal dimension of CC (AB) and the distance from the genu to the anterior edge of the anterior commissure (AD) was also measured (Fig. 1).

Three senior radiologists (each with at least 10 years of experience in brain MRI) took all of the measurements (three values for each parameter) and the combined mean values were used in the subsequent analysis of each data set.

Statistical analysis

The data was entered into a spreadsheet and analyzed using the IBM SPSS Statistics for Windows, version 19 (IBM Corp, Armonk, NY, USA). The means (± standard deviation) were calculated, and males and females in the various age groups were compared.

Differences in continuous variables between the two independent groups were assessed using the two-tailed *t* test. Relationships between each dimension and the ages were assessed using the Spearman's Rho coefficient. The significance threshold was set at 0.05. All measurements showed excellent interobserver reliability, with intraclass correlation coefficients ranging from 0.76 to 0.83. The XY scatter plots were generated using Microsoft Excel 2010 and the figures were generated using Adobe Illustrator CC 2014.

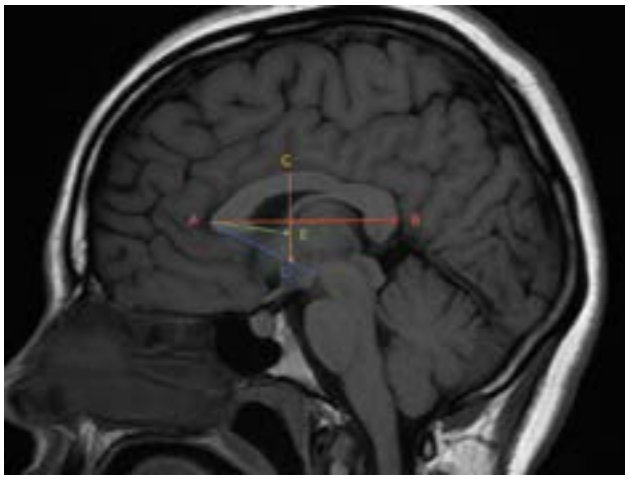

Fig. 1.- MRI showing the anteroposterior length measurement of the corpus callosum and its relation to the fornix and anterior commissure. **AB:** The length of the corpus callosum from the anterior edge of the genu to the posterior edge of the splenium. **AE**: The distance from the anterior edge of genu to the anterior edge of the fornix at its bifurcation above the anterior commissure. **CD**: The maximum height from the anterior commissure to the dorsal edge of the CC. **BAD**: The angle formed by the meeting of AB and AD (the distance from the genu to the anterior edge of the anterior commissure).

RESULTS

CC development from childhood to adulthood

MRIs from children and adults who were 18 years of age or younger were examined separately for age-related changes in CC length, and its morphometric relationship to the fornix and anterior commissure was also examined.

In males, the Spearman's Rho coefficient between age and CC parameters showed a positive relationship in children and adolescents

(≤ 18 years). A very strong positive correlation was evident with AB (r = 0.8), a moderate positive correlation was evident with CD (r = 0.5), and a very strong positive correlation was evident with AE (r = 0.8). These correlations were statistically significant (p<0.001). A very weak negative correlation between age and BAD angle was also observed (r = -0.1), but it was not statistically significant (p>0.05) (Fig. 2).

In female children and adolescents (≤ 18 years), a strong positive correlation was noted with AB (r = 0.8), and moderate positive correlations were evident with CD (r = 0.33) and AE (r = 0.5). However, the correlation between age and BAD angle was much stronger in females than males, and a moderate negative correlation was noted (r = -0.4) (Fig- 2). All correlations were statistically significant (p<0.05).

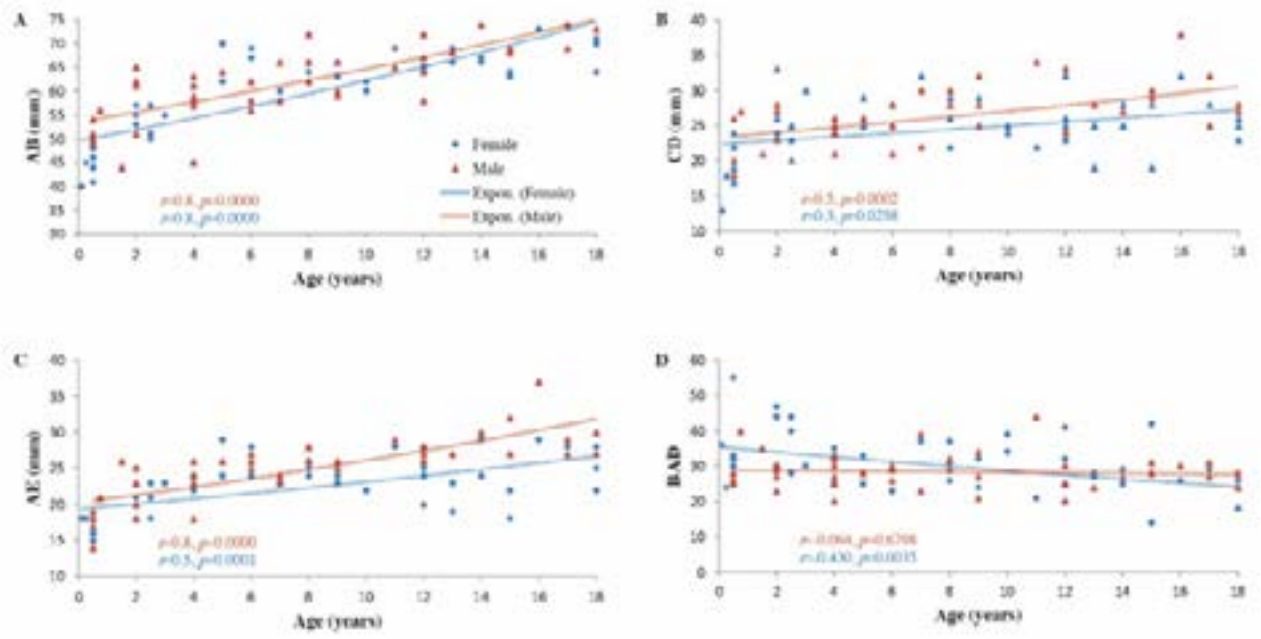

Fig. 2.- Scatter plots showing the correlations between age and: A: AB, B: CD, C: AE, and D: BAD angle in *childhood and adolescence* (0-18 years). Regression lines represent the lines of best fit. *r*: Spearman's Rho coefficient. P values were calculated using the two-tailed *t*-test, n=88.

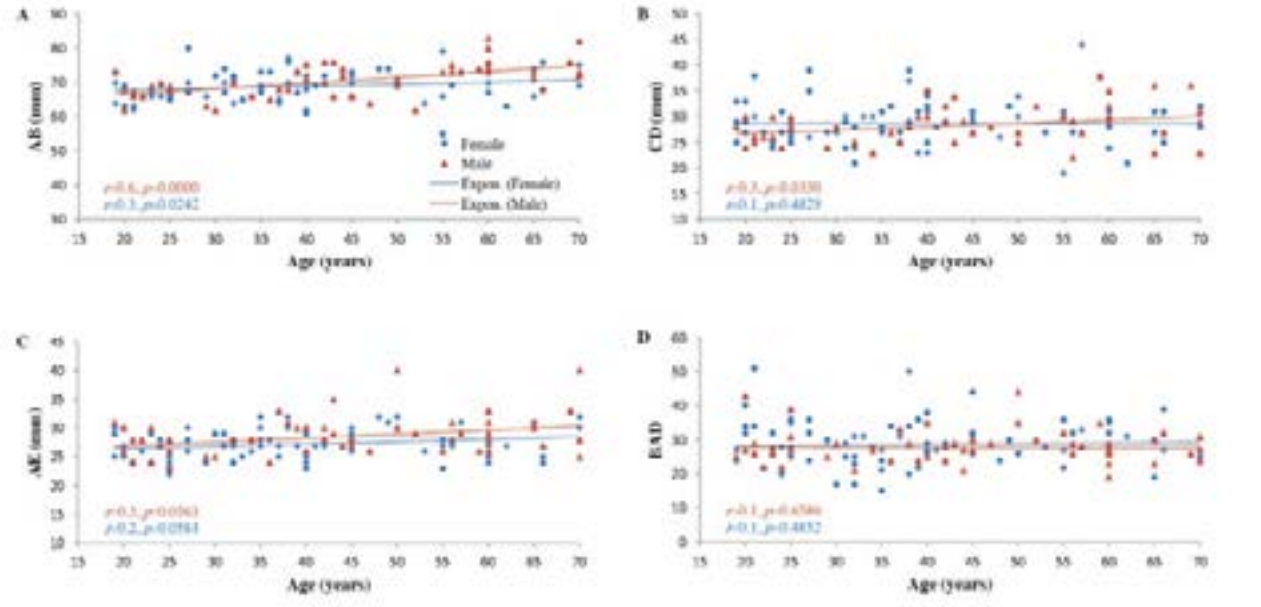

Fig. 3.- Scatter plots showing the correlations between age and: A: AB, B: CD, C: AE, and D: BAD angle in *adulthood* (19-70 years). Regression lines represent the lines of best fit. r: Spearman's Rho coefficient. P values were calculated using the two-tailed t-test, n=126.

In adult males (>18 years), a moderate positive correlation was evident with AB (r = 0.6). Weaker positive correlations were evident with CD and AE (r = 0.3), and a statistically insignificant positive correlation was observed with BAD angle (r = 0.1) (Fig. 3).

In adult females (>18 years), a weak positive correlation that was still statistically significant was noted between age and AB (r = 0.3, p<0.05). Weak positive correlations that were statistically insignificant were noted between age and both CD (r = 0.1) and AE (r = 0.2) (p>0.05). A statistically insignificant, weak positive correlation was noted between age and BAD angle (r = 0.1) (Fig. 3).

Gender and age-related differences in CC length and its morphometric relationship to the fornix and anterior commissure

The mean values (± SD) of CC length and distances to the fornix and anterior commissure in males and females of the different age subgroups are shown in Table 1. For most of the CC parameters, males tended to have higher mean values than females. In contrast, the BAD angle was higher in females. A comparison of mean CC parameters between males and females (using the two-tailed *t*-test) showed a statistically significant difference ($P<0.05$) in the longitudinal dimension of the CC (AB) and the BAD angle in only the infant subgroups (birth - 2 years old). The distance between the genu and the fornix (AE) was also significantly different between genders in the adolescent group (12-18 years old).

DISCUSSION

CC dimensions and its distances to the nearby structures can be used by neurologists to compare the findings in patients with certain neurological and psychological disease entities (Luders et al., 2010; Woldehawariat et al., 2014). Most of the studies on the size and shape of CC were performed on Caucasian (Mourgela et al., 2007), East Asian (Hwang et al., 2004), Iranian (Mohammadi et al., 2011) and Indian populations (Gupta et al., 2008). Few studies have been performed using Middle Eastern individuals. In a previous study, Yasin and Farahani (2015) reported that genetic and racial factors, in addition to educational background, play a significant role in CC size. The authors suggested that such research should be conducted in the Middle East and other countries to confirm the genetic and racial factors in anthropometry. In our study population, the mean CC length was similar to the data recorded from Iranian and Turkish populations (Mohammadi et al., 2011; Unlu et al., 2014). Our values, however, still higher than the data from the Japanese (Takeda et al., 2003), indicating that ethnicity could play an important role in CC size (Mohammadi et al., 2011).

Currently, many factors are thought to influence the variations observed in human CC morphology. The first factor considered in our study was the age of the participants. According to 3D ultrasounds of the fetal CC, rudimentary fibers of the CC begin to appear at the fetal midline in the 12th week of gestation (Pashaj et al., 2013). The number of callosal fibers is already fixed around birth, but structural changes continue to occur in the CC during postnatal development (Luders et al., 2010; Tanaka-Arakawa et al., 2015). Our data showed a rapid increase in CC length until 18 years, but slower growth in adults of both sexes (>18 years).

Numerous studies have reported that CC length changes significantly with age (Luders et al., 2010; Mohammadi et al., 2011), and our findings confirm this observation. However, few studies have reported data on CC morphology in infants. A study of healthy children with ages ranging from 1 day to 15 years reported rapid growth until three years of age, followed by continuous slower growth (Garel et al., 2011). In the study by Garel et al., the fronto-occipital diameter (anteroposterior diameter of the CC) and the thickness of the genu and isthmus were measured, but they did not directly assess the size of the CC. On the other hand, a recent MRI study of 114 healthy individuals with ages ranging from 1 month to 25 years reported significant, non-linear, age-related increases in the absolute area of the overall CC and its subregions: rostrum, genu, rostral body, anterior midbody, posterior midbody, isthmus and splenium. The growth rate then started to flatten during adolescence and adulthood in both sexes (Tanaka- Arakawa et al., 2015). Our results echo their findings, but we further showed a continued

increase in CC length after the childhood period in both sexes, with a greater slowing of growth in females. Using MRI, Vannucci et al. (2017) reported that genu, body, splenial and total corpus callosal areas increased by 40-100% during first year of life. Comparing genu and splenium, they demonstrated that the genu expanded to a greater extent than the splenium during the first 6 years, while the splenium expanded to a greater extent between 7 and 18 years. They attributed these age-related differences to the consequence of differential axonal myelination. Sex differences

Table 1. Gender and age-related differences in CC length and its relation to the fornix and anterior commissure in Jordanians.

	AB		CD		AE		BAD	
	Male	**Female**	**Male**	**Female**	**Male**	**Female**	**Male**	**Female**
(0-2 years) (4 males & 6 females)	55.3±7.1	48.9±5.6	24.0±3.7	21.8±5.0	20.4±3.6	18.6±3.1	29.1±4.7	36.5±8.9
Range	44-65	40-57	18-28	13-33	14-26	15-25	23-40	24-55
P value	0.0214*		0.2323‡		0.2149‡		0.0206*	
(3-8 years)	60.8±6.0	60.1±7.6	25.6±2.9	26.1±3.4	24.8±2.5	23.9±2.7	29.2±4.5	31.6±6.3
(8 males & 9 females)								
Range P value	45-72 0.7669‡	45-70	21-30 0.6999‡	20-32	18-28 0.3579‡	18-29	20-39 0.223‡	23-44
(9-11 years)	62.5±3.5	64.0±3.5	29.8±4.0	25.6±2.9	26.3±1.9	23.8±2.5	31.5±9.9	30.0±7.4
(9 males & 11 females)								
Range P value	59-66 0.5461‡	60-69	25-34 0.1135‡	22-29	25-29 0.1491‡	22-28	21-44 0.8011‡	21-39
(12-18 years)	70.2±5.6	67.0±3.5	28.4±4.1	25.6±3.8	28.7±3.1	24.3±3.6	26.9±3.3	27.1±7.4
(13 males & 15 females)								
Range P value	58-79 0.0819‡	63-74	24-38 0.0738‡	19-32	26-37 0.0019*	18-28	20-31 0.9491‡	14-42
(19-39 years)	67.5±3.0	68.6±4.0	26.8±2.3	28.8±4.2	27.5±2.8	26.9±2.4	27.9±5.5	28.9±7.5
(14 males & 20 females)								
Range P value	62-73 0.288‡	62-80	23-30 0.0512‡	21-39	23-33 0.477‡	22-32	21-43 0.5937‡	15-51
(40-60 years)	72.2±4.9	69.4±5.2	29.6±3.6	29.6±4.7	29.1±3.3	27.6±2.7	28.6±5.2	31.0±5.0
(16 males & 22 females)								
Range P value	62-83 0.0606‡	55-79	22-38 0.9572‡	19-44	26-40 0.0802‡	23-32	19-44 0.11‡	22-44
(> 60 years)	73.6±4.4	66.3±2.9	29.3±5.4	27.9±3.9	30.6±4.9	28.6±3.2	27.6±3.5	28.3±6.1
(31 males & 36 females)								
Range P value	68-82 0.197‡	63-76	68-82 0.5837‡	21-32	25-40 0.3858‡	24-32	23-32 0.7935‡	19-39

* Extremely significant, ‡ not significant, all dimensions in millimeters.

seem to exist during the development of the CC. The significant increase in the CC parameters in males explains the significant increase of the BAD angle in females.

Geometrically, the meeting of the AD line with a longer AB line (at A point) produces a more acute angle than the meeting of the same AD line with a shorter AB line (at a closer A point), which will produce a wider angle. Our results support the idea that structural changes of the CC continue to occur throughout life, but the most dramatic changes happen during childhood and adolescence. Progressive fiber myelination, regressive pruning processes, glial proliferation and ongoing maturation and modeling of the axonal cytoskeleton may underlie these changes (Luders et al., 2010). The adult group in the present study ranged in age from 19-70 years and a wider age range of participants could have yielded different results. Westerhausen et al. (2011) suggested sexual dimorphism in the micro-structural architecture of the CC. They claimed that clusters of significantly-higher fractional anisotropy and lower diffusion strength in males compared to females were detected in the genu and truncus of CC.

The literature concerning sexual dimorphism of the CC is not in agreement about sex differences in callosal size and shape (Ardekani et al., 2013; Gupta et al., 2008; Luders et al., 2010). In one study, the only parameter that showed significant gender dimorphism was the length of the CC, being longer in males (Suganthy et al., 2003). In Iran and Japan, however, no statistically significant differences between the sexes were found (Mohammadi et al., 2011; Takeda et al., 2003). In our study, the male to female differences in the longitudinal dimensions of the CC were not statistically significant. Of the parameters measured, only the longitudinal dimension of the CC and BAD angle in infants (≤ 2 years) and the distance between the genu and the fornix (AE) in adolescents (12-18 years old) exhibited sexual dimorphism. This may be explained by a significant difference in the growth of the CC parameters in adolescents between sexes, which may be attributed to hormonal factors. Guz et al. (2019) studied sexual parameters as regards CC including: lengths of longitudinal cross-section of CC, CC thickness in the narrowest place (isthmus), the largest linear dimension of the brain from the frontal pole to occipital pole, the longitudinal cross-section area of the CC and cerebral cross-section area. They demonstrated that in all age groups studied, there were statistically-significant differences in the values of the analysed parameters and ratios of CC size between males and females.

Several studies have reported the presence of significant sex differences in callosal measurements. DeLacoste-Utamsing and Holloway (1982) reported a sex difference in the shape and surface area of the CC, especially in its splenium. They related such observation due to gender differences in the degree of lateralization for visuospatial function, since the splenium contains peristriate, parietal and superior temporal fibers. In Korean neonates, Hwang et al. (2004) reported no significant gender differences in the width and total area of the CC, but the height of the CC was greater in males and the splenium was thicker in females. Similar results were also obtained in a Turkish population where the splenium was found to be wider in females than in males (Aydlnlioglu et al., 1996). In an Indian study, morphometric measurements of the CC and its subregions showed sexual dimorphism in several parameters: 1) a longer CC in males, 2) a longer distance between the genu and the fornix in older males, and 3) a longer distance between the splenium and superior colliculus (Gupta et al., 2008). Another earlier study reported significantly higher ratios between the whole brain and the total CC including the genu, the posterior midbody, and the splenium in females than males (Tanaka-Arakawa et al., 2015).

Little is yet known about the morphometric relationship between CC and nearby structures. In our study, the distances from the CC to the fornix and anterior commissure (CD and AE respectively) were also traced from infancy to late adulthood. In both sexes, CD and AE exhibited significant increases with advancing age until 18 years. However, the angle formed by the longitudinal dimension of the CC and the distance from the genu to the anterior edge of the anterior

commissure (BAD) decreased significantly with age in female children and adolescents only. In adulthood, the CD continued to increase significantly with age in males only. These data suggest age-related sex differences during the structural maturation of the brain. Myelination processes could also affect the anatomical relationship between the CC and the nearby structures. Additionally, gonadal hormones and sex chromosomes could contribute to differences between the sexes. Schmied et al. (2020) studied sex differences in brain-size adjusted CC area and thickness in ages of 6-24 months and reported a steeper rate of growth in males versus females. They reported that CC thickness was significantly associated with underlying microstructural organization. However, they observed that there were no sex differences in the association between microstructure and thickness, suggesting that the role of factors such as axon density and/or myelination in determining CC size is generally equivalent between sexes.

Our study was limited, because we did not measure the thickness of the CC and its subregions. We only measured the length of the CC, as it is easily applicable in daily clinical practice. However, more detailed analyses of the callosal subregions should be conducted to establish a normative reference in our population and to understand the complex changes in CC morphometry throughout life. In addition, our results only reveal differences between people of different ages rather than changes in the same individuals over time. Therefore, a longitudinal study of these changes could provide more insight into developmental changes in the CC.

In conclusion, this study offers a reference of CC length, and its distances from the anterior commissure and fornix are established. In addition, sexual dimorphisms of some CC parameters were more evident during the early years of life. Our data also indicated important sex differences in the development of the CC. Such knowledge is essential in evaluating the normal neurological development of the CC and the pathologies affecting it. Further studies with increased numbers of samples can give more evidence concerning these parameters.

REFERENCES

ALEXANDER AL, LEE JE, LAZAR M, BOUDOS R, DUBRAY MB, OAKES TR, MILLER JN, LUJ, JEONG EK, MCMAHON WM, BIGLER ED, LAINHART JE (2007) Diffusion tensor imaging of the corpus callosum in autism. *Neuroimage,* 34(1): 61-73.

ARDEKANI BA, FIGARSKY K, SIDTIS JJ (2013) Sexual dimorphism in the human corpus callosum: an MRI study using the OASIS brain database. *Cereb Cortex,* 23(10): 2514-2520.

AYDLNLIOGLU A, DIYARBAKIRLI S, YÜCEER N, KELES P, UNAL O, ERDOGAN RA (1996) The relationship of sex differences to the anatomy of corpus callosum in the living human being. *Turkish Neurosurgery,* 6: 1-4.

BARNEA-GORALY N, KWON H, MENON V, ELIEZ S, LOTSPEICH L, REISS AL (2004) White matter structure in autism: preliminary evidence from diffusion tensor imaging. *Biol Psychiatry,* 55(3): 323-326.

CYPRIEN F, COURTET P, MALAFOSSE A, MALLER J, MESLIN C, BONAFE A, LE BARS E, DE CHAMPFLEUR NM, RITCHIE K, ARTERO S (2011) Suicidal behavior is associated with reduced corpus callosum area. *Biol Psychiatry*, 70(4): 320-326.

DELACOSTE-UTAMSING C, HOLLOWAY RL (1982) Sexual dimorphism in the human corpus callosum. *Science,* 216(4553): 1431-1432.

DOWNHILL JE JR, BUCHSBAUM MS, WEI T, SPIEGEL-COHEN J, HAZLETT EA, HAZNEDAR MM, SILVERMAN J, SIEVER LJ (2000) Shape and size of the corpus callosum in schizophrenia and schizotypal personality disorder. *Schizophr Res,* 42(3): 193-208.

GAREL C, CONT I, ALBERTI C, JOSSERAND E, MOUTARD ML, DUCOU LE POINTE H (2011) Biometry of the corpus callosum in children: MR imaging reference data. *AJNR Am J Neuroradiol,* 32(8): 1436-1443.

GRIFFITHS PD, BATTY R, REEVES MJ, CONNOLLY DJ (2009) Imaging the corpus callosum, septum pellucidum and fornix in children: normal anatomy and variations of normality. *Neuroradiology,* 51(5): 337-345.

GUPTA T, SINGH B, KAPOOR K, GUPTA M,

KOCHHAR S (2008) Age and sex related variations in corpus callosal morphology. *Nepal Med Coll J,* 10(4): 215-221.

GUZ W, PAZDAN D, STACHYRA S, SWIETON F, PORĘBA P, BEDNARZ M, LIS A, KAZAŃSKA A, KRUKOWSKA J, KLĘBA J, URBANIK A (2019) Analysis of corpus callosum size depending on age and sex. *Folia Morphol,* 78(1): 24-32.

HWANG SJ, JI EK, LEE EK, KIM YM, SHIN DY, CHEON YH, RHYU IJ (2004) Gender differences in the corpus callosum of neonates. *Neuroreport,* 15(6): 1029-1032.

JOU RJ, JACKOWSKI AP, PAPADEMETRIS X, RAJEEVAN N, STAIB LH, VOLKMAR FR (2011) Diffusion tensor imaging in autism spectrum disorders: preliminary evidence of abnormal neural connectivity. *Aust N Z J Psychiatry,* 45(2): 153-162.

LUDERS E, THOMPSON PM, TOGA AW (2010) The development of the corpus callosum in the healthy human brain. *J Neurosci,* 30(33): 10985-10990.

MOELLER FG, HASAN KM, STEINBERG JL, KRAMER LA, DOUGHERTY DM, SANTOS RM, VALDES I, SWANN AC, BARRATT ES, NARAYANA PA (2005) Reduced anterior corpus callosum white matter integrity is related to increased impulsivity and reduced discriminability in cocaine-dependent subjects: diffusion tensor imaging. *Neuropsychopharmacology,* 30(3): 610-617.

MOHAMMADI MR, ZHAND P, MORTAZAVI MOGHADAM B, GOLALIPOUR MJ (2011) Measurement of the corpus callosum using magnetic resonance imaging in the north of iran. *Iran J Radiol,* 8(4): 218-223.

MOURGELA S, ANAGNOSTOPOULOU S, SAKELLAROPOULOS A, GOULIAMOS A (2007) An MRI study of sex- and age-related differences in the dimensions of the corpus callosum and brain. *Neuroanatomy,* 6(1): 63-65.

NOSARTI C, RUSHE TM, WOODRUFF PW, STEWART AL, RIFKIN L, MURRAY RM (2004) Corpus callosum size and very preterm birth: relationship to neuropsychological outcome. *Brain,* 127(Pt 9): 2080-2089.

PASHAJ S, MERZ E, WELLEK S (2013) Biometry of the fetal corpus callosum by three-dimensional ultrasound. *Ultrasound Obstet. Gynecol,* 42(6): 691-698.

SCHMIED A, SODA S, GERIG G, STYNER M, SWANSON MR, ELISON JT, SHEN MD, MCKINSTRY RC, PRUETT JR JR, BOTTERON KN, ESTES AM, DAGER SR, HAZLETT HC, SCHULTZ RT, PIVEN J, WOLFF JJ (2020) Sex differences associated with corpus callosum development in human infants: A longitudinal multimodal imaging study. *Neuroimage,* 215: 116821.

SUGANTHY J, RAGHURAM L, ANTONISAMY B, VETTIVEL S, MADHAVI C, KOSHI R (2003) Gender- and age-related differences in the morphology of the corpus callosum. *Clin Anat,* 16(5): 396-403.

TAKEDA S, HIRASHIMA Y, IKEDA H, YAMAMOTO H, SUGINO M, ENDO S (2003) Determination of indices of the corpus callosum associated with normal aging in Japanese individuals. *Neuroradiology,* 45(8): 513-518.

TANAKA-ARAKAWA MM, MATSUI M, TANAKA C, UEMATSU A, UDA S, MIURA K, SAKAI T, NOGUCHI K (2015) Developmental changes in the corpus callosum from infancy to early adulthood: a structural magnetic resonance imaging study. *PLoS One,* 10(3): e0118760.

TEICHER MH, DUMONT NL, ITO Y, VAITUZIS C, GIEDD JN, ANDERSEN SL (2004) Childhood neglect is associated with reduced corpus callosum area. *Biol Psychiatry,* 56(2): 80-85.

UNLU E, BAGCIOGLU E, ACAY MB, KACAR E, TURAMANLAR O, GONUL Y, CEVIK M, AKPINAR A, COSKUN KS (2014) Magnetic resonance imaging study of corpus callosum abnormalities in patients with different subtypes of schizophrenia. *S Afr J Psychiatr,* 20(4): 146-152.

VANNUCCI RC, BARRON TF, VANNUCCI SJ (2017) Development of the corpus callosum: an MRI study. *Dev Neuroscience,* 39(1-4): 97-106.

WALTERFANG M, WOOD AG, BARTON S, VELAKOULIS D, CHEN J, REUTENS DC, KEMPTON MJ, HALDANE M, PANTELIS C, FRANGOU S (2009) Corpus callosum size and shape alterations in individuals with bipolar disorder and their first-degree relatives. *Prog Neuropsychopharmacol Biol Psychiatry,* 33(6): 1050-1057.

WESTERHAUSEN R, KOMPUS K, DRAMSDAHL

M, FALKENBERG LE, GRÜNER R, HJELMERVIK H, SPECHT K, PLESSEN K, HUGDAHL K (2011) A critical re-examination of sexual dimorphism in the corpus callosum microstructure. *Neuroimage,* 56(3): 874-880.

WESTERHAUSEN R, KREUDER F, DOS SANTOS SEQUEIRA S, WALTER C, WOERNER W, WITTLING RA, SCHWEIGER E, WITTLING W (2004) Effects of handedness and gender on macro- and microstructure of the corpus callosum and its subregions: a combined high-resolution and diffusion-tensor MRI study. *Brain Res Cogn Brain Res,* 21(3): 418-426.

WOLDEHAWARIAT G, MARTINEZ PE, HAUSER P, HOOVER DM, DREVETS WW, MCMAHON FJ (2014) Corpus callosum size is highly heritable in humans, and may reflect distinct genetic influences on ventral and rostral regions. *PLoS One,* 9(6): e99980.

YASIN M, FARAHANI RM (2015) Corpus callosum size, is there a sexual difference. *Int J Morphol,* 33(1): 96-99.

Morphological and molecular effects of trace metals on parenchymatous organs of diabetic rat model

Ahmed S. Ahmed

Anatomy and Embryology Department, College of Medicine, Tanta University, Tanta 31511, Egypt

SUMMARY

Trace metals are naturally materials found in water, earth crust and rocks, making the exposure rate to these metals is high affecting vital organs of the body. Diabetes is an endocrinal disease that can also affect many body organs by its oxidative stress like action. The present study was conducted to examine the effect of various trace metals on some parenchymatous organs in a diabetic and non-diabetic rat model. 120 Albino Wistar rats were used, and diabetes was induced in 60 rats. All rats were divided into twelve groups. All of them received trace metals for 4 weeks, except the control groups. At the end of the study, samples from blood (for biochemical analysis), heart, pancreas, liver, kidney and spleen (for histopathological and gene expression analysis) were collected. All trace-metal-treated groups showed histopathological insult and functional disability. The extent of injury was extensive in diabetic groups if compared to non-diabetic groups. The genetic expression analysis showed increase in apoptotic genes CASP-3 and a marked decrease of anti-apoptotic genes BCL-2. The present study showed that trace metals are highly toxic to various organs of the body even in low concentration. The diabetic rats are more susceptible to trace-metal-induced cellular damage through gene-mediated pathway. CASP-3 gene plays an important role in trace-metal-associated tissue injury. The present study showed that cadmium affects mainly hepatic and splenic tissues. Chromium, arsenic and thallium affect mainly the kidney, heart and pancreas respectively.

Key words: Trace metals – Parenchymatous organs – Apoptosis – CASP-3 – BCL-2

INTRODUCTION

Diabetes mellitus (DM) is an endocrinal disorder characterized by a sustained elevation of blood glucose level, if uncontrolled, it can cause cardiovascular, renal and hepatic complications due to its effect on microvasculature. As estimated in 2017, 450 million people are affected with diabetes. World health organization (WHO) reported that diabetes causes about six million deaths per year (Piepoli et al., 2016). Economically speaking, diabetes-related expenditures in 2019 exceeded one billion dollars. The average cost of diabetic patients is three-fold nondiabetic personnel (Ashrafzadeh and Hamdy, 2019). Its classic symptoms include polyuria, polyphagia and polydipsia, together with symptoms of multi-organ complications. Diabetes affect the cardiovascular system and it doubles the risk of cardiovascular complications (Bettencourt-Silva et al., 2019). It affects small blood vessels of the eye, brain, kidney and the peripheral nervous system, causing blindness, stroke, nephropathy and peripheral neuropathy respectively (Westerberg, 2013). The main cause of diabetes is insulin

Corresponding author:
Ahmed S. Ahmed. 13 Al-Bahr street, Tanta (31511), Gharbia, Egypt.
E-mail: Ahmedsahmed.tanta@gmail.com

Submitted: May 7, 2020. **Accepted:** October 1, 2020

deficiency or insulin resistance, which result in glucose accumulation in the blood stream causing glycosuria, followed by polyuria (Gilardi et al., 2019).

Trace metal is an expression used to describe any metallic compound that is toxic in low concentrations and has high atomic weight, e.g., mercury, thallium, cadmium, chromium and arsenic (all have density more than 5 gm/cm^3). These are found in water in very limited concentrations; if their concentration crosses specific limits, they can cause cardiac and renal complications (Hwang et al., 2018).

Mercury (Hg) is one of the trace metals discovered by ancient Egyptians in 1500 BC. Historically, mercury chloride was used as a diuretic and disinfectant, as well as in syphilis treatment. It is still used in thermometers, barometers, sphygmomanometers, fluorescent light lamps and in the cosmetics industry (Kern et al., 2016) In some developing countries it is also still used in dentistry in the form of metal mixture amalgam (Andreoli and Sprovieri, 2017). Other modes of exposure include Hg toxicity during wars, as Hg is used in explosives production, or by eating fish like shellfish or tuna, which can store considerable amount of mercury (Bose-O'Reilly et al., 2017). Some water-soluble forms of Hg are present such as methylmercury, which can cause toxicity if ingested (Siblerud et al., 2019). It can be absorbed through the skin, the gastrointestinal mucous membrane and olfactory mucous membrane if mercury vapors are inhaled or during tobacco smoking (El-Badry et al., 2018). It is extremely toxic and can damage the central nervous system, kidneys, liver, lungs and other organs. The toxic effect is dose related (Vianna et al., 2019).

Thallium (Ti) is a trace metal discovered in 1861. It is used in pharmaceutical, cosmetics and glass industries, and also as a (tasteless) poison. Medically, it is used in cardiographs to examine the coronaries and the state of heart revascularization after graft surgeries. It is absorbed readily by the skin and the mucous membrane of either the gastrointestinal or respiratory tracts (Campanella et al., 2019). Cadmium (Cd) is a silvery, white and solid trace element. Discovered in 1817 in Germany. It is commonly used in batteries, pigments, the electric industry, television screen manufacturing, anticancer drugs, laser emission and immunofluorescent microscopes. It can cause cellular oxidative stress. Intoxication of cadmium can be caused by inhalation of fertilizers causing pulmonary edema (Wu et al., 2019).

Chromium (Cr) is the most abundant trace metal in the earth crust and rocks, discovered in 1797. It is used in pigment manufacturing and as a metal surface coating. In laboratories, it is used to clean glass containers (Them et al., 2018). Arsenic (As) is one of the oldest trace metals: discovered in 815 AD, it was described by the Arab chemist Jabir Ibn Haiyan. It is used in wood preservation, insecticides and in rat poisons. It is highly soluble and easily absorbed. Historically it was used in syphilis treatment and as an antibiotic (Karbowska, 2016).

All previously mentioned trace metals cause cellular stress through oxidative stress and ignition of cellular apoptosis. The programmed cell death [apoptosis] is regulated by genetic factors such as CASP-3 [apoptotic gene] and BCL-2 [anti-apoptotic gene] (Beyaert et al., 1997). Thus, the present work is designed to examine the effect of trace metals (Hg, Ti, Cd, Cr, As) on apoptosis-regulating genes (CASP-3, BCL-2) in diabetic and non-diabetic albino rats. The current study will also examine the effect of trace metals' toxicity on both the function and histological structure of the liver, heart, kidney, pancreas and spleen.

MATERIALS AND METHODS

Chemicals

20 gm of mercury Bi-chloride, 95% (HgCl2), 20 gm of thallium Bi-chloride, 95% (TiCl2), 20 gm of cadmium Bi-chloride, 95% (CdCl2), 20 gm of chromium Bi-chloride, 95% (CrCl2) and 20 gm of arsenic Tri-chloride, 95% (AsCl3) were purchased from Sino pharm Chemical Reagent Co., Ltd. (Shanghai Shi, China).

Animals

One hundred and twenty albino Wistar rats were used, with an average weight of 200 gm and an average age of 6 months. Animals were housed individually. Free access to food and water was allowed. A 12-hour light/dark cycle was kept. By the help of air conditions, the temperature was kept at

25ºC (in accordance to national and institutional guidelines). This research study was approved by the Research and Ethics Committee, Quality Assurance Unit, Faculty of Medicine, Tanta University, Egypt.

Experimental design

Diabetes was induced by injecting streptozotocin 40mg/kg b.w., one-week later, blood glucose level was measured. Rat is considered diabetic if blood glucose level > 300 mg/dl. Rats were divided into twelve groups (n=10), Group I, control nondiabetic, Group II, Hg-nondiabetic, Group III, Ti-nondiabetic , Group IV, Cd-nondiabetic, Group V, Cr-nondiabetic Group VI, As-nondiabetic, Group VII, diabetic, Group VIII, Hg-diabetic, Group IX, Ti-diabetic, Group X, Cd-diabetic, Group XI, Cr-diabetic, Group XII, As-diabetic.

All groups (except Group I and Group VII) received intraperitoneal injection of the respective trace metal salt 20 mg/kg b.w. twice weekly for four weeks. Group I and VII received intraperitoneal saline injection instead. At day 30, all rats were sacrificed, blood from heart chambers was collected, serum was separated by centrifugation (4000 rpm) and kept at -30ºC for biochemical studies. Heart, kidney, liver, pancreas and spleen samples were collected and further divided into two groups. The first group of organs was fixed in 10% neural buffered formaldehyde, dehydrated, embedded in paraffine, then sectioned at 5 µm and stained with hematoxylin and eosin. The second group was homogenized and centrifuged for gene expression analysis using reverse transcriptase PCR (Pawłowska et al., 2017).

Histopathological examinations

Fresh tissue samples were cut into cubes (1 cm^3), placed in fixative 10% paraformaldehyde solution, immersed in paraffine blocks, sectioned into 5 µm thick sections using CUT 4050 Microtome (Laborgeräte Microtec, Germany), and finally stained with hematoxylin and eosin. Histopathological examinations were performed by two histopathologists blinded to present study.

Biochemical analysis

Serum was analyzed for blood urea, creatine, Aspartate Aminotransferase of liver (ASTL), Alanine Transaminase of liver (ALTL), random blood glucose, bilirubin and total cholesterol (Kits were purchased from Sino pharm Chemical Reagent Co.,)

Gene analysis

Following sacrificing rats, the heart, kidney, liver, pancreas and spleen tissues were harvested for gene expression analysis. RNA from tissues was extracted using Trizol reagent (Invitrogen, USA) and quantified with an ND-1000 spectrophotometer (NanoDrop Technologies, USA). cDNA was synthesized from 1 µg RNA with the Revert Aid H-Minus first-strand cDNA synthesis kit (Invitrogen, USA) as the manufacturer's protocol. The qRT-PCR analysis of all heavy-metal-treated groups, as well as the non-diabetic untreated control group, was carried out for Caspase-3 (apoptotic gene) and Bcl2 (anti-apoptotic gene) using Maxima SYBR Green qPCR Master Mix (Fermentas, USA) according to the manufacturer's protocol and run on PikoReal 96 real-time PCR (Thermo Scientific, USA). The relative gene expression analysis was performed by using PikoReal software (Thermo Scientific). β-actin was used for normalization. Note: Caspase-3; forward primer: 5′-GGA CAG CAG TTA CAA AAT GGA TTA-3′, reverse primer: 5′-GTCGATGCAGTCTCAGCTCTCA-3. Bcl2; forward primer: 5′-AAG CCG GCG ACG ACT TCT-3′, reverse primer: 5′-GCCTACTCCTCAGTCTCT TC-3′.

β-actin; forward primer: 5′-GCTGCCTGCT-GACTAGT AT-3′, reverse primer: 5′-CGTGTGTAT-GCTCTGACTAC-3′. PCR conditions were [initial denaturation at 96 °C (four min.), then forty cycles of 96 °C (twenty sec.), 63 °C (thirty sec.), and 72 °C (thirty sec.)

Statistical analysis

Statistical Package for Social Sciences (SPSS) software, 20 V. (SPSS Inc., USA) was used for data analysis. The statistical significance of differences between groups was validated using one-way analysis of variance (ANOVA). Post hoc Scheffe's procedure was used for groups comparison. Data were expressed in mean ± standard deviation and probability value was considered significant if <0.05.

RESULTS

Heart

On examination of hematoxylin- and eosin-stained heart sections, the control group (G-I) showed normal histological architecture, normal cardiac myofibril with large prominent nuclei with clear intercalated discs with no capillary congestion. The diabetic group (G-VII) showed moderate tissue fibrosis, necrosis and cytoplasmic vacuolations. Trace-metal-treated nondiabetic groups (G-II, III, IV, V, VI) showed cytoplasmic vacuolation of cardiomyocytes, the nuclei appear small and pyknotic with necrotic cardiac myofibrils (Fig. 1). These histopathological chances become more extensive in trace-metal-treated diabetic groups (G-VIII-XII) congestion of small blood vessels and capillaries (Fig. 1). The extensive damage appears in As-diabetic group (G-XII) was also confirmed by statistically significant ($p < 0.05$) increased CASP-3 and decreased BCL-2 expression. The fluctuation of expression become more extensive in diabetic trace-metal-treated groups (G-VIII-XII) if compared to non-diabetic trace-metal-treated groups (G-II-VI) (Fig. 2).

Kidney

Hematoxylin- and eosin-stained kidney sections showed that the control group (G-I) revealed normal glomeruli. Tubular lining epithelium appears healthy with prominent nuclei with no cytoplasmic vacuolations. Tubular degeneration appears in the diabetic group (G-VII). Trace-metal-treated groups either diabetic (more extensive) or nondiabetic, showed cytoplasmic vacuolation, edema, small pyknotic nuclei and congested blood vessels (Fig. 3). The gene expression analysis of the kidney tissue showed that the chromium-treated (diabetic) group (G-XI) scored the highest value for CASP-3 expression and the lowest value for BCL-2 expression (Fig. 4). While the rest of trace-metal-treated groups showed relative fluctuation of apoptotic and anti-apoptotic genes in favor of the apoptotic gene (CASP-3) if compared to control group (G-I). After trace metal administration, the biochemical analysis revealed a statistically significant ($p < 0.05$) increase in blood urea and creatinine either in diabetic or non-diabetic (Fig. 5): the highest value was recorded also in chromium treated group (diabetic)(G-XI), which emphasizes the histopathological findings.

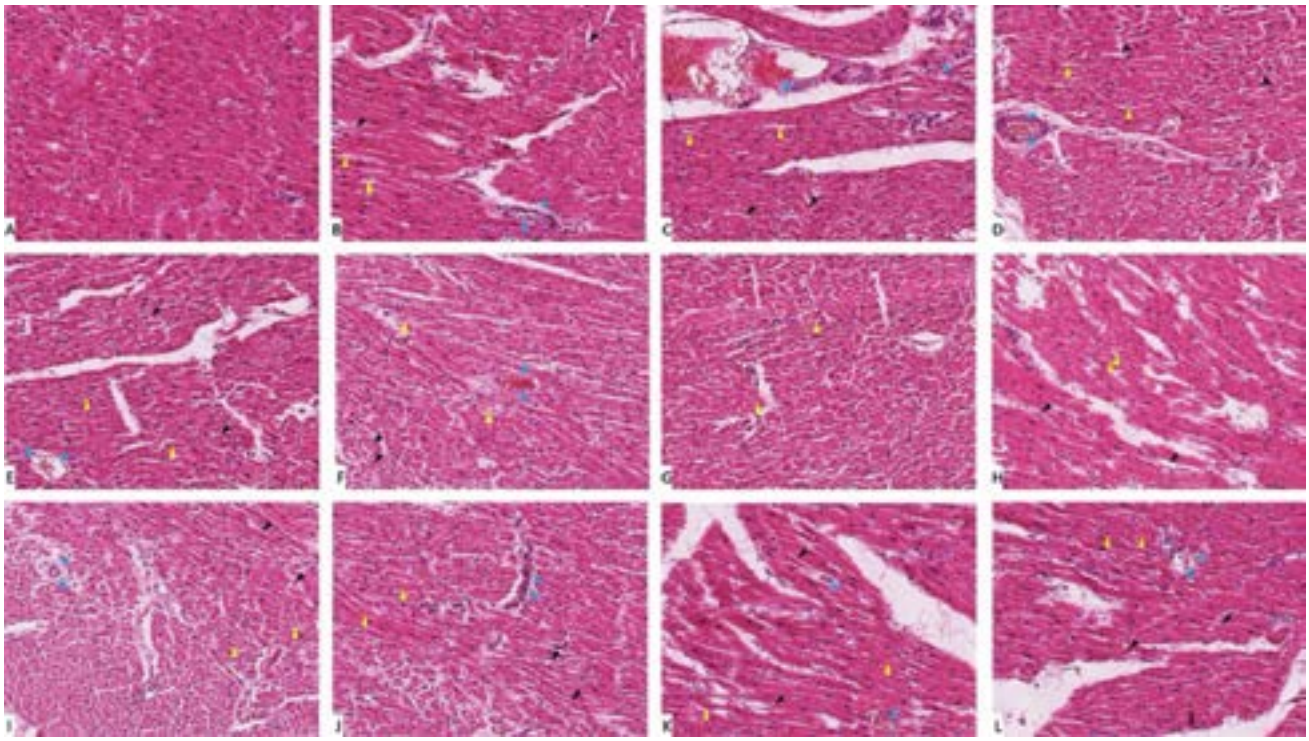

Fig. 1.- Heart tissue sections stained with hematoxylin and eosin (X 1000). (**A**) group I showed normal histological features. (**B, C, D, E and F**) **r**epresent nondiabetic groups treated with trace metals, group II, III, IV, V and VI, respectively. (G) represent diabetic non treated group VII. (**H, I, J, K and L**) represent diabetic groups treated with trace metals, group VIII, IX, X, XI and XII, respectively. Vacuolations are pointed at by yellow arrow, while degeneration and congestion are pointed into by black and blue arrows respectively.

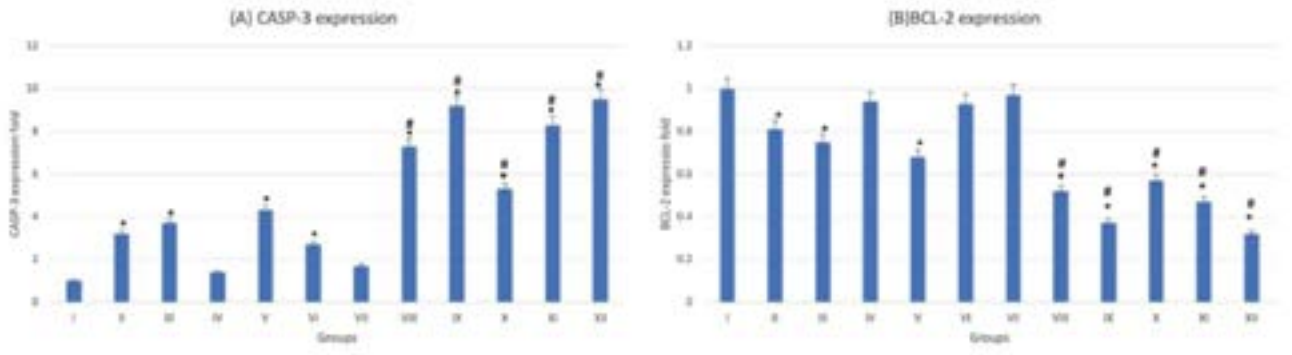

Fig. 2.- Gene expression analysis of the heart tissue of groups I-XII. **(A)** represent CASP-3. **(B)** represent BCL-2. * statistically significant ($p < 0.05$) difference in comparison to I-group. # statistically significant ($p < 0.05$) difference in comparison to VII-group. Data are presented as mean ± standard deviation, (n=10).

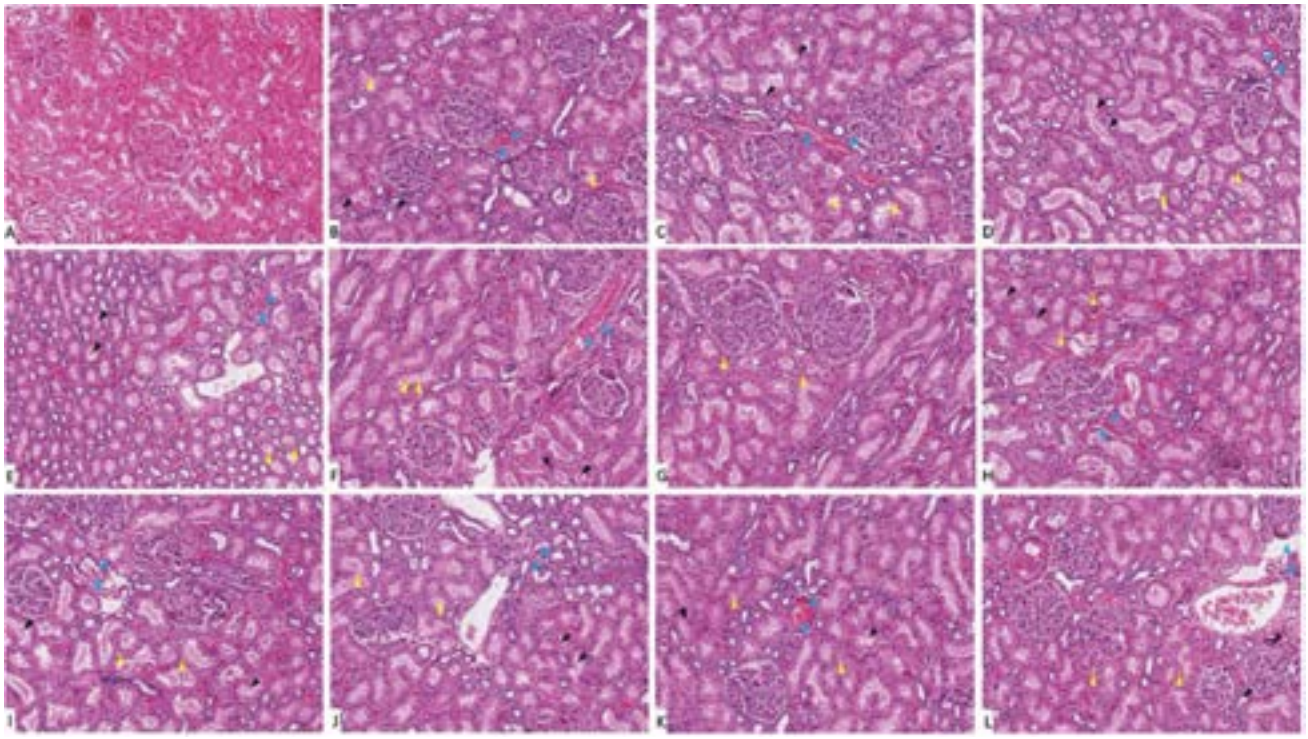

Fig. 3.- Kidney tissue sections stained with hematoxylin and eosin (X 1000). **(A)** Group I, showed normal histological features. **(B, C, D, E and F) r***epresent groups II, III, IV, V and VI, respectively.* **(G)** represent diabetic non treated group VII. **(H, I, J, K and L)** represent groups VIII, IX, X, XI and XII, respectively. Vacuolations are pointed into by yellow arrow, while degeneration and congestion are pointed into by black and blue arrows respectively.

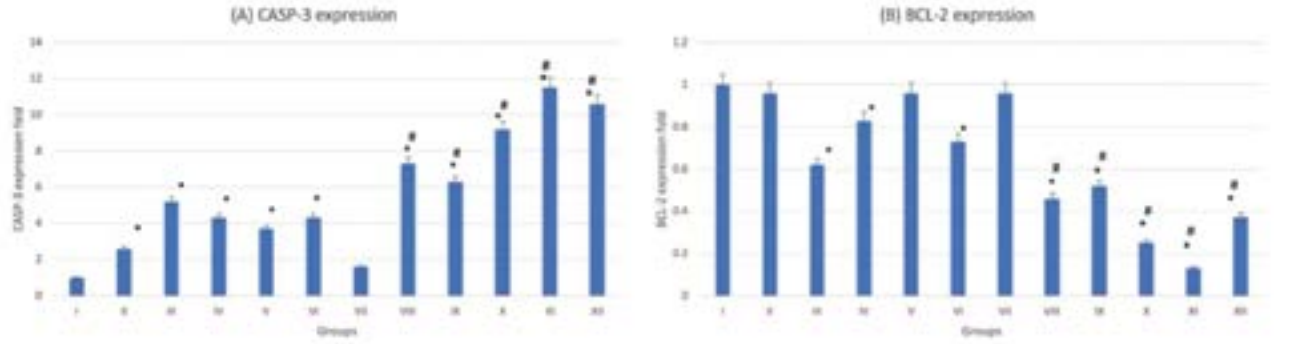

Fig. 4.- Gene expression analysis of the heart tissue of groups I-XII. **(A)** Represent CASP-3. **(B)** Represent BCL-2. * statistically significant ($p < 0.05$) difference in comparison to I-group. # statistically significant ($p < 0.05$) difference in comparison to VII-group. Data are presented as mean ± standard deviation, (n=10).

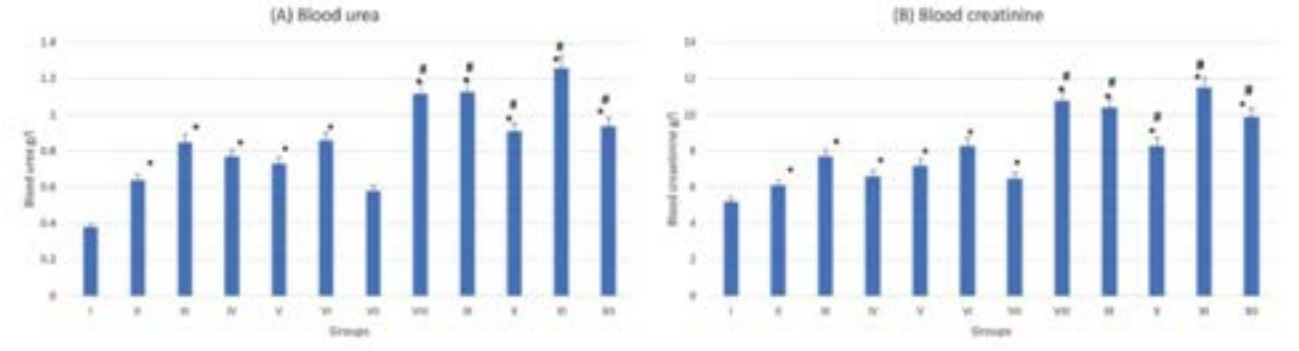

Fig. 5.- Kidney function tests of groups I-XII. **(A)** represent blood urea. **(B)** represent blood creatinine. * statistically significant ($p < 0.05$) difference in comparison to I-group. # statistically significant ($p < 0.05$) difference in comparison to VII-group. Data are presented as mean ± standard deviation, (n=10).

Liver

On examination of hematoxylin- and eosin-stained liver sections, normal histological architecture was noticed in the control group (G-I) with characteristic hexagonal structure of liver lobule. Hepatocytes diverge from the central vein towards the periphery of the lobule. Hepatocytes appear healthy with normal cytoplasm and large central nuclei. Cellular degeneration and necrosis appeared in the diabetic non-treated group (G-VII). On administration of trace metals, especially in the cadmium group (G-XI), vacuolation and inflammatory cells infiltration appears in liver sections. These changes appeared more in diabetic if compared to non-diabetic groups (Fig. 6). The gene expression analysis of CASP-3 and BCL-2 emphasizes the histopathological findings. In trace-metal-treated groups, [especially the cadmium group (G-X)] there was statistically significant ($p < 0.05$) increase in CASP-3 expression and decrease in BCL-2 expression (Fig. 7). Liver enzymes analysis (ASTL and ALTL) also emphasizes the histopathological findings denoting the functional affection of the liver after trace-metal administration in both diabetic and non-diabetic rats. The diabetic groups (trace metal treated) show more rise of enzymatic levels if compared to the non-diabetic (trace-metal-treated) groups (Fig. 8).

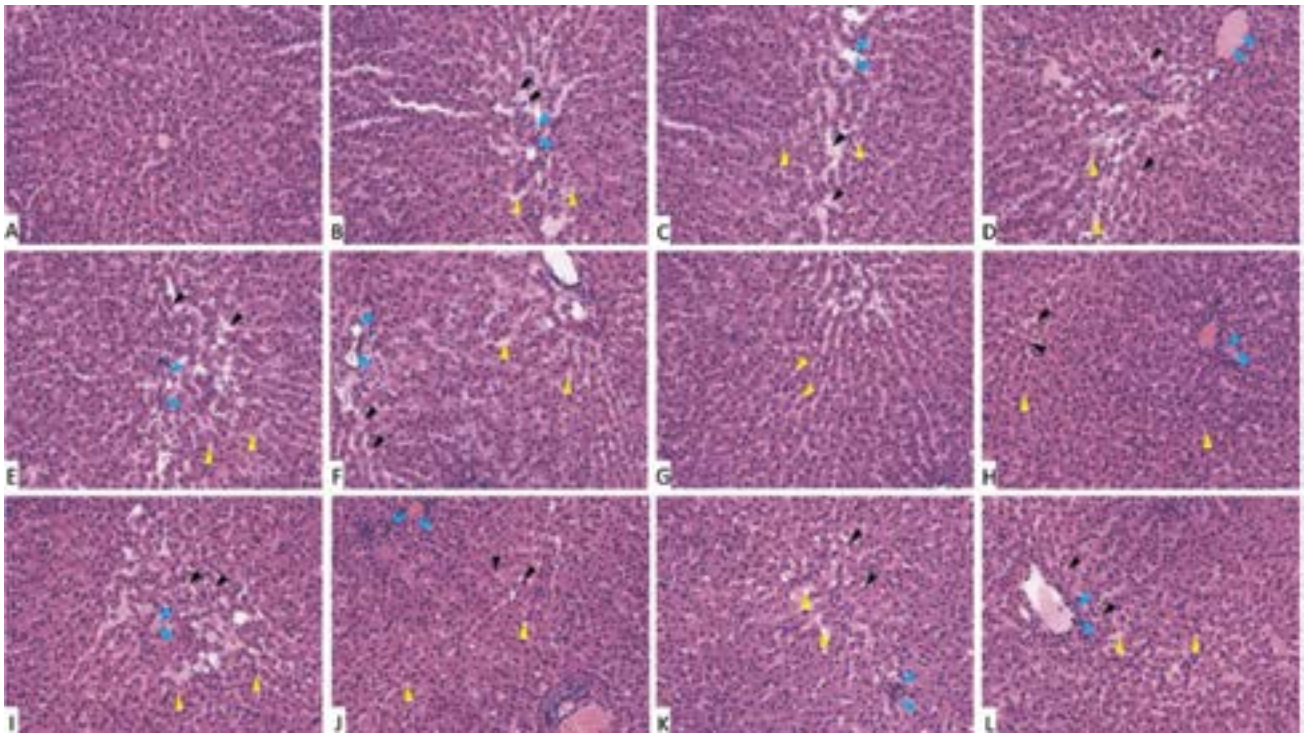

Fig. 6.- Liver tissue sections stained with hematoxylin and eosin (X 1000). (**A**) Group I showed normal histological features. (**B, C, D, E** and **F**) represent groups II, III, IV, V and VI, respectively. (**G**) represent diabetic non treated group VII. (**H, I, J, K** and **L**) represent groups VIII, IX, X, XI and XII, respectively. Vacuolations are pointed into by yellow arrow, while degeneration and congestion are pointed into by black and blue arrows respectively.

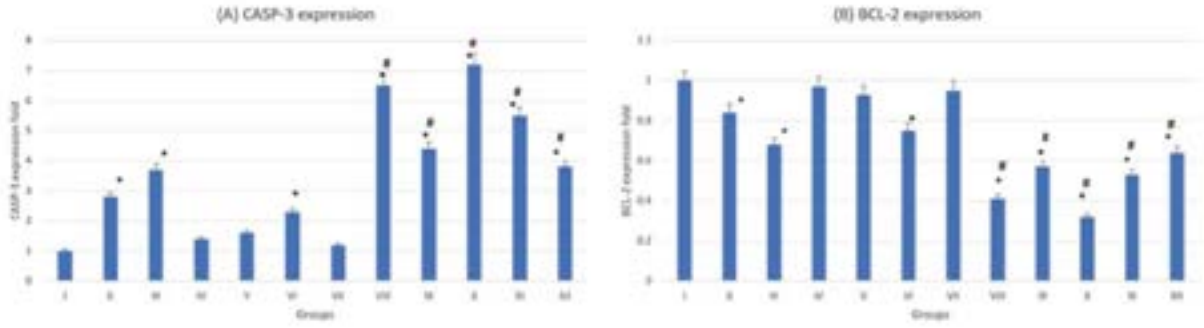

Fig. 7.- Gene expression analysis of the liver tissue of groups I-XII. (**A**) represent CASP-3. (**B**) represent BCL-2. * statistically significant ($p < 0.05$) difference in comparison to I-group. # statistically significant ($p < 0.05$) difference in comparison to VII-group. Data are presented as mean ± standard deviation, (n=10).

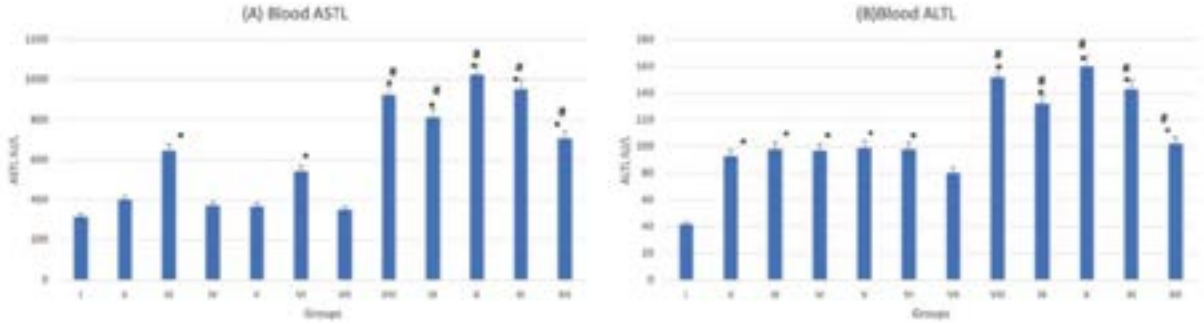

Fig. 8.- Liver function tests of groups I-XII. (**A**) Represent ASTL. (**B**) Represent ALTL. * statistically significant ($p < 0.05$) difference in comparison to I-group. # statistically significant ($p < 0.05$) difference in comparison to VII-group. Data are presented as mean ± standard deviation, (n=10).

Pancreas

Examination of stained pancreas sections showed that the control group (G-I) has normal histological architecture with healthy acini and islet of Langerhans. In the diabetic group (G-VII), the acinar cells appear swollen with small cytoplasmic vacuolations. Cells appear shrunken, degenerative and necrotic in G-II-VI. Histopathological changes were more intense in diabetic groups treated with trace metals (G-VIII-XII). The thallium group (G-IX) showed extensive histopathological changes if compared to the rest of trace-metal-related groups, either diabetic or non-diabetic (Fig. 9). The gene expression analysis of pancreatic tissue confirmed the histopathological changes, more fluctuation of CASP-3 and BCL-2-fold levels either by increase and decrease respectively (Fig. 10). Biochemical study of the serum showed that group (G-IX) (thallium related) recorded the highest blood glucose score. All other groups (with exclusion of the control group) recorded elevated blood glucose levels (Fig. 11).

Spleen

The histological examination of splenic sections showed normal histological architecture in control group (G-I). All diabetic and non-diabetic groups showed congestion of red pulp after administration of trace metals together with cell necrosis of white pulp. The cadmium-treated diabetic group (G-X) showed the most extensive tissue injury if compared to the rest of groups (Fig. 12). This was confirmed by gene expression done to the splenic tissue, which showed that the cadmium-related group (G-X) scored the highest CASP-3 level among other groups (Fig. 13). As an indicator for splenic function, serum analysis for both bilirubin and total cholesterol levels were performed, which appeared to decrease after trace-metal administration either in diabetic or non-diabetic groups (Fig. 14).

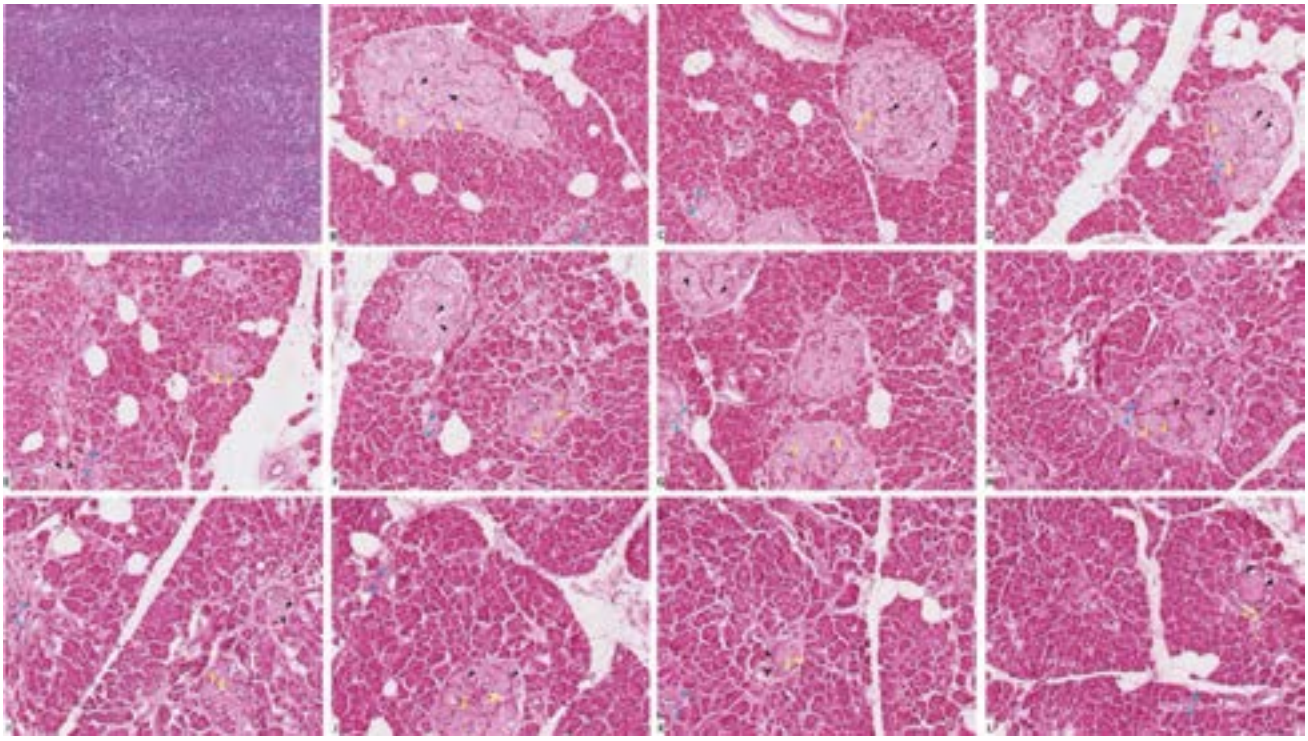

Fig. 9.- Pancreas tissue sections stained with hematoxylin and eosin (X 1000). (**A**) Group I showed normal histological features. (**B, C, D, E** and **F**) represent groups II, III, IV, V and VI, respectively. (**G**) represent diabetic non treated group VII. (**H, I, J, K** and **L**) represent groups VIII, IX, X, XI and XII, respectively. Vacuolations are pointed into by yellow arrow, while degeneration and congestion are pointed into by black and blue arrows respectively.

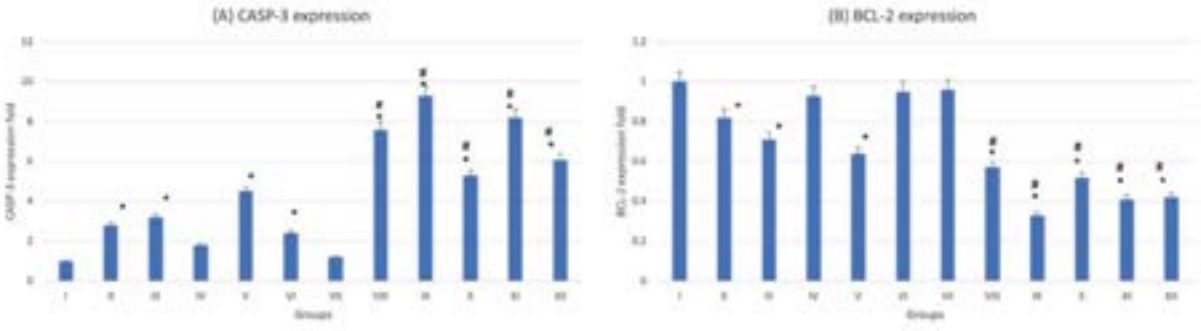

Fig. 10.- Gene expression analysis of the pancreatic tissue of groups I-XII. (**A**) represent CASP-3. (**B**) represent BCL-2. * statistically significant ($p < 0.05$) difference in comparison to I- group. # statistically significant ($p < 0.05$) difference in comparison to VII-group. Data are presented as mean ± standard deviation, (n=10).

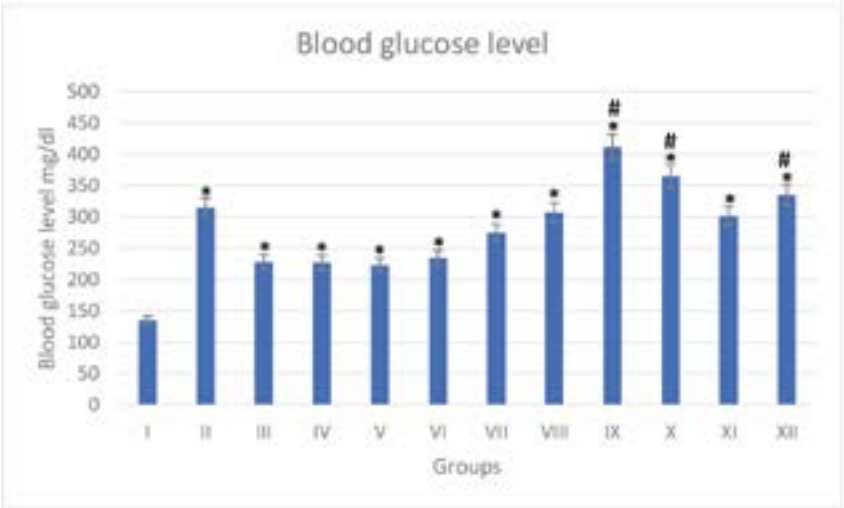

Fig. 11.- Blood glucose level of groups I-XII. * statistically significant ($p < 0.05$) difference in comparison to I-group. # statistically significant ($p < 0.05$) difference in comparison to VII- group. Data are presented as mean ± standard deviation, (n=10).

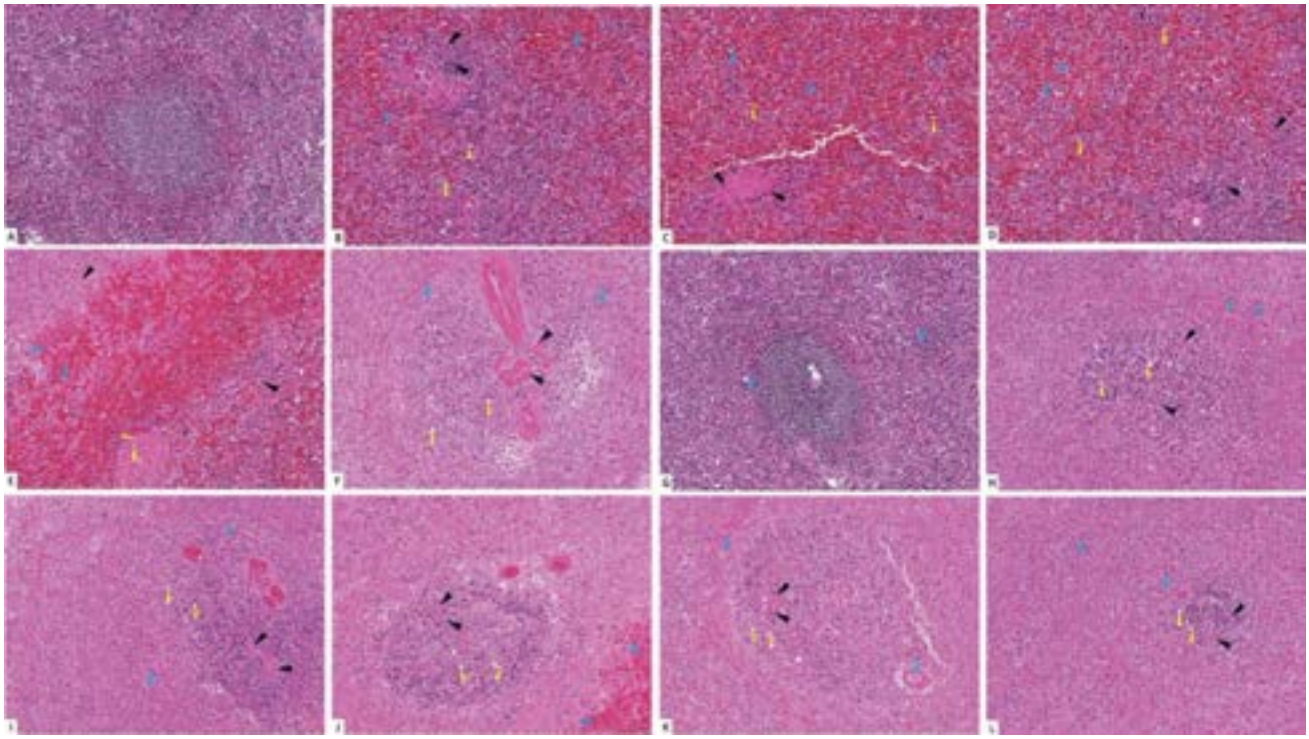

Fig. 12.- Splenic tissue sections stained with hematoxylin and eosin (X 1000). (**A**) Group I showed normal histological features. (**B, C, D, E** and **F**) represent groups II, III, IV, V and VI, respectively. (**G**) represent diabetic non treated group VII. (**H, I, J, K** and **L**) represent groups VIII, IX, X, XI and XII, respectively. Vacuolations are pointed into by yellow arrow, while degeneration and congestion are pointed into by black and blue arrows respectively.

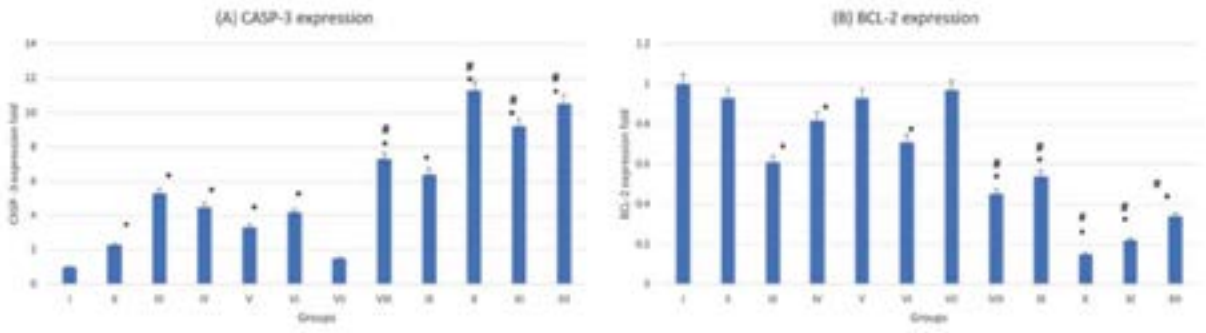

Fig. 13.- Gene expression analysis of the splenic tissue of groups I-XII. (**A**) represent CASP-3, (**B**) represent BCL-2. * statistically significant ($p < 0.05$) difference in comparison to I- group. # statistically significant ($p < 0.05$) difference in comparison to VII-group. Data are presented as mean ± standard deviation, (n=10).

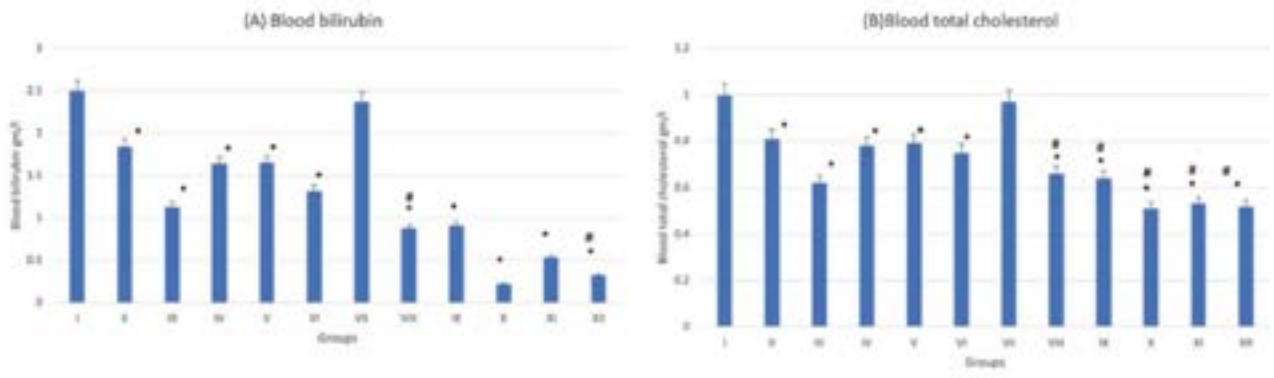

Fig. 14.- Spleen function indicators of groups I-XII. (**A**) represent blood bilirubin. (**B**) represent blood total cholesterol. * statistically significant ($p < 0.05$) difference in comparison to I-group. # statistically significant ($p < 0.05$) difference in comparison to VII-group. Data are presented as mean ± standard deviation, (n=10).

DISCUSSION

Trace metals are naturally found in sea water and earth crust, resulting in frequent exposure rate to these metals and affecting various organs of the body (Di et al., 1968). Diabetes is an endocrinal problem that can also affect many body organs (Sas-Nowosielska and Pawlas, 2015). The present study was conducted to compare between the effect of various trace metals in a diabetic and non-diabetic rat model.

Present results showed that Hg administration to non-diabetic rat groups caused cytoplasmic vacuolation of cardiomyocytes with small pyknotic nuclei and necrosis of cardiac myofibrils, which comes in agreement with Nyland et al. (2012), who reported myocarditis in a clinical case study of Hg toxicity. Other researchers (Ahn et al., 2018) reported that Hg can cause myocarditis. The changes noticed in non-diabetic rats become accentuated in diabetic groups with the appearance of congested blood vessels and capillaries, which was reported by other researchers that mercury causes cardiomyopathy and heart failure (Lombardi et al., 2016).

Gene expression analysis of the heart tissue showed increased expression of CASP-3 (apoptotic gene) while expression of BCL-2(anti-apoptotic gene) decreased after Hg administration in all rat groups, which collectively favor the apoptotic state of the heart in response to Hg: this comes in agreement with Tiexeira et al. (2016), who reported the apoptotic and toxic effect of mercury on the heart tissue. Ding et al. (2017) mentioned the increased level of mi-RNA 92 in mercury workers, which also favors apoptosis of cells. All these histological findings interfere with the normal function of the heart as stated by Furieri et al. (2011), who reported impaired contractile function of the heart as a result of Hg toxicity. The aortic endothelium as a component of cardiovascular system is also dysfunctional as mentioned by Ahmed and Maulood (2018) in case of Hg toxicity.

The cytoplasmic vacuolations and small pyknotic nuclei appeared also in the kidney tissue beside the congested capillaries of the glomeruli after Hg administration, while other researchers (Li et al., 2011) stated that Hg affect only kidney tubules with no effect on glomerular capillaries. Seno et al. (2013) added that Hg induced renal injury by inducing autoimmune state. Wang et al. (2015a) agreed with us in the glomerular engagement in the histopathological lesion as he noticed proliferation of mesangial zone of glomeruli. Other researchers (Langworth et al., 1992) agreed with Seno et al. (2013) and mentioned the increased serum antibodies after Hg administration, which result in renal tissue injury.

Our results revealed that the effect of Hg on diabetic rat kidneys is more extensive than the effect on non-diabetic rats, which comes in same page with other researchers (Cohen and Post, 2002), who added that diabetes affect kidney tissue and interferes with urine concentration function, making it more vulnerable to Hg toxic effects. The apoptotic state of the kidney, which was revealed in our research by the fluctuated level of CASP-3 and BCL-2 in favor of CASP-3, was also mentioned by other researchers (Wang et al., 2015b), who explained the apoptotic process which undergoes in the tubular epithelium. Woods et al. (2002) stated that Hg ameliorates NF-KAPPA B, increasing the liability of the renal tissue to apoptosis (Sutton and Tchounwou, 2007). The increased level of urea and creatinine after Hg administration indicate the impairment of kidney functions, which was reported by other researchers (Rojas-Franco et al., 2019) and emphasized our histopathological results of the kidney.

In our study, liver tissue showed cellular degeneration and necrosis together with inflammatory cells infiltration after Hg administration either in diabetic or non-diabetic rats' groups, which appeared as moderate and severe injury respectively. This comes in agreement with other researchers (Chandirasegaran et al., 2018). The increase in expression of CASP-3, which was evident in our results, comes in agreement with Yang et al. (2016), who stated that Hg increases production of reactive oxygen species and causes apoptosis to hepatic cells which is Hg dose dependent.

Lee et al. (2017) reported the relationship between blood mercury concentration and liver function deterioration, which was reported in our results as well. Present results showed that Hg

administration caused shrinkage of B-cells of the pancreas, which appeared with small pyknotic nuclei and cytoplasmic vacuolations: this finding was reported by other researchers (Śliwińska-Mossoń et al., 2018). Present results showed that Hg causes pancreatic inflammation and histological disturbance of both exocrinal and endocrinal components. Chen et al. (2012) reported that Hg increased the production of mi-RNA regulating caspase-3 and caspase-7 production, which comes in agreement with our findings that Hg increases the expression of apoptotic gene CASP-3 and decrease the expression of anti-apoptotic gene BCL-2.

The congested splenic red pulp with wide spread necrosis, which appeared in our results after mercury administrations in diabetic (more extensive pathology) and non-diabetic rats, comes in agreement with other researchers (Ghosh et al., 2018). The increase in expression of apoptotic genes was mentioned by other researchers (Barst et al., 2015), and the disturbed splenic function (immune related) was reported by other researchers (Gill et al., 2017), which comes in agreement with our results after examining splenic functions.

The effect of Ti on cardiac tissue, which appeared in our research, was reported by other researchers (Maublant et al., 1985). The extensive impact of Ti on diabetic rats' heart was explained by Lee and Kim (2017) by occurrence of metabolic disturbance and microvasculature dysfunction. The increase in CASP-3 gene expression recorded in our results was stated by Doue et al. (2008). The histopathological impact of Ti on kidney tissue appeared in our research was stated by (Atkins et al., 1977), who added that Ti is mainly concentrated in the heart, large intestine and kidney. Foster et al. (2012) stated that Ti intake affect mitochondrial functions of the renal tissue, which offer another explanation to the apoptosis rather than the increases expression of CASP-3 gene recorded in our results. In our study, Ti appeared to cause hepatocyte cytoplasmic vacuolation, degeneration and necrosis especially in diabetic group, which was reported by other researchers (Misiakiewicz-Has et al., 2019) who stated that fatty liver insult associated with diabetes mellitus (mainly type -2) makes the liver tissue more liable to the impact of Ti. Apoptosis of liver cells could be explained due to opposing expression of CASP-3 and BCL-2, while others (Abdel-Daim and Abdou, 2015) stated that Ti cause apoptosis by reactive oxygen species production.

The deterioration of liver functions appeared in our results, especially in diabetic rats, which was reported by Tae et al. (2014) who added that liver cirrhotic states associate Ti toxicity. In present results, Ti caused histopathological changes mainly in diabetic rats, which could be explained by effect of Ti on mitochondria and rough endoplasmic reticulum (Kizilgul et al., 2018). Also, the increase in expression of CASP-3 shown in other results comes in agreement with other researchers (Tekabe et al., 2012). The apoptotic effect of Ti on splenic tissue, which was manifest in our results, was also reported by other researchers (Vasamsetti et al., 2018). Inokuma et al. (1995) reported that high level of Ti tends to accumulate in pancreatic tissue which impacted our results as the pancreas was the most affected organ after Ti administration.

Results showed that Cd administration caused histopathological changes of the heart in the form of cytoplasmic vacuolations and nuclear pyknosis together with necrosis of the cardiac myofibrils, which was expressed more dramatically in the diabetic groups. Sarcomere disorganization and cardiac arrythmia was reported by Shen et al. (2018) as a result of Cd administration.

Present results showed the relationship between Cd administration and increased CASP-3 expression, which result in cardiomyocytes apoptosis. Nazimabashir et al. (2015) explained Cd-related apoptosis by the activation of Nrf2 apoptotic pathway. The histopathological insult caused by cadmium on both kidney and liver tissue expressed in our results together with increased apoptotic state was also reported by other researchers (Ranieri et al., 2019), who added that the extract of green olive leaf can ameliorate the effect of cadmium on kidney, and they explained apoptosis by the activation of mi-RNA 30 production.

Present results showed histopathological injury of the pancreas and increased expression of CASP-3 gene after Cd administration, especially in diabetic rats, which comes in agreement with other researchers (Śliwińska-Mossoń et al., 2019),

While the disturbed pancreatic function (showed in our result) after Cd administration was not in agreement with Trevino et al. (2015), who linked between the Cd administration and increased insulin secretion. Our results showed that Cd affects mainly the structure, apoptotic activity and function of liver and spleen, which was partially in agreement with Huo et al. (2017), who reported that liver and pancreas are mainly affected after Cd administration.

Cr administration to diabetic and non-diabetic rats, caused histopathological injury to the heart with an increase in CASP-3 gene expression, which comes in agreement with other researchers (Boşgelmez and Güvendik, 2019), who elaborated that Cr causes bradycardia in some patients. In our study the kidney reacted to Cr administration by showing disturbed histological architecture, increased apoptosis rate and disturbed renal functions either in diabetic or non-diabetic rats which was reported by other researchers (Venter et al., 2017), who showed that Cr binds to chromatin forcing its condensation mainly on the tubular lining epithelium cells, and reported the occurrence of proteinuria in Cr workers.

Present results showed cytoplasmic vacuolations and necrosis of hepatocytes, increase expression of CASP-3 gene and decrease of liver functions after Cr administration, which comes in agreement with other researchers (Yang et al., 2020), who reported disturbed histological architectures of the liver with disturbed hepatic enzymatic activity after Cr administration. Other researchers (Wang et al., 2017) reported the association between Cr and the histopathological and functional disturbance in the pancreas with increased apoptotic tendency (Same findings were reported in our results). In the present study Cr caused congested red pulp of spleen with cellular necrosis, increased expression of CASP-3 gene and disturbed splenic functions which comes in agreement with (Núñez et al., 2016). Our results showed that the kidney was the most sensitive organ to Cr administration on structural and functional levels, which was confirmed clinically by Filler and McIntyre (2019) in dialysis patients.

Present results showed that, in diabetic and non-diabetic rats, arsenic (As) administration caused histopathological disturbance and increased expression of CASP-3 gene in the heart tissue. The effect was extensive in diabetic groups if compared to non-diabetic group: this was in the same page with other researchers (Mateen et al., 2017). These histopathological and genetic disturbance was also noticed in the kidney in addition to disturbed function (Sanders et al., 2019). Our study showed that As caused histopathological findings in the liver, pancreas and spleen of non-diabetic rats; more histopathological injury was noticed in diabetic rats (Lu et al., 2019). As administration was associated with increased expression of apoptotic genes and decrease in anti-apoptotic gene expression (Jamal et al., 2020). Present results showed As mainly affected the heart of diabetic rats: this comes in agreement with Wei et al. (2018), who demonstrated the involvement of liver and kidney as well. In conclusion, the present study showed that trace metals are highly toxic to various organs of the body even with low concentration. The diabetic rats are more susceptible to trace-metal-induced cellular damage through gene mediated pathway. The organs insults include structural and functional dimensions. CASP-3 gene plays an important role in trace-metal-associated tissue injury. Cadmium affects mainly hepatic and splenic tissues. Chromium, arsenic and thallium affect mainly the kidney, heart and pancreas respectively.

REFERENCES

ABDEL-DAIM MM, ABDOU RH (2015) Protective effects of diallyl sulfide and curcumin separately against thallium-induced toxicity in rats. *Cell J,* 17(2): 379-388.

AHMED AH, MAULOOD IM (2018) The roles of potassium channels in contractile response to urotensin-II in mercury chloride induced endothelial dysfunction in rat aorta. *Iran J Vet Res*, 19(3): 208-216.

AHN H, KIM J, KANG SG, YOON S, KO H-J, KIM P-H, HONG E-J, AN B-S, LEE E, LEE G-S (2018) Mercury and arsenic attenuate canonical and non-canonical NLRP3 inflammasome activation. *Sci Rep*, 8(1): 13659.

ANDREOLI V, SPROVIERI F (2017) Genetic aspects of susceptibility to mercury toxicity: an overview. *Int J Environ Res Public Health*, 14(1): 93.

ASHRAFZADEH S, HAMDY O (2019) Patient-driven diabetes care of the future in the technology era. *Cell Metab*, 29(3): 564-575.

ATKINS HL, BUDINGER TF, LEBOWITZ E, ANSARI AN, GREENE MW, FAIRCHILD RG, ELLIS KJ (1977) Thallium-201 for medical use. Part 3: Human distribution and physical imaging properties. *J Nucl Med*, 18(2): 133-140.

BARST BD, BRIDGES K, KORBAS M, ROBERTS AP, VAN KIRK K, MCNEEL K, DREVNICK PE (2015) The role of melano-macrophage aggregates in the storage of mercury and other metals: an example from yelloweye rockfish (*Sebastes ruberrimus*). *Environ Toxicol Chem*, 34(8):1918-1925.

BETTENCOURT-SILVA R, AGUIAR B, SÁ-ARAÚJO V, BARREIRA R, GUEDES V, MARQUES RIBEIRO MJ, CARVALHO D, ÖSTLUNDH L, SILVA PAULO M (2019) Diabetes-related symptoms, acute complications and management of diabetes mellitus of patients who are receiving palliative care: a protocol for a systematic review. *BMJ Open*, 9(6): e028604.

BEYAERT R, KIDD VJ, CORNELIS S, VAN DE CRAEN M, DENECKER G, LAHTI JM, GURURAJAN R, VANDENABEELE P, FIERS W (1997) Cleavage of PITSLRE kinases by ICE/CASP-1 and CPP32/CASP-3 during apoptosis induced by tumor necrosis factor. *J Biol Chem*, 272(18): 11694-11697.

BOSE-O'REILLY S, BERNAUDAT L, SIEBERT U, ROIDER G, NOWAK D, DRASCH G (2017) Signs and symptoms of mercury-exposed gold miners. Int J Occup Med Environ Health, 30(2): 249-269.

BOŞGELMEZ Iİ, GÜVENDIK G (2019) Beneficial effects of N-acetyl-L-cysteine or taurine pre- or post- treatments in the heart, spleen, lung, and testis of hexavalent chromium-exposed mice. *Biol Trace Elem Res*, 190(2): 437-445.

CAMPANELLA B, COLOMBAIONI L, BENEDETTI E, DI CIAULA A, GHEZZI L, ONOR M, D'ORAZIO M, GIANNECCHINI R, PETRINI R, BRAMANTI E (2019) Toxicity of thallium at low doses: a review. *Int J Environ Res Public Health*, 16(23): 4732.

CHANDIRASEGARAN G, ELANCHEZHIYAN C, GHOSH K (2018) Effects of berberine chloride on the liver of streptozotocin-induced diabetes in albino Wistar rats. *Biomed Pharmacother*, 99: 227-236.

CHEN KL, LIU SH, SU CC, YEN CC, YANG CY, LEE KI, TANG FC, CHEN YW, LU TH, SU YC, HUANG CF (2012) Mercuric compounds induce pancreatic islets dysfunction and apoptosis in vivo. *Int J Mol Sci*, 13(10): 12349-12366.

COHEN M, POST GS (2002) Water transport in the kidney and nephrogenic diabetes insipidus. *J Vet Intern Med*, 16(5): 510-517.

DI LOLLO F, FAZZINI G, MORINI PL (1968) Diabete e complicanze encefaliche acute a genesi dismetabolica. Attuali aspetti patogenetici e fisiopatologici [Diabetes and acute dysmetabolic encephalic complications. Current pathogenetic and physiopathological aspects]. *Recenti Prog Med*, 44(2): 178-212.

DING E, GUO J, BAI Y, ZHANG H, LIU X, CAI W, ZHONG L, ZHU B (2017) MiR-92a and miR-486 are potential diagnostic biomarkers for mercury poisoning and jointly sustain NF-□B activity in mercury toxicity. *Sci Rep*, 7(1): 15980.

DOUE T, OHTSUKI K, OGAWA K, UEDA M, AZUMA A, SAJI H, STRAUSS HW, MATSUBARA H (2008) Cardioprotective effects of erythropoietin in rats subjected to ischemia-reperfusion injury: assessment of infarct size with 99mTc-annexin V. *J Nucl Med*, 49(10): 1694-1700.

EL-BADRY A, REZK M, EL-SAYED H (2018) Mercury-induced oxidative stress may adversely affect pregnancy outcome among dental staff: a cohort study. *Int J Occup Environ Med*, 9(3): 113-119.

FILLER G, MCINTYRE C (2019) Chromium: rise and shine in peritoneal dialysis patients? *Perit Dial Int*, 39(4): 320-322.

FOSTER DB, HO AS, RUCKER J, GARLID AO, CHEN L, SIDOR A, GARLID KD, O'ROURKE B (2012) Mitochondrial ROMK channel is a molecular component of mitoK(ATP). *Circ Res*, 111(4): 446-454.

FURIERI LB, FIORESI M, JUNIOR RF, BARTOLOMÉ MV, ARAÚJO FERNANDES A, CACHO-

FEIRO V, LAHERA V, SALAICES M, STEFANON I, VASSALLO DV (2011) Exposure to low mercury concentration in vivo impairs myocardial contractile function. *Toxicol Appl Pharmacol*, 255(2): 193-199.

GHOSH S, CHOWDHURY S, SARKAR P, SIL PC (2018) Ameliorative role of ferulic acid against diabetes associated oxidative stress induced spleen damage. *Food Chem Toxicol*, 118: 272-286.

GILARDI F, WINKLER C, QUIGNODON L, DISERENS JG, TOFFOLI B, SCHIFFRIN M, SARDELLA C, PREITNER F, DESVERGNE B (2019) Systemic PPARγ deletion in mice provokes lipoatrophy, organomegaly, severe type 2 diabetes and metabolic inflexibility. *Metabolism*, 95: 8-20.

GILL R, MCCABE MJ JR, ROSENSPIRE AJ (2017) Low level exposure to inorganic mercury interferes with B cell receptor signaling in transitional type 1 B cells. *Toxicol Appl Pharmacol*. 330: 22-29.

HUO J, DONG A, YAN J, WANG L, MA C, LEE S (2017) Cadmium toxicokinetics in the freshwater turtle, *Chinemys reevesii*. *Chemosphere*, 182: 392-398.

HWANG JS, DAHMS HU, HUANG KL, HUANG MY, LIU XJ, KHIM JS, WONG CK (2018) Bioaccumulation of trace metals in octocorals depends on age and tissue compartmentalization. *PLoS One*, 13(4): e0196222.

INOKUMA T, TAMAKI N, TORIZUKA T, FUJITA T, MAGATA Y, YONEKURA Y, OHSHIO G, IMAMURA M, KONISHI J (1995) Value of fluorine-18-fluorodeoxyglucose and thallium-201 in the detection of pancreatic cancer. *J Nucl Med*, 36(2): 229-235.

JAMAL Z, DAS J, GHOSH S, GUPTA A, CHATTOPADHYAY S, CHATTERJI U (2020) Arsenic-induced immunomodulatory effects disorient the survival-death interface by stabilizing the Hsp90/Beclin1 interaction. *Chemosphere*, 238: 124647.

KARBOWSKA B (2016) Presence of thallium in the environment: sources of contaminations, distribution and monitoring methods. *Environ Monit Assess*, 188(11): 640.

KERN JK, GEIER DA, SYKES LK, HALEY BE, GEIER MR (2016) The relationship between mercury and autism: A comprehensive review and discussion. *J Trace Elem Med Biol*, 37: 8-24.

KIZILGUL M, WILHELM JJ, BEILMAN GJ, CHINNAKOTLA S, DUNN TB, PRUETT TL, ABDULLA M, HELLER D, FREEMAN ML, SCHWARZENBERG SJ, HERING BJ, BELLIN MD (2018) Effect of intrapancreatic fat on diabetes outcomes after total pancreatectomy with islet autotransplantation. *J Diabetes*, 10(4): 286-295.

LANGWORTH S, ELINDER CG, SUNDQUIST KG, VESTERBERG O (1992) Renal and immunological effects of occupational exposure to inorganic mercury. Br J Ind Med, 49(6): 394-401.

LEE MR, LIM YH, LEE BE, HONG YC (2017) Blood mercury concentrations are associated with decline in liver function in an elderly population: a panel study. *Environ Health*, 16(1): 17.

LEE WS, KIM J (2017) Diabetic cardiomyopathy: where we are and where we are going. *Korean J Intern Med*, 32(3): 404-421.

LI SJ, ZHANG SH, CHEN HP, ZENG CH, ZHENG CX, LI LS, LIU ZH (2010) Mercury-induced membranous nephropathy: clinical and pathological features. *Clin J Am Soc Nephrol*, 5(3): 439-444.

LOMBARDI C, SPIGONI V, GORGA E, DEI CAS A (2016) Novel insight into the dangerous connection between diabetes and heart failure. *Herz*, 41(3): 201-207.

LU P, MA JQ, LI F, XU GH, GUO W, ZHOU HM (2019) A fatal case of acute arsenic poisoning. *J Forensic Sci*, 64(4): 1271-1273.

MATEEN FJ, GRAU-PEREZ M, POLLAK JS, MOON KA, HOWARD BV, UMANS JG, BEST LG, FRANCESCONI KA, GOESSLER W, CRAINICEANU C, GUALLAR E, DEVEREUX RB, ROMAN MJ, NAVAS-ACIEN A (2017) Chronic arsenic exposure and risk of carotid artery disease: The strong heart study. *Environ Res*, 157: 127-134.

MAUBLANT JC, MOINS N, GACHON P, ROSS MR, DAVIDSON WD, MENA I (1985) Effects of grisorixin on the distribution of thallium-201 and on the oxidative metabolism in cultured myocardial cells. *J Nucl Med*, 26(6): 626-629.

MISIAKIEWICZ-HAS K, MACIEJEWSKA D, KOLASA-WOŁOSIUK A, PILUTIN A, RZESZOTEK S, WILK A, SZYPULSKA-KOZIARSKA D, STACHOWSKA E, ŁUKOMSKA A, WISZNIEWSKA B (2019)

Modulatory effect of inulin with soya isoflavones on plasma lipid profile and liver SCD-18 index in rats with induced type-2 diabetes mellitus. *Histol Histopathol*, 34(10): 1131-1140.

NAZIMABASHIR, MANOHARAN V, MILTONPRABU S (2015) Cadmium induced cardiac oxidative stress in rats and its attenuation by GSP through the activation of Nrf2 signaling pathway. *Chem Biol Interact*, 242: 179-193.

NÚÑEZ O, FERNÁNDEZ-NAVARRO P, MARTÍN-MÉNDEZ I, BEL-LAN A, LOCUTURA JF, LÓPEZ-ABENTE G (2016) Arsenic and chromium topsoil levels and cancer mortality in Spain. *Environ Sci Pollut Res Int*, 23(17): 17664-17675.

NYLAND JF, FAIRWEATHER D, SHIRLEY DL, DAVIS SE, ROSE NR, SILBERGELD EK (2012) Low-dose inorganic mercury increases severity and frequency of chronic coxsackievirus-induced autoimmune myocarditis in mice. *Toxicol Sci*, 125(1): 134-143.

PAWŁOWSKA M, LEGUTKO D, STEFANIUK M (2017) Zajrzeć w głąb mózgu - nowe techniki oczyszczania optycznego i obrazowania z zastosowaniem mikroskopu arkusza światła [Getting an insight into the brain - new optical clearing techniques and imaging using light-sheet microscope]. *Postepy Biochem*, 63(1): 8-15.

PIEPOLI MF, HOES AW, AGEWALL S, ALBUS C, BROTONS C, CATAPANO AL, COONEY MT, CORRÀ U, COSYNS B, DEATON C, GRAHAM I, HALL MS, HOBBS FDR, LØCHEN ML, LÖLLGEN H, MARQUES-VIDAL P, PERK J, PRESCOTT E, REDON J, RICHTER DJ, SATTAR N, SMULDERS Y, TIBERI M, VAN DER WORP HB, VAN DIS I, VERSCHUREN WMM, BINNO S (2016) European Guidelines on cardiovascular disease prevention in clinical practice: The Sixth Joint Task Force of the European Society of Cardiology and Other Societies on Cardiovascular Disease Prevention in Clinical Practice (constituted by representatives of 10 societies and by invited experts). Developed with the special contribution of the European Association for Cardiovascular Prevention & Rehabilitation (EACPR). *Eur Heart J*, 37(29): 2315-2381.

RANIERI M, DI MISE A, DIFONZO G, CENTRONE M, VENNERI M, PELLEGRINO T, RUSSO A, MASTRODONATO M, CAPONIO F, VALENTI G, TAMMA G (2019) Green olive leaf extract (OLE) provides cytoprotection in renal cells exposed to low doses of cadmium. *PLoS One*, 14(3): e0214159.

ROJAS-FRANCO P, FRANCO-COLÍN M, TORRES-MANZO AP, BLAS-VALDIVIA V, THOMPSON-BONILLA MR, KANDIR S, CANO-EUROPA E (2019) Endoplasmic reticulum stress participates in the pathophysiology of mercury-caused acute kidney injury. *Ren Fail*, 41(1): 1001-1010.

SANDERS AP, MAZZELLA MJ, MALIN AJ, HAIR G, BUSGANG SA, SALAND JM, CURTIN P (2019) Combined exposure to lead, cadmium, mercury, and arsenic and kidney health in adolescents age 12-19 in NHANES 2009-2014. *Environ Int*, 131: 104993.

SAS-NOWOSIELSKA H, PAWLAS N (2015) Heavy metals in the cell nucleus - role in pathogenesis. *Acta Biochim Pol*, 62(1): 7-13.

SENO K, OHNO J, OTA N, HIROFUJI T, TANIGUCHI K (2013) Lupus-like oral mucosal lesions in mercury-induced autoimmune response in Brown Norway rats. *BMC Immunol,* 14: 47.

SHEN J, WANG X, ZHOU D, LI T, TANG L, GONG T, SU J, LIANG P (2018) Modelling cadmium-induced cardiotoxicity using human pluripotent stem cell-derived cardiomyocytes. *J Cell Mol Med*, 22(9): 4221-4235.

SIBLERUD R, MUTTER J, MOORE E, NAUMANN J, WALACH H (2019) A hypothesis and evidence that mercury may be an etiological factor in Alzheimer's disease. *Int J Environ Res Public Health*, 16(24): 5152.

ŚLIWIŃSKA-MOSSOŃ M, MILNEROWICZ S, MILNEROWICZ H (2018) Diabetes mellitus secondary to pancreatic diseases (type 3c): The effect of smoking on the exocrine-endocrine interactions of the pancreas. *Diab Vasc Dis Res*, 15(3): 243-259.

ŚLIWIŃSKA-MOSSOŃ M, SOBIECH K, DOLEZYCH B, MADEJ P, MILNEROWICZ H (2019) N-acetyl-beta-D-glucosaminidase in tissues of rats chronically exposed to cadmium and treated with ozone. *Ann Clin Lab Sci,* 49(2): 193-203.

SUTTON DJ, TCHOUNWOU PB (2007) Mercury induces the externalization of phosphatidyl-ser-

ine in human renal proximal tubule (HK-2) cells. *Int J Environ Res Public Health*, 4(2): 138-144.

TAE HJ, JUN DW, CHOI YY, KWAK MJ, LEE MH (2014) Assessment of risk of complications in cirrhosis using portal thallium scans. *World J Gastroenterol*, 20(1): 228-234.

TEIXEIRA FB, DE OLIVEIRA ACA, LEÃO LKR, FAGUNDES NCF, FERNANDES RM, FERNANDES LMP, DA SILVA MCF, AMADO LL, SAGICA FES, DE OLIVEIRA EHC, CRESPO-LOPEZ ME, MAIA CSF, LIMA RR (2018) Exposure to inorganic mercury causes oxidative stress, cell death, and functional deficits in the motor cortex. *Front Mol Neurosci*, 11: 125.

TEKABE Y, LUMA J, LI Q, SCHMIDT AM, RAMASAMY R, JOHNSON LL (2012) Imaging of receptors for advanced glycation end products in experimental myocardial ischemia and reperfusion injury. *JACC Cardiovasc Imaging*, 5(1): 59-67.

THEM TR II, GILL BC, CARUTHERS AH, GERHARDT AM, GRÖCKE DR, LYONS TW, MARROQUÍN SM, NIELSEN SG, TRABUCHO ALEXANDRE JP, OWENS JD (2018) Thallium isotopes reveal protracted anoxia during the Toarcian (Early Jurassic) associated with volcanism, carbon burial, and mass extinction. *Proc Natl Acad Sci USA*, 115(26): 6596-6601.

TREVIÑO S, WAALKES MP, FLORES HERNÁNDEZ JA, LEÓN-CHAVEZ BA, AGUILAR-ALONSO P, BRAMBILA E (2015) Chronic cadmium exposure in rats produces pancreatic impairment and insulin resistance in multiple peripheral tissues. *Arch Biochem Biophys*, 583: 27-35.

VASAMSETTI SB, FLORENTIN J, COPPIN E, STIEKEMA L, ZHENG KH, NISAR MU, SEMBRAT J, LEVINTHAL D, ROJAS M, STROES ES, KIM K, DUTTA P (2018) Sympathetic neuronal activation triggers myeloid progenitor proliferation and differentiation. *Immunity*, 49(1): 93-106.e7.

VENTER C, OBERHOLZER HM, CUMMINGS FR, BESTER MJ (2017) Effects of metals cadmium and chromium alone and in combination on the liver and kidney tissue of male Spraque-Dawley rats: An ultrastructural and electron-energy-loss spectroscopy investigation. *Microsc Res Tech*, 80(8): 878-888.

VIANNA ADS, MATOS EP, JESUS IM, ASMUS CIRF, CÂMARA VM (2019) Human exposure to mercury and its hematological effects: a systematic review. *Cad Saude Publica*, 35(2): e00091618.

WANG C, CHEN Z, PAN Y, GAO X, CHEN H (2017) Anti-diabetic effects of Inonotus obliquus polysaccharides-chromium (III) complex in type 2 diabetic mice and its sub-acute toxicity evaluation in normal mice. *Food Chem Toxicol*, 108(Pt B): 498-509.

WANG Y, WANG D, WU J, WANG B, GAO X, WANG L, MA H (2015a) Cinnabar-induced subchronic renal injury is associated with increased apoptosis in rats. *Biomed Res Int*, 2015: 278931.

WANG Y, WANG D, WU J, WANG B, WANG L, GAO X, HUANG H, MA H (2015b) Cinnabar induces renal inflammation and fibrogenesis in rats. *Biomed Res Int*, 2015: 280958.

WEI H, HU Q, WU J, YAO C, XU L, XING F, ZHAO X, YU S, WANG X, CHEN G (2018) Molecular mechanism of the increased tissue uptake of trivalent inorganic arsenic in mice with type 1 diabetes mellitus. *Biochem Biophys Res Commun*, 504(2): 393-399.

WESTERBERG DP (2013) Diabetic ketoacidosis: evaluation and treatment. *Am Fam Physician*, 87(5): 337-346.

WOODS JS, DIEGUEZ-ACUÑA FJ, ELLIS ME, KUSHLEIKA J, SIMMONDS PL (2002) Attenuation of nuclear factor kappa B (NF-kappaB) promotes apoptosis of kidney epithelial cells: a potential mechanism of mercury-induced nephrotoxicity. *Environ Health Perspect*, 110 (Suppl 5): 819-822.

WU M, SHU Y, SONG L, LIU B, ZHANG L, WANG L, LIU Y, BI J, XIONG C, CAO Z, XU S, XIA W, LI Y, WANG Y (2019) Prenatal exposure to thallium is associated with decreased mitochondrial DNA copy number in newborns: Evidence from a birth cohort study. *Environ Int*, 129: 470-477.

YANG D, TAN X, LV Z, LIU B, BAIYUN R, LU J, ZHANG Z (2016) Regulation of Sirt1/Nrf2/TNF-α signaling pathway by luteolin is critical to attenuate acute mercuric chloride exposure induced hepatotoxicity. *Sci Rep*, 6: 37157.

YANG Y, WANG W, LIU X, SONG X, CHAI L (2020) Probing the effects of hexavalent chromium exposure on histology and fatty acid metabolism in liver of Bufo gargarizans tadpoles. *Chemosphere*, 243: 125437.

Gonial angle measures in Medieval and contemporary skeletons

Borja Faus-Valero[1], Susanna Llidó-Torrent[1], Marcos Miquel-Feutch[1], Laura Quiles-Guiñau[1], Marcelino Perez-Bermejo[1], Shahed Nalla[1,2], Juan A. Sanchis-Gimeno[1]

[1] GIAVAL Research Group, Department of Anatomy and Human Embryology, University of Valencia, Faculty of Medicine, Avda. Blasco Ibanez 15, E46010 - Valencia, Spain

[2] Department of Human Anatomy and Physiology, Faculty of Health Sciences, University of Johannesburg, Auckland Park, 2006, South Africa

SUMMARY

We aimed to test the possible differences in gonial angle values between a Medieval sample and a contemporary sample because literature suggests that modern skulls tend to have larger gonial angles. We analyzed the gonial angle values in a Medieval sample (n=69) and a current sample (20th century sample; n=146). We found that current gonial angle values were 3.6º (CI95% 2.2-4.9) larger than the Medieval angle values ($p<0.001$). No significant differences between the right and left angle values in both the Medieval ($p=0.131$) and current sample ($p=0.120$) were observed. The right angle values of the current sample were 3.6º larger (CI95% 1.9-5.3) than the medieval right angle values while the left angle values of the current sample were 3.5º larger (CI95% 1.9-5.2) than the Medieval left angle values. Our research suggests that the present population have larger angle values than the Medieval population.

Key words: Mandibular anatomy – Diet – Mandibular injuries – Risk factors

INTRODUCTION

The gonial (mandibular) angle is the angle of the mandible (Fig. 1) formed between the ramus line and the mandibular line as viewed from the lateral aspect of the mandible. The ramus line is the tangent to the posterior border of the mandible, and the mandibular line is the lower border of the mandible through the gnathion (Ohm and Silness, 1999; Dhara et al., 2019).

Fig. 1.- Schematic representation of the gonial angle (GoA). RL: ramus line; ML: mandibular line; gn: gnathion.

The gonial angle values have been studied in present day populations (Dutra et al., 2004; Uthman, 2007; Upadhyay et al., 2012; Chole et al., 2013; Bhardwaj et al., 2014; Leversha et al., 2016; Larrazabal-Moron and Sanchis-Gimeno, 2018). Questions

Corresponding author:
Juan A. Sanchis-Gimeno. GIAVAL Research Group, Department of Anatomy and Human Embryology, University of Valencia, Faculty of Medicine, Avda. Blasco Ibanez 15, E46010 - Valencia, Spain. E-mail: juan.sanchis@uv.es

Submitted: June 13, 2020. **Accepted:** August 14, 2020

about factors that influence the morphology and morphometry of the gonial angle is the focus of research in the scientific community. In this context, different researchers (Varrella, 1990; Luther, 1993; Kaifu, 1997; Gungor et al., 2007; Hayashi et al., 2011; Rando et al., 2014; Toro-Ibacache et al., 2016; Toro-Ibacache et al., 2019) have presented contradictory results after analyzing the jaw size and shape by means of traditional morphometry measurements and geometric morphometrics in order to determine possible morphological changes of the jaw during past centuries, the presence of sexual dimorphism, and the possibility of asymmetry in gonial angle values.

One of the most controversial aspects is the possible larger gonial angle values in contemporary subjects when compared to past subjects. Some authors have suggested that modern skulls tend to have larger gonial angles (Varrella, 1990; Luther, 1993; Rando et al., 2014) due to a modern diet of softer foods (Rando et al., 2014) in comparison to the coarser pre-industrialized diet that required more vigorous masticatory activity (Varrella, 1990). The possible angle changes in line with research that has revealed that mandibular shape varies as a function of the forces applied to it by the temporalis and masseter muscles (Sella-Tunis et al., 2018). However, Gungor et al. (2007) compared the gonial angle values of present subjects with skeletal series from different Anatolian populations to investigate possible changes since the Mesolithic period, and concluded that there is no clear evidence in the change of gonial degree angle in the passage of time.

The study of medieval and contemporary skeletal remains will allow us to answer some of the related research questions mentioned. Following on from this, we aimed to test the possible differences in gonial angle values between medieval and contemporary mandibles in order to test the hypothesis of an increase of the gonial angle values during the past centuries. Secondly, we also aimed to analyze the possible differences in left and right angles and the sexual dimorphism of gonial angle values.

MATERIALS AND METHODS

We carried out an observational transversal study that analyzed the gonial angle values in a medieval sample and a twentieth-century sample. This study was approved by the institutional review board of the University of Valencia (reference number: H1491206464387).

Inclusion criteria of the mandibles in the study are that each specimen of both sample populations required to be of a Caucasian adult, with an age at death ranging from 20 to 50 years old, and have at least one quarter of the dentition presenting teeth numbers 35, 36, 37, 45, 46 and 47. In addition to the above inclusion criteria, the twentieth-century mandibles were obtained from skeletons of subjects who had passed away before 1970 in order to avoid the possible effect of current orthodontic treatments on mandibular morphometric values (Furquim et al., 2018).

The medieval sample was composed of 208 skeletons discovered during the restoration works at a Medieval Muslim burial site of L'Alcudiola (Favara, Valencia, Spain) (Fig. 2). L'Alcudiola Necropolis lies 6 km away from the Mediterranean coast of Spain, around 49 km south of the modern city of Valencia. The human remains found were dated between the eleventh and fourteenth centuries, and after application of the inclusion criteria, 69 of the 208 mandibles (33.2%) found were used in the study.

Fig. 2.- Image of the recovery of the human remains found in the Medieval burial site of L'Alcudiola.

Due to the lack of availability of old registers on age-at-death of each individual skeleton, the age and sex of said skeletons was determined by evaluation of the metamorphosis at the sternal extremity of the rib, thyroid cartilage ossification, cranial bone synostosis and pubic symphysis morphology (Burns, 2008). The twentieth-century skeletal mandibles (n=146; 100%) with known sex

and age at death were obtained from the Raymond A. Dart Collection of Human Skeletons (Dart Collection) housed in the School of Anatomical Sciences, University of the Witwatersrand Medical School, Johannesburg, South Africa. Table 1 presents the demographic characteristics of the samples analyzed.

Table 1. Description of the samples analyzed.

Medieval	n (%)	mean age±SD	Age range	CI 95%
Total	69 (100%)	33.2±7.5	20 - 50	31.4-35.0
Male	36 (52.2%)	34.6±6.9	20 - 50	32.2-36.9
Female	33 (47.8%)	31.8±7.8	20 - 50	29.0-34.6
p-value	0.610 *	0.124 †	---	---
20th century	n (%)	mean age±SD	Age range	CI 95%
Total	146 (100%)	38.6±8.6	21 - 50	37.2-40.0
Male	76 (52.1%)	37.7±8.3	22 - 50	35.8-39.6
Female	70 (47.9%)	39.6±8.8	21 - 50	37.5-41.7
p-value	0.483 *	0.174 †	---	---

* Proportion difference z-test; † Unpaired Student t-test. No significant differences were observed in the proportion of female and male in both samples. Neither were found significant age differences in both samples.

Measurement of the gonial angles was carried out by means of a conventional mandibulometer. The gonial angle value used was the mean of three consecutive measurements taken on the same day by the same researcher. We also analyzed the sexual dimorphism and the potential differences in the left and the right gonial angle values.

Data were entered and stored in an MS-Excel file, and then transferred to SPSS v.23 software (SPSS Inc., Chicago, IL, USA) for statistical analysis. Continuous variables were presented as mean ± standard deviation. Categorical variables were expressed by count and percentage. Normality of the data distribution was determined by using the Kolmogorov-Smirnov test. Difference between proportions was evaluated utilizing the z-test. Differences between means were analyzed with the paired or unpaired Student t-test as required in the case of two means. Although angles are not meant to be compared using linear statistics, we used a t-test because the differences were within a very small angle range (<10º). Two-sided $p<0.05$ was considered to be statistically significant. Intraclass correlation coefficient (ICC) estimates and their 95% confident intervals (CI) were calculated based on a 2-way mixed-effects model. ICC values less than 0.5 are considered to be indicative of poor reliability, values between 0.5 and 0.75 indicate moderate reliability, values between 0.75 and 0.9 indicate good reliability, and values greater than 0.90 indicate excellent reliability (Koo and Li, 2016).

RESULTS

In order to evaluate the reliability of our measurements, the gonial angle was measured thrice by the same researcher, and the ICC among the 3 different measurements was calculated. The ICC used to assess measurement accuracy for the gonial angle measurements was 0.995, with a CI95% from 0.991 to 0.997 ($F= 193.38$, $p<0.001$), which reflects an excellent reliability. In addition, we also evaluated the results obtained by two different researchers who measured the gonial angles, and we found that the ICC was 0.992 with a CI95% from 0.984 to 0.996 ($F= 120.37$, $p<0.001$) which also reflects an excellent reliability.

Table 2 presents the gonial angle results obtained in the samples analyzed. We found that the 20th century values were 3.6º (CI95% 2.2-4.9) larger than the Medieval values ($p<0.001$; Unpaired Student t-test).

Table 2. Results obtained in the samples analyzed (grades) *.

Sample	n	Mean±SD	range	CI 95%
Medieval	138	119.1±3.6 †	110-127	118.5 - 119.7
20th century	292	122.7±6.6 †	108-140	121.9 - 123.4

* All angles analyzed (both left and right angles included). † Statistically significant differences between medieval and 20th century values ($p<0.001$; Unpaired Student t-test)

Table 3 reveals no significant differences between the right and the left angle values in the medieval ($p=0.131$; Paired Student t-test) and twentieth-century samples ($p=0.120$; Paired Student t-test). Nevertheless, we found significant differences when comparing the right angle values of the medieval sample and the right angle

values of the twentieth-century sample (p<0.001; Unpaired Student t test). The twentieth-century right angle values were 3.6º larger (CI95% 1.9-5.3) than the medieval right angle values. We found similar results for the left angles (p<0.001; Unpaired Student t-test): the twentieth-century left angle values were 3.5º larger (CI95% 1.9-5.2) than the medieval left angle values.

Table 3. Left and right gonial angle values obtained in the samples analyzed.

Angle	Sample	n	mean±SD	range	CI 95%
Right	Medieval	69	118.9±3.5 *	110-126	118.1-119.8
	20th century	146	122.5±6.7 †	108-139	121.4-123.6
Left	Medieval	69	119.3±3.7 *	110-127	118.4-120.2
	20th century	146	122.8±6.4 †	109-140	121.8-123.9

* Significant differences between the Medieval right angles and the 20th century right angles (p<0.001; Unpaired Student t test); † Significant differences between the Medieval left angles and the 20th century left angles (p<0.001; Unpaired Student t test)

The differences in gonial angle values between females and males are presented in Table 4. Analysis of the medieval sample revealed significant differences between the right values of female and male (p<0.001; Unpaired Student t test): female right angle values were 3.8º larger than male right values (CI95% 2.4-5.2); we also found significant differences between sexes in the left angle values (p<0.001; Unpaired Student t-test), female having left angle values 4.2º larger than male (CI95% 2.8-5.7). The twentieth-century females had right angle values 3.6º larger than that presented by males (p<0.001; Unpaired Student t-test; CI95% 1.4-5.7) while female left values were 3.5º larger than those presented by males (p<0.001; Unpaired Student t-test; CI95% 1.5-5.6).

DISCUSSION

We have carried out a study in two different skeletal samples of subjects aged 20 to 50 years old at death. We measured the gonial angles of adult subjects, and none younger than 20 years old, because the angle values show a continuous decrease until the age of 21 years when it stops changing (Larrazabal-Moron and Sanchis-Gimeno, 2018).

Focusing on the main objective of our research, we observed larger gonial angle values in the twentieth-century sample. In this context, it must be noted that we analyzed skeletons of subjects that passed away before 1970 in order to avoid the effect of current orthodontic treatments in mandibular morphometric values (Furquim et al. 2018), and that the ICC analysis reflected an excellent reliability of the measurements carried out.

Table 4. Analysis of the gonial angle values in female and male (grades) *.

Medieval	n	mean±SD	range	CI 95%
Right male	36	117.1±2.9	110-123	116.1-118.1
Right **female**	33	120.9±2.9	116-126	119.9-121.9
Left male	36	117.3±2.9	110-123	116.3-118.3
Left female	33	121.5±3.1	114-127	120.4-122.6
20th century	n	mean±SD	range	CI 95%
Right male	76	120.8±7.1	108-139	119.2-122.4
Right **female**	70	124.4±5.8	111-139	123.0-125.8
Left male	76	121.1±7.0	109-140	119.5-122.7
Left female	70	124.7±5.2	112-136	123.4-125.9

* Female presented statistically significant larger right and left angle values in both the medieval (p<0.001; Unpaired Student t test) and 20th century sample (p<0.001; Unpaired Student t test)

Rando et al. (2014) analyzed two skeletal samples from the late medieval period (years 1050-1550) and the post-medieval period (years 1550-1850), and found larger gonial angle values in the post-medieval period sample. Luther (1993) found larger gonial angle values in modern mandibles when compared to medieval mandibles. Our results concur with these authors, as our twentieth-century mandibles present larger gonial angle values than the medieval mandibles.

Similar results were presented by Varrella (1990) as the smaller gonial angles found in fifteenth- and sixteenth-century skulls compared to contemporary; Varrella (1990) suggested that the observed changes in gonial angle values were related to the differences in intensity of chewing

between the samples, possibly due to changes in diet (with the present diet being softer), but also concluded that masticatory activity, in addition to breathing, is an important factor in the determination of facial growth direction. Furthermore, Toro-Ibacache et al., (2019) in their study of current and past populations based on the intensity of masticatory loads, found that modern urban subjects with lower intensity of masticatory loads tend to have more gracile features, as well as wider mandibular angles. However, they also indicated that the large variation in the mandible shape of modern subjects may be affected by genetics and nutrition. It must be noted that malnutrition related to social status cannot be factored in a skeletal study undertaken on past skeletal remains like these, as the material properties of food items cannot be measured in extinct populations (Toro-Ibacache et al., 2019), and because malnutrition is a factor that affects the appearance of the jaw (Suazo-Galdames et al., 2008). Thus, Hayashi et al. (2012) recommended identification of the social class of a subject prior to a physical anthropology comparison or examination. The results of their geometric morphometrics analysis revealed a clear difference in craniomandibular shape between the early modern (Edo) Japanese (seventeenth- to nineteenth-century) group, which presented an obtuse gonial angle, and the contemporary Japanese group. Possibly these factors (social and nutrition status), also with the lack of samples from different periods, may be the reason of the non-significant differences between mean gonial angle degrees between late Byzantine, medieval and the contemporary periods observed in the study done in Anatolian populations by Gungor et al., (2007).

Luther (1993) and Rando et al. (2014) also suggested that dietary differences were likely to be major explanatory factors of the differences between medieval and modern mandibles. The daily diet of medieval populations similar to the one studied by us has been analyzed before (Alexander et al., 2015; Guede et al., 2017). These studies have revealed that the diet was based on cereals, pulses, lamb, poultry, fish, fruit, honey, eggs, milk and cheese, which was similar to twentieth- and twenty-first-century daily diet comprising plant foods, olive oil, fish, poultry, red meat, fresh fruit, refined white maize meal, bran, sugar, and vegetables (Abramson et al., 1960; Widmer et al., 2015). Nonetheless, the current human diet is softer than pre-industrialized diet because of food processing technologies (Rando et al., 2014) may imply that less force is needed to be applied by the temporalis and masseter muscles during biting, being a possible explanation for the current larger gonial angle values, because of the relationship between the force input and the cranial skeletal deformation during biting (Toro-Ibacache et al., 2016). This may be one possible cause of the larger gonial angle values observed in the twentieth-century sample. Moreover, it is known that the mandible is considered to be a bone whose morphology is adaptable (Nicholson and Harvati, 2006; Smith, 2009). Kaifu (1997) found a human mandibular reduction in the Japanese remains between the Kofun and the Edo periods that may be related to a reduction of chewing stress. Similarly, May et al. (2018) and Pokhojaev et al. (2019) suggested that changes in mandibular size and orientation during the terminal Pleistocene to Holocene can be explained by a reduction in the biomechanical demands of the masticatory system.

All this raises a question about the comparability of the samples we studied, as the modern sample was obtained from a South African skeletal collection housed in a modern urban city, whereas the Medieval sample was composed of Mediterranean skeletons from a small rural location. It could be argued that both samples were not comparable due to a number of factors, for example, possible different social status, sample composition, geographical differences as well as ancestry and genetic differences. Therefore, we have compared the twentieth-century gonial angles from the Dart collection we used with the gonial angles of a twentieth-century Mediterranean skeletal sample from our lab, and we found no significant differences between both the twentieth-century Mediterranean and South African samples (Table 5). The gonial angles were also significantly larger in the contemporary Mediterranean sample than in the medieval Mediterranean sample ($p<0.001$; Unpaired Student t-test).

Table 5. Values obtained in the 20th century samples (all grades analyzed) *.

Sample	n	Mean±SD	range	CI 95%
Mediterranean	64	123.3±3.9 *	116-133	122.3-124.7
South African	292	122.7±6.6 *	108-140	121.9-123.4

* There were no statistically significant differences between the samples (p=0.353; Unpaired Student t-test)

Regarding asymmetry and sexual dimorphism, we found no significant differences between the right and the left angle values in the medieval and twentieth-century samples, but females presented statistically significant larger angle values in both the medieval and twentieth-century samples, our samples being well balanced between sexes. Gungor et al. (2007) found no asymmetrical difference between the right and left gonial angle degrees of individuals belonging to the same sex, but females have larger gonial angles, which leads to concluding that mandibular gonial angle showed sexual dimorphism with female having higher values starting from the early settlement times in Anatolia through time. In addition, Hayashi et al. (2012) found morphological differences between early modern (Edo) Japanese women and contemporary Japanese women using human female remains, and although they noted that the reason of their results remained unclear, they related the results possibly to both environmental changes and genetic variation over the past 100 years. Similarly, Katz et al. (2017) also proposed that genetic mechanisms are involved in skull shape. In this context, Coquerelle et al. (2011) highlight that sexual dimorphism in the mandible is closely related to the soft tissues of the oral cavity, because these are a major component of facial growth.

Anatomical analysis of ancient and present skeletons allows for reverse translational research to be undertaken. For example, the detected increased gonial angle values in present subjects, when compared to skeletons of populations who lived several centuries ago, may provide information about possible clinical symptoms and/or pathologies that current people may indicate. In this context, our results may have future research implications, as it appears that there is a positive correlation between high gonial angle values and the presence of an angle fractures (Panneerselvam et al., 2017; Bereznyak-Elias et al., 2018; Dhara et al., 2019), which are the most common mandibular fractures (Aleysson et al., 2008). Subjects with smaller gonial angles (as observed in our medieval sample) are assumed to have greater muscle activity and thus greater cortical bone thickness (Jonasson and Kiliaridis, 2004; Osato et al., 2012), while subjects with larger gonial angle values (as observed in our twentieth-century sample) that generate relatively decreased bite forces or masticatory loads will present decreased cortical bone thickness (Panneerselvam et al., 2017). Thus, results obtained in this study may be complemented with further skeletal research in order to determine whether modern skeletons present a high incidence of angle fractures than historical skeletons.

In summary, our study suggests that contemporary skeletons present larger gonial angle values than Medieval skeletons maybe due to a current softer diet. Further research is required in order to determine the possible effect on mandibular shape and gonial angle values of factors such as social status, nutrition, geographical differences, ancestry, and genetic differences.

ACKNOWLEDGEMENTS

The authors wish to thank Miss Manuela Raga y Rubio, Head of Archeological Intervention in L'Alcudiola, for her assistance in different phases of this research work.

REFERENCES

ABRAMSON JH, SLOME C, WARD NT (1960) Diet and health of a group of African agricultural workers in South Africa. Am J Clin Nutr, 8: 875-884.

ALEXANDER MM, GERRARD CM, GUTIÉRREZ A, MILLARD AR (2015) Diet, society, and economy in late medieval Spain: stable isotope evidence from Muslims and Christians from Gandía, Valencia. Am J Phys Anthropol, 156: 263-273.

ALEYSSON PO, ABUABARA A, PASSERI LA (2008) Analysis of 115 mandibular angle fractures. J Oral Maxillofac Surg, 66: 73-76.

BEREZNYAK ELIAS Y, SHILO D, EMODI O, NOY D, RACHMIEL A (2018) The Relation Between Morphometric Features and Susceptibility to Mandibular Angle Fractures. J Craniofac Surg, 29: e663-e665.

BHARDWAJ D, KUMAR JS, MOHAN V (2014) Radiographic evaluation of mandible to predict the gender and age. J Clin Diagn Res, 8: 66-69.

BURNS KR (2008) Forensic Anthropology Manual. Edicions Bellaterra SL, Barcelona.

CHOLE RH, PATIL RN, BALSARAF CHOLE S, GONDIVKAR S, GADBAIL AR, YUWANATI MB (2013) Association of mandible anatomy with age, gender, and dental status: a radiographic study. ISRN Radiol, 2013: 453763.

COQUERELLE M, BOOKSTEIN FL, BRAGA J, HALAZONETIS DJ, WEBER GW, MITTEROECKER P (2011) Sexual dimorphism of the human mandible and its association with dental development. Am J Phys Anthropol, 145: 192-202.

DHARA V, KAMATH AT, VINEETHA R (2019) The influence of the mandibular gonial angle on the occurrence of mandibular angle fracture. Dent Traumatol, 35: 188-193.

DUTRA V, YANG J, DEVLIN H, SUSIN C (2004) Mandibular bone remodelling in adults: evaluation of panoramic radiographs. Dentomaxillofac Radiol, 33: 323-328.

FURQUIM BD, JANSON G, COPE LCC, FREITAS KMS, HENRIQUES JFC (2018) Comparative effects of the mandibular protraction appliance in adolescents and adults. Dental Press J Orthod, 23: 63-72.

GUEDE I, ORTEGA LA, ZULUAGA MC, ALONSO-OLAZABAL A, MURELAGA X, PINA M, GUTIERREZ FJ, IACUMIN P (2017) Isotope analyses to explore diet and mobility in a medieval Muslim population at Tauste (NE Spain). PLoS One, 12: e0176572.

GUNGOR K, SAGIR M, OZER I (2007) Evaluation of the gonial angle in the Anatolian populations: from past to present. Coll Antropol, 31: 375-378.

HAYASHI K, SAITOH S, MIZOGUCHI I (2011) Morphological analysis of the skeletal remains of Japanese females from the Ikenohata-Shichikencho site. Eur J Orthod, 34: 575-581.

JONASSON G, KILIARIDIS S (2004) The association between the masseter muscle, the mandibular alveolar bone mass and thickness in dentate women. Arch Oral Biol, 49: 1001-1006.

KAIFU Y (1997) Changes in mandibular morphology from the Jomon to modern periods in eastern Japan. Am J Phys Anthropol, 104: 227-243.

KATZ DC, GROTE MN, WEAVER TD (2017) Changes in human skull morphology across the agricultural transition are consistent with softer diets in preindustrial farming groups. PNAS, 114: 9050-9055.

KOO TK, LI MY (2016) A guideline of selecting and reporting intraclass correlation coefficients for reliability research. J Chiropr Med, 15: 155-163.

LARRAZABAL-MORON C, SANCHIS-GIMENO JA (2018) Gonial angle growth patterns according to age and gender. Ann Anat, 215: 93-96.

LEVERSHA J, MCKEOUGH G, MYRTEZA A, SKJELLRUP-WAKEFILED H, WELSH J, SHOLAPURKAR A (2016) Age and gender correlation of gonial angle, ramus height and bigonial width in dentate subjects in a dental school in Far North Queensland. J Clin Exp Dent, 8: e49-54.

LUTHER F (1993) A cephalometric comparison of medieval skulls with a modern population. Eur J Orthod, 15: 315-325.

MAY H, SELLA-TUNIS T, POKHOJAEVA A, PELED D, SARIG R (2018) Changes in mandible characteristics during the terminal Pleistocene to Holocene Levant and their association with dietary habits. J Archaeol Sci Rep, 22: 413-419.

NICHOLSON E, HARVATI K (2016) Quantitative analysis of human mandibular shape using three-dimensional geometric morphometrics. Am J Phys Anthropol, 131: 368-383.

OHM E, SILNESS J (1999) Size of the mandibular jaw angle related to age, tooth retention and gender. J Oral Rehabil, 26: 883-891.

OSATO S, KUROYAMA I, NAKAJIMA S, OGAWA T, MISAKI K (2012) Differences in 5 anatomic parameters of mandibular body morphology by gonial angle size in dentulous Japanese subjects. Ann Anat, 194: 446-451.

PANNEERSELVAM E, PRASAD PJ, BALASUBRAMANIAM S, SOMASUNDARAM S, RAJA KV, SRINI-

VASAN D (2017) The influence of the mandibular gonial angle on the incidence of mandibular angle fracture-a radiomorphometric study. J Oral Maxillofac Surg, 75: 153-159.

POKHOJAEV A, AVNI H, SELLA-TUNIS T, SARIG R, MAY H (2019) Changes in human mandibular shape during the Terminal Pleistocene-Holocene Levant. Sci Rep, 9: 8799.

RANDO C, HILLSON S, ANTOINE D (2014) Changes in mandibular dimensions during the medieval to post-medieval transition in London: a possible response to decreased masticatory load. Arch Oral Biol, 59: 73-81.

SELLA-TUNIS T, POKHOJAEV A, SARIG R, O'HIGGINS P, MAY H (2018) Human mandibular shape is associated with masticatory muscle force. Sci Rep, 8: 6042.

SMITH HF (2009) Which cranial regions reflect molecular distances reliably in humans? Evidence from three-dimensional morphology. Am J Hum Biol, 21: 36-47.

SUAZO-GALDAMES IC, ZAVANDO-MATAMALA DA, LUIZ-SMITH R (2008) Evaluating accuracy and precision in morphologic traits for sexual dimorphism in malnutrition human skull: a comparative study. Int J Morphol, 26: 877-881.

TORO-IBACACHE V, UGARTE F, MORALES C, EYQUEM A, AGUILERA J, ASTUDILLO W (2019) Dental malocclusions are not just about small and weak bones: assessing the morphology of the mandible with cross-section analysis and geometric morphometrics. Clin Oral Investig, 23: 3479-3490.

TORO-IBACACHE V, ZAPATA MUÑOZ V, O'HIGGINS P (2016) The relationship between skull morphology, masticatory muscle force and cranial skeletal deformation during biting. Ann Anat, 203: 59-68.

UPADHYAY RB, UPADHYAY J, AGRAWAL P, RAO NN (2012) Analysis of gonial angle in relation to age, gender, and dentition status by radiological and anthropometric methods. J Forensic Dent Sci, 4: 29-33.

UTHMAN AT (2007) Retromolar space analysis in relation to selected linear and angular measurements for an Iraqi sample. Oral Surg Oral Med Oral Pathol Oral Radiol Endod, 104: e76-82.

VARRELA J (1990) Effects of attritive diet on craniofacial morphology: a cephalometric analysis of a Finnish skull sample. Eur J Orthod, 12: 219-223.

WIDMER RJ, FLAMMER AJ, LERMAN LO, LERMAN A (2015) The Mediterranean diet, its components, and cardiovascular disease. Am J Med, 128: 229-238.

Deep external rotator muscles of the hip: an anatomical and architectural study

Ian A. Scagnetti, Lorraine C. Jadeski, Stephen H.M. Brown

Department of Human Health and Nutritional Sciences, University of Guelph, Guelph, ON, Canada

SUMMARY

The number and organization of sarcomeres within a muscle (referred to as muscle architecture) can be used to predict functional capability. The six deep external rotator muscles of the hip (piriformis (PI), quadratus femoris (QF), obturator internus (OI), obturator externus (OE), superior gemellus (SG), and inferior gemellus (IG)) play a role in both hip stabilization and rotation and are damaged and relocated during total hip arthroplasty surgery. Understanding the architectural details of these muscles could lead to improved clinical understanding of their function. Therefore, muscles were excised from 12 embalmed cadavers (6 male, 6 female aged 56-88 years) to measure muscle mass, fascicle length, and sarcomere length. These variables were used to calculate the architectural parameters physiological cross-sectional area (PCSA) and normalized fascicle length (LF_n). Results demonstrated that in the measured neutral cadaveric posture all six muscles had mean sarcomere lengths (2.40 to 2.57 μm) that placed them on the ascending limb of the force-length relationship where they could theoretically generate more than 90 percent of their maximum capable force. The OI had the largest PCSA, and thus largest force-generating capability, while the PI had the longest normalized fascicle length, and thus largest excursion and shortening velocity capabilities. SG and IG were the smallest in both regards. These data provide valuable insight into the force-generating capability of the hip deep external rotator muscles and can be used as inputs to biomechanical models to predict function in healthy movement or within a variety of clinical conditions.

Key words: Functional anatomy – Muscle – Architecture – Sarcomere – Force – Length

INTRODUCTION

External rotation of the femur and stabilization of the hip joint are performed in part by the group of six muscles defined anatomically as the deep external rotators of the hip (Dostal, 1987; Agur and Dalley, 2016). These muscles are: piriformis (PI), quadratus femoris (QF), obturator internus (OI), obturator externus (OE), superior gemellus (SG), and inferior gemellus (IG) (Fig. 1). These six muscles extend between their attachments at various points on the ischium and pubis and the greater trochanter, trochanteric fossa and quadrate tubercle of the femur. The bony attachments make it possible for the muscles to cross the hip joint from several different angles, thereby facilitating the generation of external rotation throughout the hip joint's range of motion. These muscles also work to

Corresponding author:
Dr. Stephen H. M. Brown. Department of Human Health and Nutritional Sciences, University of Guelph, 50 Stone Rd East, Guelph ON Canada N1G 2W1. E-mail: shmbrown@uoguelph.ca

Submitted: July 27, 2020. **Accepted:** August 22, 2020

stabilize the head of the femur within the acetabulum (Agur and Dalley, 2016). This important group of muscles is damaged during total hip arthroplasty surgery (THA) in varying levels of severity depending on the surgical approach and technique employed (Bottner and Pellici, 2006; Meneghini et al., 2006), and as a result, long-term weakness and instability of the hip joint is often observed in THA patients' post-surgery (Winther et al., 2016; Kawasaki et al., 2017). In Canada alone, approximately 55,000 THA surgeries are done per year, and 4,500 revision surgeries performed per year due to failure in stability of the hip joint (Canadian Institute for Health Information, 2017). Unfortunately, the architecture of the deep hip external rotator muscle group has not been well documented.

Muscle architecture describes the internal organization of contractile elements called sarcomeres. The number and organization of sarcomeres within a muscle can be used to predict a muscle's functional capacity regarding the excursion and velocity potential of the muscle fibres, as well as the ability of the muscle to produce force. The best predictor of a muscle's excursion and velocity potential is normalized fascicle length (LF_n), which represents the number of sarcomeres arranged in-series along the length of the muscle. The best predictor of a muscle's ability to produce force is its physiological cross-sectional area (PCSA), which represents the number of sarcomeres arranged in-parallel within the muscle. Mean sarcomere length also plays an important role in determining a muscle's ability to produce force, as described by the well-known sarcomere force-length relationship (Gordon et al., 1966; Walker and Schrodt, 1974). These important architectural variables have not been well defined for the deep external rotator muscles of the hip.

Therefore, the current study was designed to measure the mass, sarcomere length and fascicle length of the six external rotator muscles of the hip from cadaveric donors, and use those measurements to calculate the architectural parameters normalized fascicle length and physiological cross-sectional area.

MATERIALS AND METHODS

All dissection and photography was performed in the University of Guelph Human Anatomy Laboratory. Permission is given by the Chief Coroner of Ontario to use cadaveric specimens donated to the University of Guelph for research purposes. Permission is also given by whole body donors and their families via the Anatomy Act (Province of Ontario) to utilize tissue for scientific research at the University of Guelph.

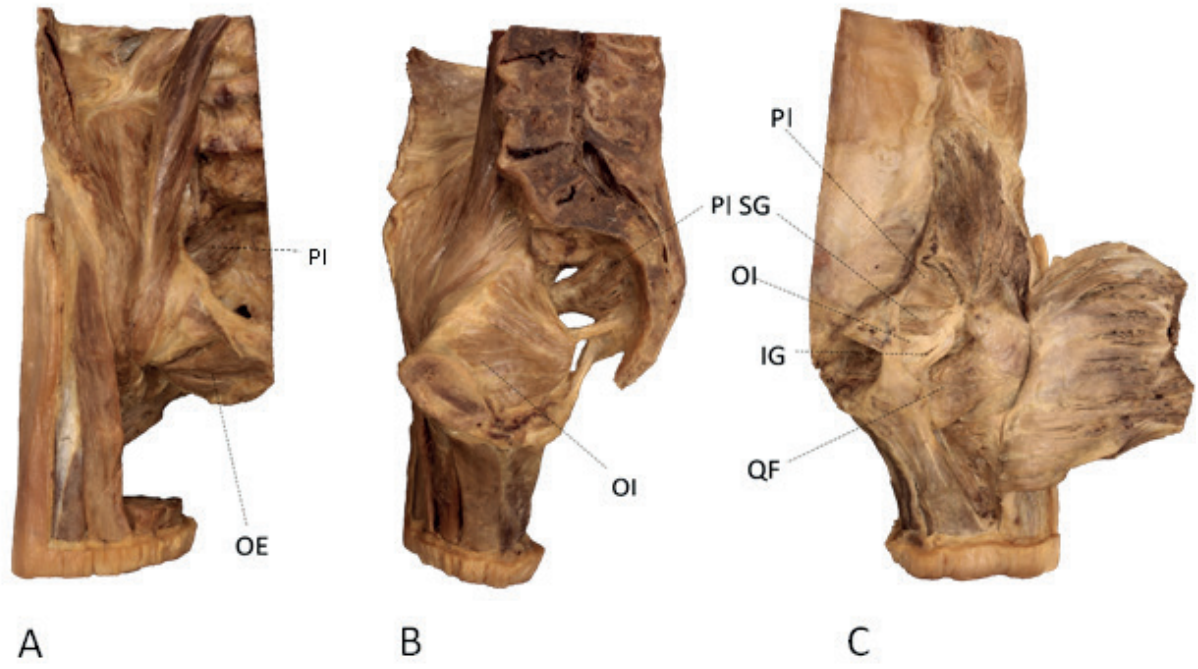

Fig. 1.- (**A**) Anterior view of right-side bisected pelvis, origin of piriformis (**PI**) and origin of obturator externus (**OE**) shown. (**B**) Mid-sagittal view of right-side bisected pelvis, origin of obturator internus (**OI**), and origin of piriformis (**PI**) shown. (**C**) Posterior view of right-side bisected pelvis, insertions of piriformis (**PI**), superior gemellus (**SG**), obturator internus (**OI**), inferior gemellus (**IG**) and quadratus femoris (**QF**) shown.

The cadavers in this study were embalmed by arterial perfusion using a 2.5% formaldehyde solution (60% ethanol, 30% propylene glycol, 5% phenol, 2.5% formaldehyde, 2.5% Dettol disinfectant), which results in approximate muscle density of 1.112 gm/cm^3 (Ward and Lieber, 2005). The current study followed the protocol for muscle dissection and removal described by Sacks and Roy (1982) in their study on feline hind-limb muscles and previously used for human muscles by multiple authors (e.g. Ward et al., 2009). The six muscles were harvested from one side of the body of each of 12 formaldehyde-fixed human cadavers [6 male and 6 female aged 56 – 88 years (mean = 79.3 years)] by carefully dissecting the muscles away from their origins and insertions using hand tools. Specimens were excluded if the medical history of the body donor reported any hip-related injury, surgery, chronic condition or wheelchair confinement. Specimens were also excluded if damage to the muscle or hip joint was observed during dissection. After the muscles were removed from their bony attachments, they were dissected to remove as much superficial fat and connective tissue as possible. Each muscle was then weighed to an accuracy of ±0.01 g using a digital scale. Next, using digital calipers (resolution of 0.01 mm), fascicle length was measured at three different locations (one central and two lateral) for each muscle (Fig. 2). The fascicle measurements were taken in these proximal, middle and distal areas of the muscle belly to represent the average fascicle length. To measure sarcomere length, three small biopsies were taken from each of the three fascicle regions described above (example of proximal, middle and distal locations along the fascicle marked with asterisks on the obturator externus muscle shown in Figure 2) and subjected to laser diffraction (Baskin and Lieber, 1983). Measured fascicle lengths and sarcomere lengths were averaged to provide a representative value for each muscle.

The mean fascicle length was normalized to the optimal sarcomere length for human muscle (2.7µm) using the equation below (Ward et al., 2009):

$$LF_n\,(cm) = \frac{LF_m\,(cm) \times L_{so}\,(\mu m)}{Lsm\,(\mu m)}$$

Where LF_n represents normalized fascicle length, LF_m represents measured fascicle length, Ls_o represents optimal sarcomere length for human muscle (2.7 µm; Walker and Schrodt, 1974) and Ls_m represents measured sarcomere length.

Each muscle's PCSA was then determined using the following equation (Ward and Lieber, 2005):

$$PCSA\,(cm^2) = \frac{M\,(g) \times \cos(\theta)}{\rho \times LFn\,(\mu m)}$$

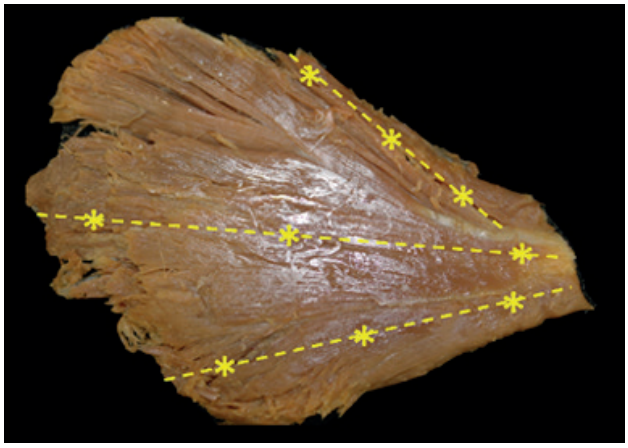

Fig. 2.- Excised obturator externus muscle (left side, anterior view) with fat, connective tissue and tendon removed. Yellow dotted lines indicate measurement locations for fascicle length, and asterisks indicate locations biopsied for sarcomere length measurement. Similar fascicle locations and biopsy locations were chosen for measurement from each muscle in the current study..

Where M is the muscle mass in grams (g), θ is the angle of pennation of the muscle fibres (negligible for the muscles studied here), LF_n is the average normalized fascicle length of the muscle, and ρ is muscle density (gm/cm^3).

Mean sarcomere lengths were also represented relative to the established sarcomere force-length relationship for human muscle. Based on the cross-bridge theory of muscle contraction, the shape of this relationship is governed by the overlap between actin and myosin proteins (Gordon et al., 1966); this overlap is dependent upon the length of these proteins. As these lengths are relatively consistent across muscles within a species, a defined force-length relationship can be presented (Walker and Schrodt, 1974; Burkholder and Lieber, 2001).

Using a two-way mixed-model analysis of variance (ANOVA) test, independent variables (muscle, sex) were compared within each

dependent variable (architectural parameters: sarcomere length, PCSA, LF_n) for all cadavers (n=12) with muscle as a repeated factor for each cadaver. If significant differences were found ($p < 0.05$), Tukey post-hoc tests were conducted where appropriate.

RESULTS

Mean architectural values, separated for males and females, of the six deep hip external rotator muscles fixed in neutral cadaveric posture are found in Table 1.

A significant effect of sex on PCSA was found, with muscles from male donors demonstrating greater mean PCSA than muscles from female donors ($p < 0.0001$), indicating a greater capacity for force production in male muscles (Fig. 3). There were also significant differences in PCSA amongst muscles of all donors ($p < 0.0001$) (OI > PI, SG, and IG; OE, PI, and QF > SG, IG). There was no statistically significant interaction effect for PCSA (p = 0.23).

There was no significant difference in LF_n between male and female muscles ($p = 0.14$) (Fig. 4). There was a significant main effect of muscle ($p = 0.0002$) for LF_n amongst muscles (PI > QF, SG, and IG; OE > SG and IG). There was no statistically significant interaction effect for LF_n (p = 0.27).

There were no significant differences in sarcomere length amongst muscles (p = 0.26), nor between sexes ($p = 0.29$), nor a significant interaction (p = 0.98) between muscle and sex. Mean sarcomere lengths for each muscle were between 2.40µm and 2.57µm, indicating that they acted between 90.7% and 96.1% of their maximal ability to produce force, according to the well-established force-length curve (Gordon et al., 1966; Walker and Schrodt, 1974). Mean sarcomere lengths of each muscle from all donors are shown with their relative positions on the force-length curve in Fig. 5.

Mean PCSA and LF_n for each muscle from all donors, separated by sex, are plotted in Fig. 6.

Table 1. Mean (SEM) measured mass, sarcomere length (SL), normalized fascicle length (LF_n) and calculated PCSA of the six deep external rotator muscles for male (M) and female (F) cadaveric donors.

Muscle	Mass (g)		SL (µm)		LF_n (cm)		PCSA (cm^2)	
	M	F	M	F	M	F	M	F
Piriformis	18.9 (2.6)	12.3 (1.4)	2.60 (0.14)	2.49 (0.08)	6.24 (0.25)	6.86 (0.23)	2.93 (0.44)	1.69 (0.22)
Quadratus Femoris	17.9 (2.1)	11.5 (1.0)	2.40 (0.04)	2.38 (0.07)	5.34 (0.54)	5.25 (0.43)	3.26 (0.55)	2.01 (0.23)
Obturator Externus	23.1 (1.5)	19.0 (2.5)	2.58 (0.08)	2.60 (0.07)	6.28 (0.23)	6.33 (0.49)	3.50 (0.29)	2.92 (0.41)
Obturator Internus	29.5 (3.1)	15.1 (3.1)	2.50 (0.13)	2.49 (0.11)	6.54 (0.51)	5.45 (0.51)	4.49 (0.84)	2.78 (0.63)
Superior Gemellus	4.9 (1.3)	2.2 (0.2)	2.56 (0.16)	2.45 (0.10)	4.96 (0.61)	4.59 (0.39)	0.96 (0.30)	0.45 (0.04)
Inferior Gemellus	5.0 (0.9)	2.9 (0.6)	2.45 (0.07)	2.40 (0.13)	5.42 (0.41)	4.50 (0.35)	0.86 (0.16)	0.58 (0.11)

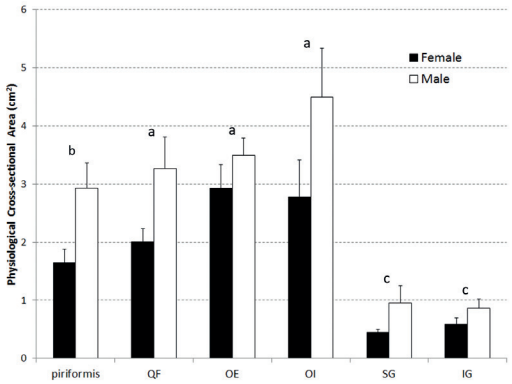

Fig. 3.- Mean (+ Standard Error of the Mean (SEM)) PCSA for both male and female muscles. Male and female were significantly different for all muscles. The same letters above the bars indicate muscles were not significantly different from one another.

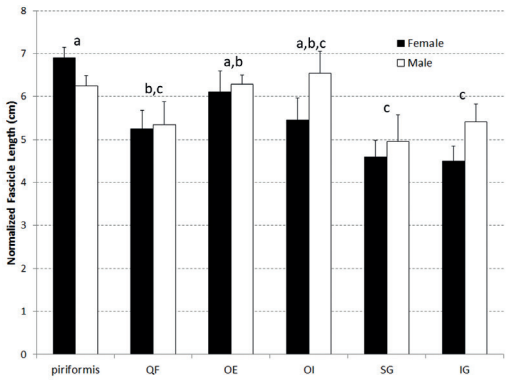

Fig. 4.- Mean (+ SEM) normalized fascicle length for both male and female muscles. The same letters above the bars indicate muscles were not significantly different from one another.

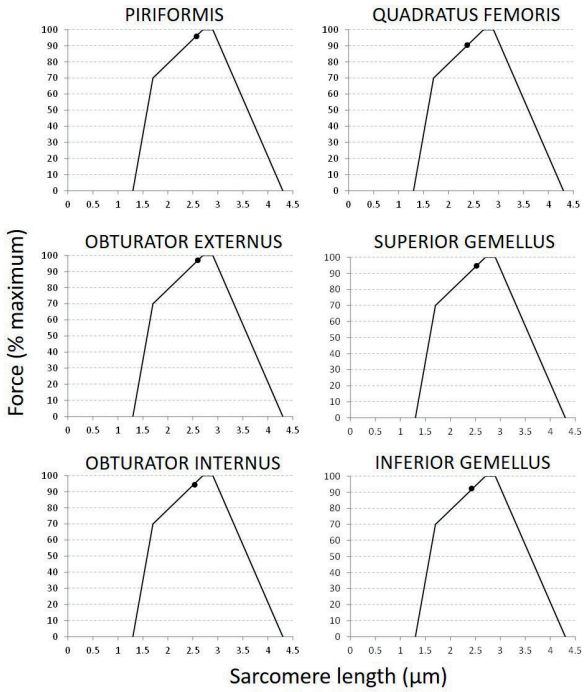

Fig. 5.- Mean sarcomere length for each muscle represented on the force-length curve as a percentage of maximal force production capable by the sarcomere in neutral cadaveric posture.

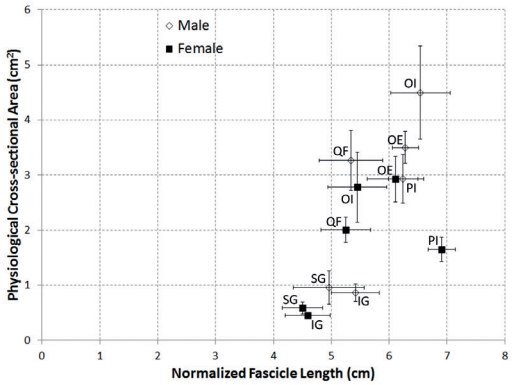

Fig. 6.- Mean (± SEM) PCSA and LFn for both male and female muscles.

DISCUSSION

This is the first study to examine and provide a high-resolution data set for the muscle architecture of the deep external rotator muscles of the hip. Interpretation of muscle functional capability, in terms of force generating capability and excursion potential, can be interpreted based on the architectural parameters PCSA and normalized fascicle length, respectively, and Figure 6 is provided to facilitate this comparison for both male and female muscles. Specifically, this enables visualization of which muscles are best suited to generating high forces and which muscles are best suited to generating force over a wide range of lengths and at high velocities. Further, these data can provide input for the development of biomechanical models of the pelvis and lower limb to study a variety of topics ranging from gait related disorders, childbirth and related muscle weakness, to surgical techniques including posterior approach total hip arthroplasty that involves the cutting and re-attachment of the PI, OI, SG, and IG.

Expected differences were observed between male and female muscles regarding PCSA. PCSA was significantly greater for males ($p < 0.0001$), indicating that male deep external hip rotator muscles are able to produce more force than female muscles. This result was expected, because PCSA is largely dictated by the mass of the muscle, which is generally correlated to the mass of the whole body (Janssen et al., 2000). There were also significant differences in PCSA amongst muscles of all donors ($p < 0.0001$) (OI > PI, SG, and IG; OE, PI, and QF > SG, IG). Thus, it can be concluded that the OI has the greatest force generating potential while SG and IG have the lowest.

Significant differences ($p = 0.0002$) were observed between the LF_n of the deep hip external rotator muscles (PI > QF, SG, and IG; OE > SG and IG), indicating that PI has the greatest excursion and contraction velocity potentials and SG and IG have the least. No statistically significant differences were found for normalized fascicle length between males and females, which was of itself interesting. Males on average have greater body height, and therefore body segments and associated muscles would be expected to be longer (Statistics Canada, 2008). However, this was not the case for the hip external rotator group (Figure 4). A potential explanation for this lack of sex-based difference in normalized fascicle length relates to the differences in the anatomy of male and female pelvises. The difference in male and female pelvic bone shape observed during dissection for this study is well documented (DeSilva and Rosenberg, 2017). Namely, the male pelvis is generally taller and narrower than the female pelvis, with anterior angling of the sacrum. Conversely, the female pelvis is generally shorter and wider than the male pelvis, and has a more posterior angle of the sacrum to accommodate childbirth. The increased width of the female pelvis results in a broader and more

lateral position of the hip joints. These differences in pelvis shape appear to offset expected differences in overall body height and ultimately result in normalized muscle fascicle lengths (LF_n) of the deep hip external rotator muscles that are not different between males and females.

The mean sarcomere length of a muscle in neutral cadaveric posture can be used to infer the muscles' ability to produce contractile force (Gordon et al., 1966). Each of the six muscles had mean sarcomere lengths, measured in the neutral cadaveric posture, between 2.40-2.57μm, indicating that in this position they were all capable of generating greater than 90 % of their maximum isometric force based on their location on the ascending limb of the force-length curve. This reveals that as the muscles are initially lengthened during movement or potential hip joint instability, they will become more effective at producing force until they surpass approximately 2.8μm, at which point force production capability would drop off. Interestingly, Suh et al (2004) demonstrated that reattachment of the external rotator muscles to the greater trochanter via a pair of transosseous sutures significantly lowered the chance of hip dislocation post-THA surgery. It is possible that the sarcomere length data presented in the current study could be used to further improve function of these muscles after reinsertion; specifically, intraoperative sarcomere length measurements (Lieber and Friden, 2001) have the potential to increase the likelihood that muscles are reattached at their natural in vivo lengths. Exploring this might further reduce the muscle weakness and instability that can be observed in patients after THA surgery. The results of this study are limited by the age-range of the individuals from which the specimens were collected (mean 79.3 years; range 56-88 years). Therefore, the data reported here are representative of an older demographic. If and how these would change in a younger group is unclear, but one previous study of the OI has demonstrated that PCSA was significantly lower in a group older than 60 years of age compared with younger groups, with no changes in LF_n or sarcomere length with age (Cook et al., 2017). Based on this, it is reasonable to expect a younger population to have larger PCSAs of all of the hip external rotator muscles than those reported here, but there is nothing to suggest that mean sarcomere lengths or LF_ns would be different between younger and older populations.

In summary, this study has yielded a high-quality muscle architecture data-set for the deep hip external rotator muscle group. Sarcomere lengths measured in the neutral cadaveric posture were between 2.40μm and 2.57μm for all six muscles, indicating that they act in this position on the ascending limb of the force-length relationship where they can generated greater than 90% of their maximal isometric force. OI had the greatest force-generating capability and PI the greatest length excursion and velocity potentials, while SG and IG were the smallest in both regards. The data reported here are required parameters that can be used to add these muscles to existing software models of the hip joint (e.g. OpenSim; Delp and Loan, 1995) which can be used to improve the understanding of the functional importance of these muscles and their potential role in preventing or treatment of hip disorders, including post-THA surgery (e.g. Myers et al., 2019).

REFERENCES

ABDELMOHSEN AM (2019) Leg dominance effect on isokinetic muscle strength of the hip joint. *J Chiropr Med,* 18: 27-32.

AGUR AMR, DALLEY AF (2016) *Grant's Atlas of Anatomy*. Wolters Kluwer.

BASKIN RJ, LIEBER RL (1983) Light diffraction: studies on striated muscle. *Trends Biomech,* 8: 197-200.

BOTTNER F, PELLICCI PM (2006) Review: posterior soft tissue repair in primary total hip arthroplasty. *HSS J,* 2: 7-11.

BURKHOLDER TJ, LIEBER RL (2001) Sarcomere length operating range of vertebrate muscles during movement. *J Exp Biol,* 204: 1529-1536.

CANADIAN INSTITUTE FOR HEALTH INFORMATION (2017) 'Hip and knee replacements in Canada'. Canadian Joint Replacement Registry Annual Report https://secure.cihi.ca/free_products/cjrr-annual-report-2018-en.pdf

COOK MS, BOU-MALHAM L, ESPARZA MC, ALPERNIN M (2017) Age-related alterations in female obturator internus muscle. *Int Urogynecol J,* 28: 729-734.

DESILVA JM, ROSENBERG KR (2017) Anatomy, development, and function of the human pelvis. *Anat Rec,* 300: 628-632.

DOSTAL WR, SODERBERG GL, ANDREWS JG (1987) Actions of hip muscles. *Phys Ther,* 66: 351-361.

GORDON AM, HUXLEY AF, JULIAN FJ (1966) The variation in isometric tension with sarcomere length in vertebrate muscle fibres. *J Physiol,* 184: 170-192.

JANSSEN I, HEYMSFIELD SB, WANG Z, ROSS R (2000) Skeletal muscle mass and distribution in 468 men and women aged 18-88 yr. *J Appl Physiol,* 89: 81-88.

KAWASAKI M, HASEGAWA Y, OKURA T, OCHIAI S, FUJIBAYASHI T (2017) Muscle damage after total hip arthroplasty through the direct anterior approach for developmental dysplasia of the hip. *J Arthroplasty,* 32: 2466-2473.

LIEBER RL, YEH Y, BASKIN RJ (1984) Sarcomere length determination using laser diffraction: effect of beam and fibre diameter. *Biophys J,* 45: 1007-1016.

LIEBER RL, FRIDEN J (2001) Clinical significance of skeletal muscle architecture. *Clin Orthop Relat Res,* 383: 140-151.

MENEGHINI RM, PAGNANO MW, TROUSDALE RT, HOZACK WJ (2006) Muscle damage during MIS total hip arthroplasty: Smith-Petersen versus posterior approach. *Clin Orthop Relat Res,* 453: 293-298.

MYERS CA, LAZ PJ, SHELBURNE KB, JUDD DL, WINTERS JD, STEVENS-LAPSLEY JE, DAVIDSON BS (2019) Simulated hip abductor strengthening reduces peak joint contact forces in patients with total hip arthroplasty. *J Biomech,* 93: 18-27.

SACKS RD, ROY RR (1982) Architecture of the hind limb muscles of cats: functional significance. *J Morphol,* 173: 185-195.

STATISTICS CANADA (2008) 'Mean height, weight, body mass index (BMI) and prevalence of obesity, by collection method and sex, household population aged 18 to 79, Canada, 2008, 2007 to 2009, and 2005'. http://statcan.gc.ca

SUH KT, PARK BG, CHOI YJ (2004) A posterior approach to primary total hip arthroplasty with soft tissue repair. *Clin Orthop Relat Res*, 418: 162-167.

WALKER SM, SCHRODT GR (1974) I segment lengths and thin filament periods in skeletal muscle fibers of the Rhesus monkey and the human. *Anat Rec,* 178: 63-81.

WARD RL, LIEBER RL (2005) Density and hydration of fresh and fixed human skeletal muscle. *J Biomech,* 38: 2317-2320.

WARD SR, ENG CM, SMALLWOOD LH, LIEBER RL (2009) Are current of lower extremity muscle architecture correct? *Clin Orthop Relat Res,* 467: 1074-1082.

WINTHER BS, VIGDIS HS, FOSS OA, TINA WS, SVENNINGSEN S, ENGDAL M, HAUGAN K, HUSBY OS (2016) Muscular strength after total hip arthroplasty: A prospective comparison of 3 surgical approaches. *Acta Orthop,* 87: 22-28.

Variations of the celiac trunk in Mexican population by MDCT angiography

Rodrigo A. Estrada León[1], Gustavo Barraza Aguirre[2], Vicente Toledo Coronado[2], Dulce A. Sánchez Nava[2], Monica Chapa Ibargüengoitia[2], Mariana Díaz Zamudio[2], Jorge Alanis Mendizabal[1], José J. Martínez De Anda[1], Diego Pineda-Martinez[1]

[1] Department of Innovation in Human Biological Material, Faculty of Medicine, National Autonomous University of Mexico
2 Department of Radiology and Image, National Institute of Medical Sciences and Nutrition "Salvador Zubirán" CDMX, Mexico

SUMMARY

The aim of this study is to describe the morphology and prevalence of anatomical variants of the celiac trunk (CT) in Mexican population, a crucial vascular structure while planning interventional radiology or surgery of the abdominal region. 127 Multidetector-row CT angiographies (MDCTA) from patients in the National Institute of Medical Sciences and Nutrition "Salvador Zubirán" (Mexico) were analyzed. Sixty-seven were women and sixty were men, with age range between 20 and 74 years old and with not previous pathologies reported. Ethics committee approval was obtained for this study. Anatomical variants were classified according to Marco-Clement's classification (2016). Type I, Complete CT, was found in 109 patients (109/127; 85.8%). The mean length of the CT was 20.4 mm ± 6.5 mm (range: 6.1-44 mm). Ostium mean diameter was 7.7 mm ± 1.9 (range 4.1-18.9 mm). Mean distance between the CT and the superior mesenteric artery was 7.3 mm ± 3.5 mm (range: 0.7-17.2 mm). Type II, incomplete CT, was found in 17 patients (17/127; 13.4%): subtype IIa, hepato-splenic trunk, was found in 9 patients (9/127; 7.1%), and subtype IIb, gastro-splenic trunk, in 8 patients (8/127; 6.3%). We did not observe Type III, independent origin of all arteries of the trunk or absence of CT. Type IV, celiac-mesenteric trunk, was found in 1 patient (1/127, 0.8%). No significant differences between genders were observed. This is the first study in Mexican population that describes CT variants by MDCTA using the newest classification with clinical significance prior to surgery or radiologic intervention.

Key words: Celiac trunk – Superior mesenteric artery – Splenic artery – Left gastric artery – Hepatic artery – Anatomical variations

INTRODUCTION

Assessment of the upper abdominal circulation is crucial while planning interventions involving the liver, bile duct, stomach, pancreas and spleen. Awareness of the anatomical variants improves outcomes in radiologic diagnosis, interventions and surgery by decreasing the rate of complications and morbidity (Ugurel et al., 2010; Nghiem et al., 1999; Clark, 2006; Winston et al., 2007; Osman and Abdrabou, 2016).

The celiac trunk morphology was described in 1756 by Albrecht von Haller, a Swiss anatomist

Corresponding author:
Diego Pineda. National Autonomous University of Mexico, Faculty of Medicine, Department of Innovation in Human Biological Material, University avenue 3000, Cp. 04510, México city, Mexico. Phone: +52 1 5560707995. E-mail: drpineda@unam.mx

Submitted: June 21, 2020. **Accepted:** August 31, 2020

and physiologist (Haller, 1756; Venara et al., 2013; Osman and Abdrabou, 2016). The classic pattern or complete trunk is made up by the left gastric artery (LGA), the splenic artery (SA) and the common hepatic artery (CHA) (Vandamme and Bonte, 1985). The superior mesenteric artery (SMA), which irrigates the pancreas, small intestine, cecum, ascending colon and the proximal transverse colon, has been reported also taking part in the celiac trunk as a fourth branch or celiac-mesenteric trunk (Sehgal et al., 2013).

The morphology and variations of the CT have been reported since the late nineteenth century. Furthermore, as usual in anatomical studies, no single universal classification has been proposed, resulting in a wide range of classifications (Lipshutz, 1917; Adachi, 1928; Michels, 1955; Song et al., 2010; Panagouli et al., 2013). There is only one study that made a meta-analysis of this variations using previous classifications proposals (Marco-Clement et al., 2016), and there is a research study made by our group based on pathological dissections analyzing TC variations in Mexican population (Pineda et al., 2019). Therefore, we have undertaken this study with the aim of using a simpler and unified classification of the celiac trunk's variations in patients.

MATERIALS AND METHODS

This retrospective study was approved by the institutional review board. Informed consent requirement was waived.

Patient population

The study was performed analyzing the MDCT scans from 200 consecutive patients from the radiological archive of the National Institute of Medical Sciences and Nutrition "Salvador Zubirán" in Mexico City between January and March of 2017.

Patients with tomographic studies that included an early arterial angiographic phase were included. The indication for such studies were: preoperative evaluations or follow-up for pancreatic or hepatobiliary neoplasms, kidney donation protocols, and monitoring of hyper-vascular gastrointestinal neoplasms. Patients with history of surgery, neoplasia, or atheroma plaques involving the celiac trunk or their branches were excluded.

Technical Parameters

The tomographic images were obtained using two 64-detector helical tomography equipments. The Somatom Sensation 64 equipment (Siemens, Germany) with the following technical parameters: 120 kV, 220 mAs, 64 x 0.6 mm acquisition, 0.5 sec rotation time, 0.95 pitch reconstruction at 3 mm, and the LightSpeed VCT equipment (General Electric Medical Systems, Milwaukee, Wisconsin, USA) with parameters 120 kV, 700 mAs, acquisition 40 x 2.5 mm, rotation time of 0.5 sec. 1,375 pitch, 3 mm reconstruction. 80-100 ml of intravenous non-ionic contrast medium (Iopromide, Ultravist 370; Schering, Berlin, Germany) were used at an infusion rate of 3 - 4 ml / sec followed by a 40 ml bolus of saline, using an automatic injector.

The injection was performed through a 16-18G forearm route or through a jugular central venous catheter in hospitalized patients. Arterial acquisition was performed at 35 seconds with a craniocaudal scan in apnea after deep inspiration. Most of the arterial tomographic series evaluated were part of multiphasic protocols with subsequent acquisitions in portal phases (40-60 sec), venous (80 sec) or late (3 min).

Image analysis

Three radiologists in training: (G.B., V.I.T.C., D.A.S.N.) with 4, 3 and 3 years of experience in abdominal imaging, respectively, jointly reviewed all the MDCTAs and the angiographic images on a picture archiving and communication systems (PACS) workstation (Carestream Vue, version 12.1.5, Carestream Health, Rochester, NY, USA).

CT variants were registered on a database using the Microsoft Excel calculation program (Microsoft Corporation, USA), and the data analysis was performed with the Stata statistical program (StataCorp, USA). To perform the different measurements, multiplanar reconstructions and the linear or curved measurement tools were used in the Picture Archiving and communications system "PACS" (Carestream, Rochester, NY, USA).

Three-dimensional volumetric reconstructions and maximum intensity projections were obtained to demonstrate the most representative variants. The morphology of CT was classi-

fied according to Marco-Clement (Marco et al., 2016).

Statistical analysis

Data are presented as number and relative percentages. Quantitative variables are expressed as mean value. We compared categorical variables with the Fisher or the Chi-square test, as appropriate. For continuous variables, we used Student's t-test for parametric data distribution. P- value < 0.05 was considered statistically significant.

RESULTS

Patients

During this research, MDCT angiographies from 200 patients were analyzed, of which 73 were excluded due to surgical history, neoplasia or atheroma plaques involving the celiac trunk or branches. In total 127 patients were included for the main analysis, 67 (52.8%) female and 60 (47.2%) male. The mean age was 49.3 ± 14.1 years (range: 20-85 years).

CT Classification

We describe variations according to the previously commented classification that use four main types of CT (Marco-Clement et al., 2016). Distribution according Type and Gender is shown in Table 1.

Type I

Complete trunk in which LGA, SA and CHA arise from a common trunk was found in 109 patients (109/127; 85.8%) (Fig. 1). As Type I is considered to be a proper celiac trunk, morphometric values were analyzed only in this group. We measured the CT length, ostium diameter and distance between the CT and the superior mesenteric artery. The mean length of the CT was 20.4 mm ± 6.5 mm (range: 6.1-44 mm). Ostium mean diameter was 7.7 mm ± 1.9 (range 4.1-18.9 mm). Mean distance between the CT and the Superior mesenteric artery was 7.3 mm ± 3.5 mm (range: 0.7-17.2 mm) (Table 2).

In Type Ia, LGA arise from the CT prior to the origin of CHA and SA. It was observed in 81 patients (81/127; 63.8 %). Type Ib corresponds to the classical Haller's Tripod, a trifurcated entity with an equidistant origin of LGA, SA and CHA. It was observed in 27 of patients (27/127; 21.3%). Type Ic is a trunk with an additional arterial branch (accessory common hepatic, dorsal pancreatic, phrenic or gastroduodenal). This pattern was observed in 1 patient (1/127; 0.8%).

Table 1. Incidence of variations of the celiac trunk by gender in our MDCT-angiography research.

Our series	Female	Male	Total
Type I (Complete Trunk)	57/67 (44.9 %)	52/60 (40.9 %)	109/127 (85.8 %)
Ia	42/67 (33.1 %)	39/60 (30.7 %)	81/127 (63.8 %)
Ib	14/67 (11 %)	13/60 (10.2 %)	27/127 (21.3 %)
Ic	1/67 (0.8 %)	0/60 (0 %)	1/127 (0.8 %)
Type II (Incomplete Trunk)	9/67 (7.1 %)	8/60 (6.3 %)	17/127 (13.4 %)
IIa	5/67 (3.9 %)	4/60 (3.1 %)	9/127 (7.1 %)
IIb	4/67 (3.1 %)	4/60 (3.1 %)	8/127 (6.3 %)
IIc	0/67 (0 %)	0/60 (0 %)	0/127 (0 %)
III "Absence of CT"	0/67 (0 %)	0/60 (0 %)	0/127 (0 %)
IV "Celiac-mesenteric trunk"	1/67 (0.8 %)	0/60 (0 %)	1/127 (0.8 %)

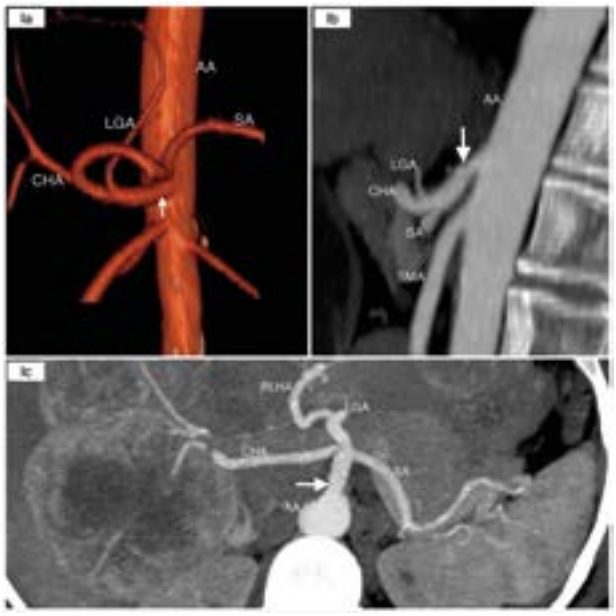

Fig. 1.- Type I" Complete Trunk: **Ia:** Complete bifurcated celiac trunk (LGA arises first); **Ib:** Complete trifurcated celiac trunk and **Ic:** Complete celiac trunk with extra branch. Abdominal Aorta (AA), Left Gastric Artery (LGA), Common Hepatic Artery (CHA), Splenic Artery (SA), Replaced Left Hepatic Artery (RLHA), White arrow (Celiac Trunk). In max intensity projection of sagittal reconstruction (first image) In three dimensional volumetric reconstruction (Ia) and Max intensity projection of sagittal reconstruction (Ib & Ic).

Table 2. Morphometric values of the Celiac Trunk (CT) Type I (complete Trunk).

n= 109/127 (85.8%)	CT l length (mm)	CT diameter (mm)	Distance between CT and SMA (mm)
Mean	20.45	7.72	7.35
Standard deviation	6.51	1.93	3.52
Range	37.9	14.8	16.5
Minimum	6.1	4.1	0.7
Maximum	44	18.9	17.2

Type II

Incomplete trunk in which either LGA, CHA and SA do not participate in the CT was found in 17 patients (17/127; 13.4 %). Gender distribution is shown in Table 1.

Type II is divided into three subtypes:

- Type IIa, hepato-splenic trunk was detected in 9 patients (9/127;7.1 %) (Fig. 2).
- Type IIb, gastro-splenic trunk was reported in 8 patients (8/127; 6.3%) (Fig. 3).
- Type IIc, hepato-gastric trunk, was not found in our patients.

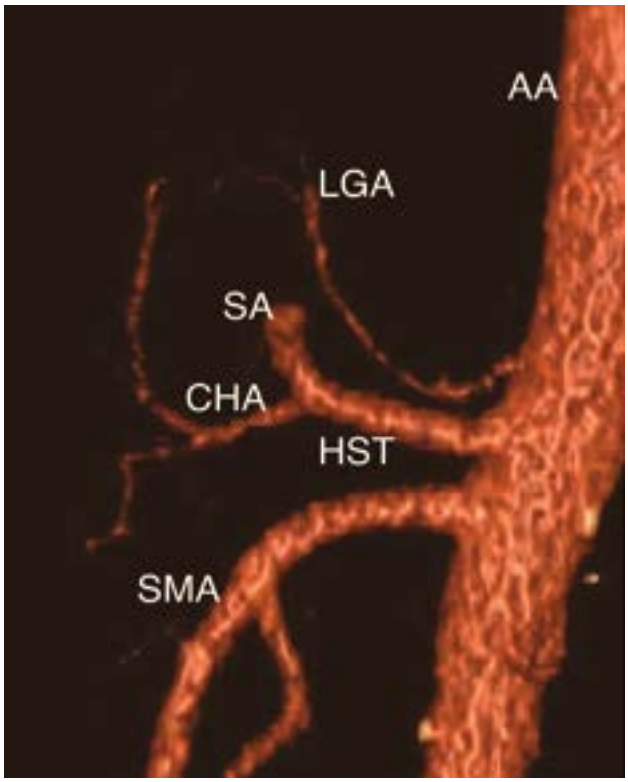

Fig. 2.- Three-dimensional volumetric reconstruction. "Type IIa" Hepatosplenic trunk (HST) with Left Gastric Artery (LGA) arising from the Abdominal Aorta (AA). Common hepatic Artery (CHA), Splenic Artery (SA) and Superior Mesenteric Artery (SMA) were identified.

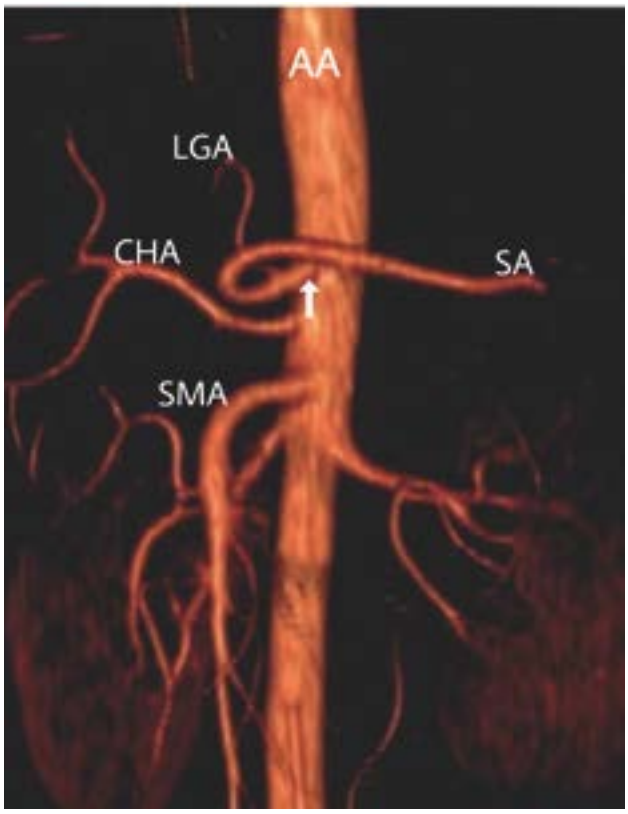

Fig. 3.- Three-dimensional volumetric reconstruction. "Type IIb" Gastrosplenic trunk (white arrow), Common Hepatic Artery (CHA) arising from the Abdominal Aorta (AA). Left Gastric Artery (LGA), Splenic Artery (SA) and Superior Mesenteric Artery (SMA) are shown.

***Type III*,** absence of the celiac trunk was not found in our patients (0%).

Type IV

Celiac-mesenteric trunk was found in 1 female (1/127; 0.8%) (Fig. 4).

Statistical analysis using Chi square test (a = 0.05) revealed no significant differences between genders in the presence of a CT variants, types or subtypes between genders.

DISCUSSION

MDCT angiography has become the primary tool for the evaluation of patients with suspected abnormalities of abdominal vessels. Three-dimensional and multiplanar imaging are non-invasive ways to examine the morphology of the celiac trunk and its branches, playing an important role by providing proper description and roadmaps of arterial morphology, previous surgical and radiological procedures such as liver transplantation or arterial chemoembolization (Nghiem et al., 1999; Winston et al., 2007; Song et al., 2010). This image

techniques reduce morbidity and mortality in pathologies as median arcuate ligament syndrome, celiac trunk aneurysm, celiac artery stenosis and occlusion. They are also used for detecting early vascular complications in post-intervention surveillance (Hiatt et al., 1994; Clark, 2006; Osman and Abdrabou, 2016).

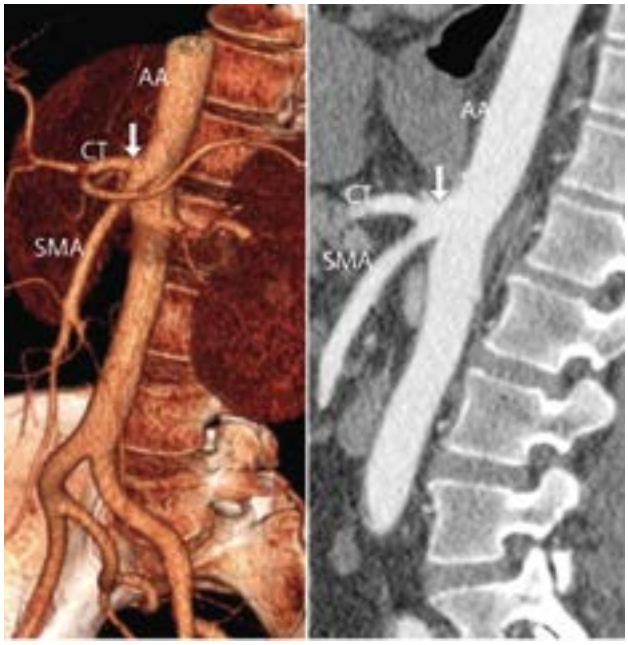

Fig. 4.- "Type IV" Celiac Trunk (CT) and Superior Mesenteric Artery (SMA) arising together from the Abdominal Aorta (AA) in a Celiac mesenteric Trunk (white arrow). Three-dimensional volumetric reconstruction (left image) and max intensity projection of sagittal reconstruction (right image).

The morphology of the abdominal vascular anatomy is highly variable and the celiac trunk (CT) is not an exception to this fact (Lippert Hans, 1985). Michels (1955) reported variation of the CT in 11% of its cadaver dissections. Similar rates have been reported on cadaveric studies with a range from 26.6 %, 15.7% (Lipshutz, 1917; Winter et al., 1995). In the MDCT era, Song et al. (2010) reported variations in 10.9% of their patients. Several image studies have reported prevalence of: 27.9%, 14.1 % and 9.5 (Eaton, 1917; Vandamme and Bonte, 1985; Hazirolan et al., 2009; Johnson et al., 2013; Marco-Clement et al., 2016). We found CT variations in 18 patients (18/127; 14.2%). In contrast, a previous cadaveric study in Mexican population reported a variation rate of 6% (Pineda et al., 2019).

Although using MDCT-angiography we obtained a higher prevalence of CT variation (14.2%), there was no statistically significant difference (p>0.05) with the prevalence of CT variations (6%) obtained in the first Mexican dissection study (Pineda et al., 2019).

Previous researches made by cadaver dissection and MDCT angio-tomography have described and published different classification systems according with their particular. Lipshutz (1917) described four CT patterns; Eaton (1917) proposed four geometrical categories; Adachi (1928) and Michels (1955) described six main groups based on cadaveric dissection, and Song et al. (2010) divided CT morphology in three categories. A recent study made a compilation of published cadaveric and radiological series, unifying and proposing a simpler and useful classification of 4 main Types (Marco-Clement et al., 2016). In Table 3 we describe the results and discussion according to this new and universal classification.

Type I

Type I (complete trunk), in which LGA, SA and CHA arise from a common trunk, was the most frequent Type reported in researches among general population with an observed prevalence of 72.1% to 90.5% (Iezzi et al., 2008; Marco-Clement et al., 2016). It was present in 109 of our patients (109/127; 85.8%). We agree with previous studies in the statement that Type I is the most common pattern observed. As Type I is considered to be a proper celiac trunk, morphometric values were analyzed only in this group (see Table 2).

Type II

Type II (incomplete trunk) can be divided in three subtypes, type IIa, IIb and IIIc. This pattern was observed in 17 patients (17/127; 13.4 %). Previous studies have reported a Type II prevalence of 7.5%, 10.9 and 11% (Rossi, 1904; Uflacker, 2007; Song et al., 2010). As an incomplete pattern, this can be considered the most frequent morphology variation CT can acquire. Although not all the studies can be adjusted to the new classification criteria due to insufficient anatomy description, the ones that could be adapted were included in the following Subtypes II analysis.

For Subtypes II the following analysis was made.

Type IIa (hepato-splenic trunk), with independent emergence of the LGA, was the most frequent

CT variation described in 9 patients (9/127; 7.1 %). It was also the most frequent type in studies made around in other countries such as Spain 4.45% (Marco-Clement et al., 2016), South Korea 4.42% (Song et al., 2010), Greece 3.34% (Panagouli et al., 2013) and Egypt 3% (Osman and Abdrabou, 2016).

Type IIb (gastro-splenic trunk), with independent emergence of CHA, was found in 8 patients (8/127; 6.3 %). The presence of this variation has been reported in range of between 0.22% and 5% in several studies (Winston et al., 2007; Song et al., 2010; Marco-Clement et al., 2016; Osman and Abdrabou, 2016). Although Michels (1955) and Eaton (1917) reported it as the most frequent variant present in 5.5% and 4.9% of their patients, it was the second most frequent variant reported in our study (distribution is shown in Table 3).

Type III

Type III (absence of celiac trunk) was not found in our sample. It has the lowest incidence reported: as with our research team, some other groups could not find it (Chen et al., 2009; Song et al., 2010; Marco-Clement et al., 2016). Other groups have reported its presence from 0.6% to 2% (Morita, 1935; Iezzi et al., 2008).

Type IV

Type IV (celiac-mesenteric trunk), the rarest variation form that the celiac trunk can acquire, interpreted as the result of the persistence of the large primitive ventral anastomosis between the early segmental celiac trunk and superior mesenteric groups (Tandler, 1904), was observed in only 1 female patient (1/127; 0.8%). This rare variation has been identified from 0.4% to 2.4% (Rossi, 1904; Lipshutz, 1917; Iezzi et al., 2008; Song et al., 2010; Osman and Abdrabou, 2016).

Statistical analysis using Chi square test (a = 0.05) revealed no significant differences in the presence of CT variants, types or subtypes between genders. Several studies have confirmed this lack of relation between gender and the presence of CT variation, although a relation with ethnicity has

Table 3. Compilation of results from worldwide researches, divided in four Types according to the new classification. Abbreviations: I, complete trunk; II, incomplete trunk, III, absence of CT; IV, Celiac-mesenteric trunk; Types are displayed on percentage (%); n, number of samples; c, cadavers; MDCT, Multidetector- row CT.

Author	n	T I				II				III	IV
			Ia	Ib	Ic		IIa	IIb	IIc		
(Rossi, 1904)	102 C	84.3	-	-	-	11.8	-	-	-	2	2
(Leriche, 1907)	55 C	89	-	-	-	10.9	-	-	-	0	0
(Descomps, 1910)	50 C	88			-	12				0	0
(Branco, 1912)	50 C	90				8				0	2
(Lipshutz, 1917)	83 C	73.4		25.3		24.1	13.3	4.8	6	0	2.4
(Eaton, 1917)	206 C	90.2				9.2	4.4	4.9	0	0	0
(Adachi, 1928)	252 C	87.7				8.8	6.4	2.4	0	0	3.5
(Michels, 1955)	200 C	89		25		11	4	5.5	1.5	0	0
(Vandamme and Bonte, 1985)	156 C	85.9				12.8				1.3	0
(Iezzi et al., 2008)	524 MDCT	72.1	50.4	19.4		10.9	5	2.3	3.6	0.6	0.4
(Chen et al., 2009)	974 C	89.8	66.6	23.2		8.5	4.4	3.9	0.2	0	1.5
(Song et al., 2010)	5002 MDCT	89.1				7.5	4.4	2.9	.2	00	1.8
(Ugurel et al., 2010)	100 MDCT	89				8	3	4	1	11	2
(Marco-Clement et al., 2016)	639 C + MDCT	90.5	57.6	32.1	0.8	9.5	4.5	5	0	0	0
Current series	127 MDCT	85.9	63.8	21.3	0.8	13.4	7.1	6.3	0	0	0.8

been shown (Panagouli et al., 2013). More studies should be made to assure it.

REFERENCES

ADACHI B (1928) Das Arteriensystem der Japaner. Vol II. Maruzen Publishing Co, Kyoto.

DO RIO-BRANCO P (1912). Essai sur l'anatomie et la medecine operatoire du tronc coeliaque et de ses branches, de l'artere hepatique en particulier. Paris: G. Steinheil.

CHEN H, YANO R, EMURA S, SHOUMURA S (2009) Anatomic variation of the celiac trunk with special reference to hepatic artery patterns. Ann Anat, 191: 399-407.

CLARK TWI (2006) Complications of hepatic chemoembolization. Semin Intervent Radiol, 23: 119-125.

DESCOMPS P (1910). Le tronc coeliaque. Paris: G. Steinheil.

EATON PB (1917) The coeliac axis. Anat Rec, 13: 369-374.

HAZIROLAN T, METIN Y, KARAOSMANOGLU AD, CANYIGIT M, TURKBEY B, OGUZ BS, ARI-YUREK M (2009) Mesenteric arterial variations detected at MDCT angiography of abdominal aorta. Am J Roentgenol, 192: 1097-1102.

HIATT JR, GABBAY J, BUSUTTIL RW (1994) Surgical anatomy of the hepatic arteries in 1000 cases. Ann Surg, 220: 50-52.

IEZZI R, COTRONEO AR, GIANCRISTOFARO D, SANTORO M, STORTO ML (2008) Multidetector-row CT angiographic imaging of the celiac trunk: Anatomy and normal variants. Surg Radiol Anat, 30: 303-310.

JOHNSON PB, CAWICH SO, ROBERTS P, SHAH S, GARDNER MT, GORDON-STRACHAN G, PEARCE NW (2013) Variants of hepatic arterial supply in a Caribbean population: A computed tomography based study. Clin Radiol, 68: 823-827.

LERICHE FV (1907) Recherches anatomiques sur les artères de l'estomac. Bibliogr Anat, 16: 111.

LIPPERT HANS PR (1985) Arterial Variations in Man: Classification and Frequency. J.F. Bergmann Verlag, München, pp 30-47.

LIPSHUTZ B (1917) A composite study of the celiac axis artery. Ann Surg, 65: 159-169.

MARCO-CLEMENT I, MARTINEZ-BARCO A, AHUMADA N, SIMON C, VALDERRAMA JM, SANUDO J, ARRAZOLA J (2016) Anatomical variations of the celiac trunk: cadaveric and radiological study. Surg Radiol Anat, 38: 501-510.

MICHELS NA (1955) Blood supply and anatomy of the upper abdominal organs with a descriptive atlas. Lippincott Company, Philadelphia, pp 136-147.

MORITA M (1935) Reports and conception of three anomalous cases in the area of the celiac and superior mesenteric arteries [in Japanese]. Igaku Kenkyu, 9: 1993-2006.

NGHIEM HV, DIMAS CT, MCVICAR JP, PERKINS JD, LUNA JA, WINTER TC, HARRIS A, FREENY PC (1999) Impact of double helical CT and three-dimensional CT arteriography on surgical planning for hepatic transplantation. Abdom Imaging, 24: 278-284.

OSMAN AM, ABDRABOU A (2016) Celiac trunk and hepatic artery variants: A retrospective preliminary MSCT report among Egyptian patients. Egypt J Radiol Nucl Med, 47: 1451-1458.

PANAGOULI E, VENIERATOS D, LOLIS E, SKANDALAKIS P (2013) Variations in the anatomy of the celiac trunk: A systematic review and clinical implications. Ann Anat, 195: 501-511.

PINEDA M, FIGUEROA V, CASTILLO S, ANDA M, PRADEL A, LEÓN E, MENDIZÁBAL A (2019) Morfometría y variantes anatómicas del tronco celíaco en población mexicana. Int J Morphol, 37: 174-177.

ROSSI EC (1904) Studio morfologico delle arterie dello stomaco. Arch Ital Anat Embryol, 255: 278-288.

SEHGAL G, SRIVASTAVA AK, SHARMA PK, KUMAR N, SINGH R, PARIHAR A, AGA P (2013) Morphometry of the celiac trunk: A multidetector computed tomographic angiographic study. J Anat Soc India, 62: 23-27.

SONG SY, CHUNG JW, YIN YH, JAE HJ, KIM HC, JEON UB, CHO BH, SO YH, PARK JH (2010) Celiac axis and common hepatic artery variations in

5002 patients: Systematic analysis with spiral CT and DSA. Radiology, 255: 278-288.

TANDLER J (1904) Über die Varietäten der Arteria coeliaca und deren Entwicklung. Beiträge Ref Anat Entwicklungsgesch, 25: 473-500.

UFLACKER R (2007). Atlas of Vascular Anatomy: An Angiographic Approach. LWW medical book collection. 2ª Ed. Lippincott Williams & Wilkins. ISBN: 078176081X, 9780781760812.

UGUREL MS, BATTAL B, BOZLAR U, NURAL MS, TASAR M, ORS F, ET AL (2010). Anatomical variations of hepatic arterial system, coeliac trunk and renal arteries: an analysis with multidetector CT angiography. Br J Radiol, 83: 661-7.

VANDAMME JPJ, BONTE J (1985) The branches of the celiac trunk. Cells Tissues Organs, 122: 110-114.

VENARA A, PITTET O, LU TL, DEMARTINES N, HALKIC N (2013) Aberrant right hepatic artery with a prepancreatic course visualized prior to pancreaticoduodenectomy. J Gastrointest Surg, 17: 1024-1026.

VON HALLER A (1756) Icones Anatomicae Quibus Praecipuae Aliquae Partes Corporis Humani Delineatae Proponuntur & Arteriarum Potissimum Historia. Göttingen.

WINSTON CB, LEE NA, JARNAGIN WR, TEITCHER J, DEMATTEO RP, FONG Y, BLUMGART LH (2007) CT angiography for delineation of celiac and superior mesenteric artery variants in patients undergoing hepatobiliary and pancreatic surgery. Am J Roentgenol, 189: 123.

WINTER TC, NGHIEM HV, FREENY PC, HOMMEYER SC, MACK LA (1995) Hepatic arterial anatomy: demonstration of normal supply and vascular variants with three-dimensional CT angiography. Radiographics, 15: 771-780.

Potential protective effect of eicosapentaenoic and docosahexaenoic acids versus necrotizing enterocolitis, mitochondrial and rough endoplasmic reticulum stress mediated pathway

Ahmed S. Ahmed

Anatomy and Embryology Department, College of Medicine, Tanta University. Tanta 31511, Egypt

SUMMARY

Necrotizing enterocolitis (NE) is a medical condition mediated by oxidative stress to the small intestine. Fish oil is a natural component rich in healthy fatty acids such as eicosapentaenoic and docosahexaenoic acids with anti-inflammatory anti-apoptotic role. Endoplasmic reticulum stress mediates many oxidative diseases such as diabetes mellitus and neurodegeneration, associated by the release of many caspase subtypes that promotes cellular apoptosis. Mitochondrial stress also causes the release of many caspase variants together with mitochondrial Deoxyribonucleic acid (mtDNA). The aim of the present study is to appraise the role mediated by both endoplasmic reticulum (ER) &mitochondria stress in the pathogenesis of necrotizing enterocolitis and to explore the therapeutic effects of eicosapentaenoic and docosahexaenoic acids. Ninety rats' pups were used (one day old), divided into three groups, (1) C-group: control group; (2) NE-group: necrotizing enterocolitis group, and (3) NE-FO-group: necrotizing enterocolitis pre-fed with fish oil group. At day 11, 12 and 13 ten pups from each group were sacrificed for intestinal sample collection. Histological examinations, Enzyme-linked immunosorbent assay, and western and Southern blot were performed. NE group showed severe histopathological changes. NE-FO group showed regain of most of normal histopathological feature. Levels of TNF-α and IL-6 increased markedly in NE group if compared to NE-FO group. Caspase 12 and caspase 9 levels in NE group were higher than in NE-FO group. The levels of GRB-78 and mtDNA were high in NE-FO group if compared to control group, but lower than levels of NE group. In conclusion, eicosapentaenoic acid and docosahexaenoic acid can protect against neonatal necrotizing enterocolitis. Mitochondrial and endoplasmic reticulum stress pathway demonstrated to mediate necrotizing enterocolitis pathological changes. Thus, fish oil offers a natural option to prevent and treat the clinical manifestation of NE.

Key words: Eicosapentaenoic – Docosahexaenoic – Mitochondria – Rough endoplasmic reticulum – Stress

Corresponding author:
Ahmed S. Ahmed. 13 Al-Bahr street, Tanta (31511), Gharbia, Egypt.
E-mail: Ahmedsahmed.tanta@gmail.com

Submitted: May 7, 2020. **Accepted:** September 17, 2020

INTRODUCTION

Necrotizing enterocolitis (NE) is a medical emergency (Mehdi et al., 2012), first described in the eighteenth century and affecting mainly newborn infant of both sexes during the first four weeks of life. The underlying cause is poor blood supply to the intestine; resulting in tissue hypoxia, oxidative stress, inflammation [mediated by tumor necrosis factor-α (TNF-α) and interleukin-6(IL-6)] and cellular apoptosis (Li and Sheng, 2018). Drinking breast milk [rich in docosahexaenoic acid (DHA)] during the first days of life is considered prophylactic to the intestine from such pathology, as announced in 2012 by American Academy of Pediatrics (Pet et al., 2018). The typical clinical picture is feeding intolerance, abdominal distention and bloody stool. It may cause intestinal perforation and peritonitis. Many promising approaches for medical treatment appear in the horizon such as usage of DHA and arachidonic acid (Najm et al., 2017). Fish oil (FO) is extracted from fish, especially oily ones; it is marketed as a dietary supplement and ointments. Salmon-, sardine- and mackerel-extracted FO is the richest in content of healthy fatty acids (Serdarevic et al., 2019). To gain relative prophylaxis against prostate cancer, cardiovascular diseases, hypertension, Alzheimer disease and psoriasis, the daily dietary recommended intake of fish oil is 200 mg (Parker et al., 2019). FO was found to be very protective against many inflammatory bowel diseases such as Crohn's disease (Parian and Limketkai, 2016), as it contains many anti-inflammatory compounds (Goel et al., 2018). It is very rich in omega-3 and omega-6 fatty acids, such as eicosapentaenoic acid (EPA) AND docosahexaenoic acid (DHA), which have anti-inflammatory role protecting the mucosal lining of the intestine (Zhang et al., 2018). These two fatty acids have an anti-apoptotic effect on hepatic, cardiac and nervous tissue cells through their rough endoplasmic reticulum and mitochondrial supporting role (Ajith, 2018).

Endoplasmic reticulum (ER) is a membranous cellular organelle which is classified as a cytoplasmic organelle (Phillips and Voeltz, 2016). Two types of ER are found, smooth (SER) and rough (RER). Both are formed of interconnected cisternae (Di, 2013), and they can be distinguished from each other by the ribosomes that are attached to the cytoplasmic surface of RER and absent from SER. RER is responsible for protein synthesis by transferring unfolded proteins to the Golgi apparatus, while SER is involved in lipid synthesis (Wang and Kaufman, 2016). Hypoxia, glucose deprivation and viral infection slow down the transfer of proteins from RER, which result in accumulation of unfolded proteins and glucose regulated protein-78 (GRP-78) in the cytoplasm of the cell, which is considered rough endoplasmic stress (RES) condition (Li et al., 2019). RES is the common share of many diseases such as diabetes mellitus, viral infection, neurodegeneration and neoplasm. RES is associated by the release of many caspase subtypes located on RER surface, causing cellular apoptosis (Lin et al., 2017).

Mitochondria is a double membrane enclosed organelle found in most of eukaryotic cells with some exceptions such as red blood cells (Nadalutti, 2020). It is responsible for adenosine triphosphate (ATP) synthesis (Hemono et al., 2020). It has an outer (smooth) membrane and inner (thrown into folds) membrane forming a shelf-like projection into the matrix of mitochondria called cristae. Obesity and excess oxidation results in mitochondrial stress with release of many caspase subtypes and mitochondrial Deoxyribonucleic acid (mtDNA) (Mohamed and Eltony, 2020; Lyu et al., 2020; Xie et al., 2020).

The aim of the present study is to appraise the role mediated by both RER and mitochondria stress in the pathogenesis of necrotizing enterocolitis and to explore the therapeutic effects of EPA and DHA.

MATERIALS AND METHODS

Chemicals

Fish oil, lipopolysaccharide water soluble (5 mg/ml), western and southern blot kits were purchased from Sino pharm Chemical Reagent Co., Ltd., Shanghai Shi, China.

Animals

Ninety albino Wistar rat pups were used (one day old), with an average weight of 20 gm. Animals were housed individually and fed with milk formula by gavage. 12-hour light/dark cycle was kept. By the

help of air conditions, the temperature was kept at 25º C (in accordance to national and institutional guidelines), and humidity at 55%. This research study was approved by the Research and Ethics Committee, Quality Assurance Unit, Faculty of Medicine, Tanta University, Egypt.

Experimental design

Rats are divided into three groups (n=30). The control group (C-group) received saline by gavage for seven days (5ml/d); the necrotizing enterocolitis group (NE-group) received saline by gavage for seven days (5ml/d); and the necrotizing enterocolitis fed with fish oil group (NE-FO-group) received fish oil by gavage for seven days (5ml/d). Throughout the whole first ten days, the general appearance of abdominal size and stool was checked daily. NE rat model was performed along days 8, 9 and10 by creating as state of hypoxia and hypothermia to the pups, by placing them twice daily in hypoxic chamber for ninety seconds, and then Çransferring them to hypothermic chamber (4ºC) for 600 seconds. Between the two settings, 10 mg/kg b.w. of lipopolysaccharides were administered by gavage to pups (Zhu et al., 2020). On day 11, 12 and 13, ten pups from each group were sacrificed for intestinal sample collection.

Clinical score

Pups body weight, abdominal distention, stool macroscopic blood, response to touch and color of skin were recorded daily and a score is given ranging from zero (worst) to twelve (best) (Table 1).

Histological examinations

Samples from the terminal part of the ileum were collected on days 11,12 and 13, and were fixed in 10% buffered paraformaldehyde, dehydrated, embedded in paraffin, and then sectioned at 5 µm by using 7manually operated rotary microtome CUT 4050 (4050F, R) (Microtec Laborgeräte GMBH, Germany). Sections were stained with hematoxylin and eosin for histopathological assessment. Histopathological examinations were performed by two expert histopathologists blinded to our study. Scoring was done as per lesion severity, as shown in (Table 2).

Table 1. Clinical score criteria.

Score	Abdomen distention	Stool blood	Touch response	Skin color
12	Non	Non	Normal	Pink
9	Mild	Mild	Sluggish	Pale on pressure
6	Moderate	Moderate	Response to crude touch	Pale without pressure
3	Sever	Sever	Response to pain	Limbs cyanosis
0	Extensive	Extensive	Non	Generalized cyanosis

Table 2. Scoring of histopathological sections, if score is > 2 NE was considered.

Score	Feature
0	Intact villous and mucosa
1	Mild separation between submucosa and lamina propria
2	Moderate separation between submucosa and lamina propria
3	Sever separation between submucosa and lamina propria or fall out of villi
4	Villi necrosis and disappearance

Enzyme-linked immunosorbent assay

Intestinal tissue was homogenized and centrifuged at 4000 rpm. Supernatant was used to detect TNF-α and IL-6 by help of the ELIZA kit (Sino pharm). Coating, blocking, incubation with enzyme-labelled antibody, substrate addition and signal detection are the main steps followed to detect the inflammatory markers (Kragstrup et al., 2013).

Western and southern blot

They are used to estimate the intestinal tissue content of caspase-9 and mtDNA as indicators for mitochondrial stress, and caspase-12 & GRB-78 as indicator of endoplasmic reticulum stress. Western blotting methodology started by extraction of proteins from intestinal tissues by the help of radioimmunoprecipitation assay (RIPA) buffer, followed by protein separation by gel electrophoresis, transfer to polyvinylidene fluoride (PVDF) membrane, blocking the rest of surface of high protein affinity membrane, incubation with primary antibody (caspase-12, caspase-9 & GRB-

78) overnight, then incubation with secondary antibody for one hour finally analysis of the data expressed. Southern Blot kits were purchased from Thermo Fisher Scientific Inc. (USA). Anza™ T4 DNA Ligase Master Mix, IVGN2108 was used for mtDNA digestion. Fragmented DNA was typically electrophoresed on an Acrylamide gels; then DNA was transferred to a positively charged nylon membrane. Nucleic acid probe, RadPrime DNA Labeling System, 18428011 was incubated with the substrate, followed by hybridization and washing. BrightStar BioDetect Kit was used for mitochondrial DNA detection. (Dandelot and Gourdon, 2018).

RESULTS

Clinical score

The control group scored the best results after daily observation and scoring of each pup according to body weight, abdominal distention, stool macroscopic blood, response to touch and skin color. NE group showed significant ($p < 0.05$) score decrease, while NE-FO regained good results if compared to NE group, but its scoring was non-significantly ($p > 0.05$) lowered if compared to control group (Fig. 1).

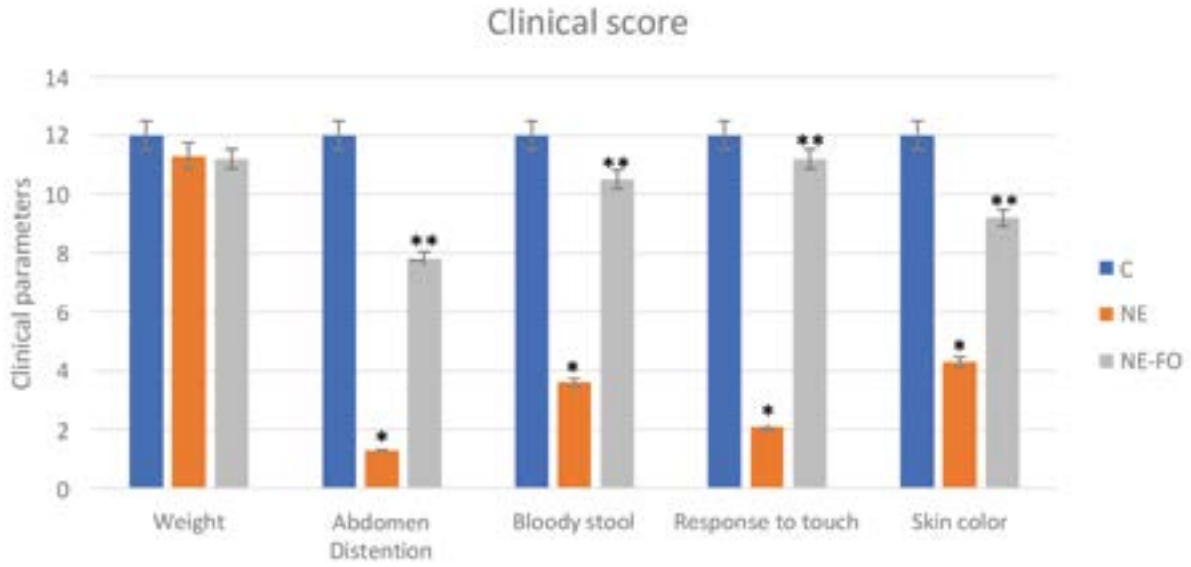

Fig. 1.- Clinical score represents changes in body weight, abdominal distention, stool macroscopic blood, response to touch and color of skin. (C) control group, (NE) necrotizing enterocolitis group, (NE-FO) necrotizing enterocolitis fed with fish oil group. * significant difference ($p < 0.05$) in comparison to C-group. ** significant difference ($p < 0.05$) in comparison with NE-group. Data are presented as mean ± standard deviation, ($n = 30$).

Statistical analysis

Statistical Package for Social Sciences (SPSS) software, 20 V. (SPSS Inc., USA) was used for data analysis. The statistical significance of differences between groups was validated using one-way analysis of variance (ANOVA). Post hoc Tukey-Kramer test was used for group comparison. Data were expressed in mean ± standard deviation and probability value was considered significant if < 0.05.

Histological examinations

Histopathological examination of the intestinal wall showed normal histological architecture of intestinal wall layers in the control group, the four layers of intestinal wall (mucosa, submucosa, muscularis propria & adventitia) appeared healthy. NE group showed severe histopathological changes on day 13, mucosal inflammation, sloughing of villi, inflammatory cells infiltration and spacing between submucosa & muscularis mucosa were noticed. NE-FO group showed regain of most healthy histological feature if compared to control group, while some inflammatory cell infiltration was noticed on day 13 (Fig. 2).

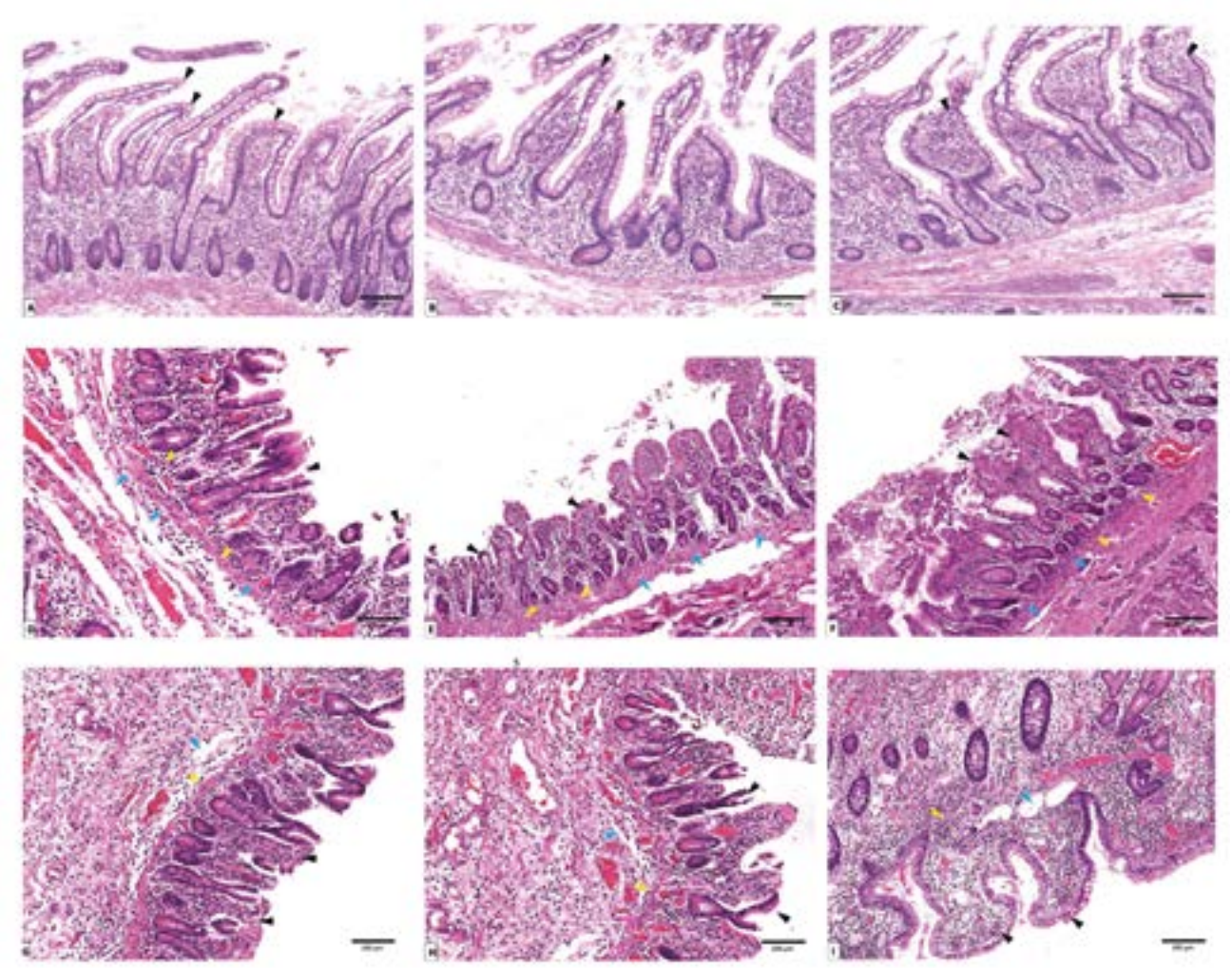

Fig. 2.- Photomicrograph of sections of rats' terminal part of the ilium stained with hematoxylin and eosin, magnification (x 1000). (A, B, C) represent control group on days 11, 12 and 13 respectively. (D, E, F) represent NE group on days 11, 12 and 13 respectively. (G, H, I) represent NE-FO group on days 11, 12 and 13 respectively. Note: villi (black arrow), submucosal edema (blue arrow), inflammatory cells infiltration (yellow arrow).

Scoring of histopathological findings are shown in (Fig. 3). On day 11, 12 and 13, NE-FO group score was significantly ($p < 0.05$) lower than that of NE group, by 40.81%, 23.53%, and 34.34%, respectively.

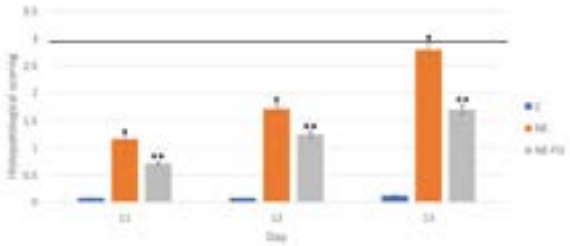

Fig. 3.- Scoring of histopathological finding done by blinded observer to our study. * significant difference ($p < 0.05$) in comparison to C-group. ** significant difference ($p < 0.05$) in comparison with NE-group. Data are presented as mean ± standard deviation, (n = 30).

Enzyme-linked immunosorbent assay

Levels of TNF-α and IL-6 increased significantly ($p < 0.05$) in NE group if compared to NE-FO group. Inflammatory markers levels in NE-FO group were significantly ($p < 0.05$) higher than that of the control group (Fig. 4). IL-6 scores of NE group on day 11,12 and13 were higher than those of control group by 8.08%, 61.74%, and 78.58%, respectively, and those of TNF-α in the NE group were higher than C group by 5.62%, 42.01%, and 72.82%, respectively.

Western and southern blot

Blotting of intestinal tissue proteins showed that caspase - 9, 12 levels in NE group were significantly ($p < 0.05$) increased if compared to NE-FO group. The levels of GRB-78 & mtDNA were significantly ($p < 0.05$) higher if NE-FO group was compared to control group, but significantly ($p < 0.05$) lower than that of NE group (Fig. 5).

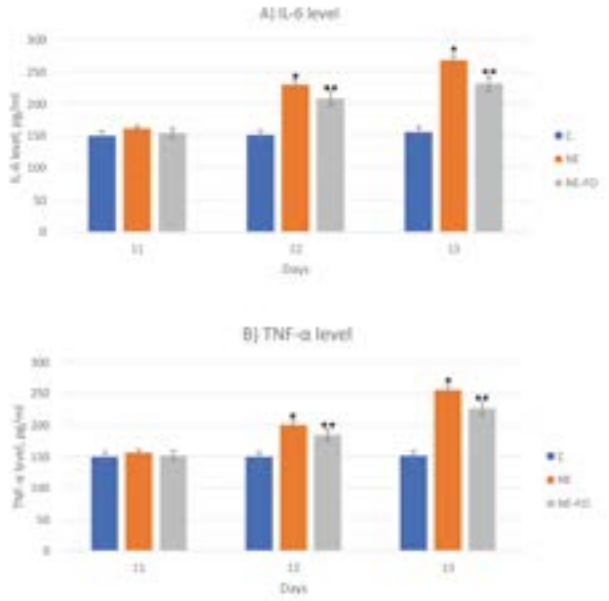

Fig. 4.- Level of inflammatory markers in the intestinal tissueon days 11, 12 and 13 (**A**) IL-6 level. (**B**) TNF-α level. * significant difference ($p < 0.05$) in comparison to C-group. ** significant difference ($p < 0.05$) in comparison with NE-group. Data are presented as mean ± standard deviation, (n = 30).

DISCUSSION

Necrotizing enterocolitis is a medical problem that came to the surface along the past 30 years. 90% of NE patients are premature infants with 20% mortality rate. This research paper was designed to understand the underlying mechanism NE on a cellular basis and to explore the protective effects of some omega-3 fatty acids.

Our results showed that there is a marked decrease in NE clinical score if compared to the control group, which comes in agreement with other researchers. Aktaş et al. (2017) reported massive fecal blood as a common sign of NE, mainly in premature infants. Abdominal distention and absence of intestinal sound was reported by Lin et al. (2019). We found a decrease in response to touch with peripheral cyanosis in NE group, and to a less extent in NE-FO group in certain parameters such as abdominal distention. The clinical score of NE-FO was enhanced due to the effect of the ingested fish oil as agreed by Najm et al. (2017), who reported the beneficial effects of fish oil on necrotizing enterocolitis, bronchopulmonary dysplasia and patency of ductus arteriosus.

Histopathological examination of terminal part of the ileum in the control group showed healthy layers of intestinal wall with vivid villi, submucosa, muscle layer and the outer serosa covering (Inamoto et al., 2008). In NE group, our results showed a severe intestinal wall inflammation with inflammatory cells infiltration (mainly mucosal lining) with necrosis and sloughing of villi. Edema and spacing appeared between mucosa and submucosa, which comes in agreement with Gross et al. (2017), who added that inhibition of 5-hydroxytryptamine synthesis reduced the mucosal inflammation on intestine. McElroy et al. (2013) hypothesized that blood vessels vasculitis and occlusion may be the direct cause of villous necrosis in NE. While, MohanKumar et al. (2019) reported that submucosal edema occurs within twelve hours of NE onset associated with sever mucosal inflammation and villous necrosis.

In the present study, the intestinal histological architectureinNE-FOgroupappearedtobehealthy, with regain of most of normal histopathological feature after fish oil pretreatment: this could be explained by its content of both docosahexaenoic and eicosapentaenoic acids with their anti-inflammatory and antioxidant potential. Molfino et al. (2017) reported that DHA has the ability to inhibit different inflammatory pathways by inhibiting inflammatory-related cytokines synthesis. This anti-inflammatory potential was reported by Irún et al. (2019), who reported that the anti-inflammatory potential of DHA is not associated with immunosuppression. Ochi et al. (2018) reported the antioxidant and anti-inflammatory capacity of EPA mainly in muscle tissue after exercise related stress.

Our study showed that Levels of TNF-α and IL-6 increased markedly in NE group if compared to NE-FO group. This comes in concession with Li et al. (2018), who reported that inflammatory markers reach their peak within twenty-four hours and start to fall after seventy-two hours. This could be due to the anti-inflammatory capacity of eicosapentaenoic acid as stated by Augimeri et al. (2019).

However, Gomes et al. (2017) mentioned that NE is associated with elevated levels of caspase-3 which mediate cellular apoptosis. In addition, Buyuktiryaki et al. (2019) reported elevated levels of caspase 3, 8 and 9 in NE. In our study, NE group showed elevated caspase 9 and caspase 12 levels in intestinal tissue higher than those of NE-FO group. Katoh et al. (2004) mentioned that caspase-9

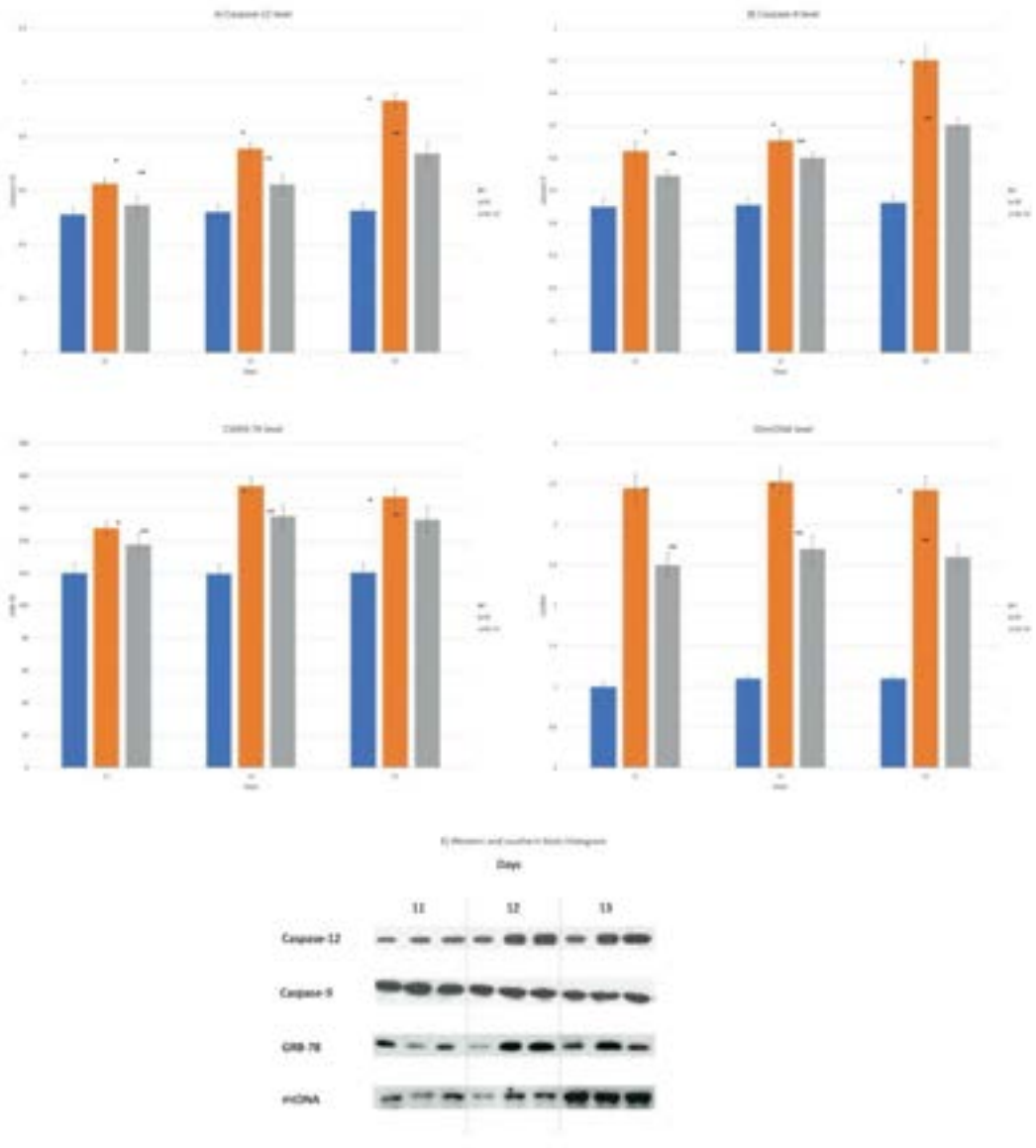

Fig. 5.- (**A, B** and **C**) represent western blot quantitative analysis of caspase 12, caspase 9 and GRB-78, respectively. (**D**) represents southern blot quantitative analysis of mtDNA in the intestinal tissue (days 11, 12 and 13). (**E**) Histogram represents the ratio of optical density of caspase-12, caspase-9, GRB-78 and mtDNA. * significant difference ($p < 0.05$) in comparison to C-group. ** significant difference ($p < 0.05$) in comparison with NE-group. Data are presented as mean ± standard deviation, (n = 30).

accumulate in the stressed mitochondria. Other researcher stated that caspase-12 is elevated in ischemic brain tissue after ischemia-reperfusion model as a sign of endoplasmic reticulum stress (Xing et al., 2019). The relative decrease in apoptotic markers noticed at our research in NE-FO group could be related to the anti-apoptotic effect of EPA. Fayez and Zaafan (2018) reported the potent antiapoptotic, anti-inflammatory and antioxidant capacity of EPA.

In our study, levels of GRB-78 and mtDNA were high in NE-FO group if compared to control group, but lower than levels of NE group which could result from endoplasmic reticulum and mitochondrial stress respectively. Zhu et al. (2020) linked between ER stress and elevated tissue level of GRP-78. Ding et al. (2011) mentioned also the elevated level of GRB-78 in the kidney tissue resulting from ER stress. Baregamian et al. (2009) stated that necrotizing enterocolitis is associated with disturbed mitochondrial functions and elevated levels of mtDNA in intestinal tissue. Other researcher (Sas et al., 2018) related healthy mtDNA to properly functioning mitochondria. Shao et al. (2006) reported the upregulated mtDNA in cases of mitochondrial stress. The decreased levels of GRB-78 and mtDNA after fish oil pretreatment in NE-FO group may be

due to the anti-apoptotic effect of DHA, as stated by Bazan et al. (2010). In conclusion, the present study revealed the shielding effect of eicosapentaenoic acid and docosahexaenoic acid against neonatal necrotizing enterocolitis through their anti- inflammatory and antioxidant effects. We also demonstrated that necrotizing enterocolitis is mediated by mitochondrial and endoplasmic reticulum stress pathway. So, fish oil offers a natural option to prevent and treat the clinical manifestation of NE. Further studies are requires determining the exact signaling pathway mediating NE pathological changes.

REFERENCES

AJITH TA (2018) A recent update on the effects of omega-3 fatty acids in Alzheimer's disease. Curr Clin Pharmacol, 13(4): 252-260.

AKTAŞ S, ERGENEKON E, ÜNAL S, TÜRKYILMAZ C, HIRFANOĞLU İM, ATALAY Y (2017) Different presentations of cow` s milk protein allergy during neonatal period. Turk J Pediatr, 59(3): 322-328.

AUGIMERI G, PLASTINA P, GIONFRIDDO G (2019) N-Eicosapentaenoyl dopamine, a conjugate of dopamine and eicosapentaenoic acid (EPA), exerts anti-inflammatory properties in mouse and human macrophages. Nutrients, 11(9): 2247.

BAREGAMIAN N, SONG J, BAILEY CE, PAPACONSTANTINOU J, EVERS BM, CHUNG DH (2009) Tumor necrosis factor-alpha and apoptosis signal-regulating kinase 1 control reactive oxygen species release, mitochondrial autophagy, and c-Jun N-terminal kinase/p38 phosphorylation during necrotizing enterocolitis. Oxid Med Cell Longev, 2(5): 297-306.

BAZAN NG, CALANDRIA JM, SERHAN CN (2010) Rescue and repair during photoreceptor cell renewal mediated by docosahexaenoic acid-derived neuroprotectin D1. J Lipid Res, 51(8): 2018-2031.

BUYUKTIRYAKI M, TAYMAN C, KOYUNCU I (2019) Therapeutic and preventative effects of ankaferd blood stopper in an experimental necrotizing enterocolitis model. Biomed Pharmacother, 110: 105-110.

DANDELOT E, GOURDON G (2018) The flash-small-pool PCR: how to transform blotting and numerous hybridization steps into a simple denatured PCR. Biotechniques, 64 (6): 262-265.

DI GIROLAMO M, FABRIZIO G, SCARPA ES, DI PAOLA S (2013) NAD+-dependent enzymes at the endoplasmic reticulum. Curr Top Med Chem, 13(23): 3001-3010.

DING Y, ZOU J, LI Z (2011) Study of histopathological and molecular changes of rat kidney under simulated weightlessness and resistance training protective effect. PLoS One, 6(5): e20008.

FAYEZ AM, ZAAFAN MA (2018) Eicosapentaenoic acid and vitamin E against doxorubicin induced cardiac and renal damages: role of cytochrome c and iNOS. Arch Iran Med, 21(11): 502-508.

GOEL A, POTHINENI NV, SINGHAL M, PAYDAK H, SALDEEN T, MEHTA JL (2018) Fish, fish oils and cardioprotection: promise or fish tale? Int J Mol Sci, 19(12): 3703.

GOMES RO, ARTIGIANI R NETO, GUIMARÃES JF NETO, NUNES AP, MONTERO EF, MARTINS JL (2017) Neonatal necrotizing enterocolitis rat model attenuated by a remote ischemic preconditioning in the pregnant. Acta Cir Bras, 32(3): 236-242.

GROSS MARGOLIS K, VITTORIO J, TALAVERA M (2017) Enteric serotonin and oxytocin: endogenous regulation of severity in a murine model of necrotizing enterocolitis. Am J Physiol Gastrointest Liver Physiol, 313(5): G386-G398.

HEMONO M, UBRIG É, AZEREDO K, SALINAS-GIEGÉ T, DROUARD L, DUCHÊNE AM (2020) Arabidopsis voltage-dependent anion channels (VDACs): overlapping and specific functions in mitochondria. Cells, 9(4): E1023.

INAMOTO T, KAWATA Y, QI WM (2008) Ultrastructural study on the epithelial responses against attachment of indigenous bacteria to epithelial membranes in Peyer's patches of rat small intestine. J Vet Med Sci, 70(3): 235-241.

IRÚN P, LANAS A, PIAZUELO E (2019) Omega-3 polyunsaturated fatty acids and their bioactive metabolites in gastrointestinal malignancies related to unresolved inflammation. a review. Front Pharmacol, 10: 852.

KATOH I, TOMIMORI Y, IKAWA Y, KURATA S (2004) Dimerization and processing of pro-

caspase-9 by redox stress in mitochondria. J Biol Chem, 279(15): 15515-15523.

KRAGSTRUP TW, VORUP-JENSEN T, DELEURAN B, HVID M (2013) A simple set of validation steps identifies and removes false results in a sandwich enzyme-linked immunosorbent assay caused by anti-animal IgG antibodies in plasma from arthritis patients. Springer plus, 2(1): 263.

LI J, LI X, LIU D (2019) EIF2α signaling regulates autophagy of osteoblasts and the development of osteoclasts in OVX mice. Cell Death Dis, 10(12): 921.

LI Z, SHENG L (2018) Significance of dynamic evolution of TNF-α, IL-6 and intestinal fatty acid-binding protein levels in neonatal necrotizing enterocolitis. Exp Ther Med, 15(2): 1289-1292.

LIN L, XIA X, LIU W, WANG Y, HUA Z (2019) Clinical characteristics of neonatal fulminant necrotizing enterocolitis in a tertiary Children's hospital in the last 10 years. PLoS One, 14(11): e0224880.

LIN Y, HUANG JJ, DAHMS HU, ZHEN JJ, YING XP (2017) Cell damage and apoptosis in the hepatopancreas of Eriocheir sinensis induced by cadmium. Aquat Toxicol, 190: 190-198.

LYU AR, KIM TH, PARK SJ (2020) Mitochondrial damage and necroptosis in aging cochlea. Int J Mol Sci, 21(7): E2505.

MCELROY SJ, UNDERWOOD MA, SHERMAN MP (2013) Paneth cells and necrotizing enterocolitis: a novel hypothesis for disease pathogenesis. Neonatology, 103(1): 10-20.

MEHDI I, AL BAHRANI B (2012) Chemotherapy-induced neutropenic necrotizing enterocolitis: a review. J Pak Med Assoc, 62(7): 718-723.

Mohamed HK, Eltony SA (2020) Effect of acute pentylenetetrazol injection induced epileptic seizures on rat dentate gyrus at different postnatal ages. Anat Cell Biol, 53(1): 84-94.

MOHANKUMAR K, NAMACHIVAYAM K, SONG T (2019) A murine neonatal model of necrotizing enterocolitis caused by anemia and red blood cell transfusions. Nat Commun, 10(1): 3494.

MOLFINO A, AMABILE MI, MONTI M, MUSCARITOLI M (2017) Omega-3 polyunsaturated fatty acids in critical illness: anti-inflammatory, proresolving, or both? Oxid Med Cell Longev, 2017: 5987082.

NADALUTTI CA, STEFANICK DF, ZHAO ML (2020) Mitochondrial dysfunction and DNA damage accompany enhanced levels of formaldehyde in cultured primary human fibroblasts. Sci Rep, 10(1): 5575.

NAJM S, LÖFQVIST C, HELLGREN G (2017) Effects of a lipid emulsion containing fish oil on polyunsaturated fatty acid profiles, growth and morbidities in extremely premature infants: A randomized controlled trial. Clin Nutr ESPEN, 20: 17-23.

OCHI E, TSUCHIYA Y (2018) Eicosapentaenoic acid (EPA) and docosahexaenoic acid (DHA) in muscle damage and function. Nutrients, 10(5): 552.

PARIAN A, LIMKETKAI BN (2016) Dietary supplement therapies for inflammatory Bowel disease: Crohn's disease and ulcerative colitis. Curr Pharm Des, 22(2): 180-188.

PARKER HM, COHN JS, O'CONNOR HT (2019) Effect of fish oil supplementation on hepatic and visceral fat in overweight men: a randomized controlled trial. Nutrients, 11(2): 475.

PET GC, MCADAMS RM, MELZER L (2018) Attitudes surrounding the management of neonates with severe necrotizing enterocolitis. J Pediatr, 199: 186-193, e3.

PHILLIPS MJ, VOELTZ GK (2016) Structure and function of ER membrane contact sites with other organelles. Nat Rev Mol Cell Biol, 17(2): 69-82.

SAS K, SZABÓ E, VÉCSEI L (2018) Mitochondria, oxidative stress and the kynurenine system, with a focus on ageing and neuroprotection. Molecules, 23(1): 191.

SERDAREVIC N, PASALIC A, DJIDO V, PECAR M, TRTAK N, GOJAK R (2019) The vitamine source, usual food intake at students. Mater Sociomed, 31(1): 53-56.

SHAO H, LAN D, DUAN Z (2006) Upregulation of mitochondrial gene expression in PBMC from convalescent SARS patients. J Clin Immunol, 26(6): 546-554.

WANG M, KAUFMAN RJ (2016) Protein misfolding in the endoplasmic reticulum as a

conduit to human disease. Nature, 529 (7586): 326-335.

XIE W, JIAO B, BAI Q (2020) Chemoptogenetic ablation of neuronal mitochondria in vivo with spatiotemporal precision and controllable severity. Elife, 9: e51845.

XING J, XU H, LIU C (2019) Melatonin ameliorates endoplasmic reticulum stress in N2a neuroblastoma cell hypoxia-reoxygenation injury by activating the AMPK-Pak2 pathway. Cell Stress Chaperones, 24(3): 621-633.

ZHANG T, WANG N, YAN W (2018) Effect of a fish oil-based lipid emulsion on intestinal failure-associated liver disease in children. Eur J Clin Nutr, 72(10): 1364-1372.

ZHU X, CUI N, YU L (2020) Potential role of endoplasmic reticulum stress is involved in the protection of fish oil on neonatal rats with necrotizing enterocolitis. Sci Rep, 10 (1): 6448.

Effects of MSG on the lymph nodes of the albino rat: Ultrastructural and morphometric studies

Tetiana Harapko[1], Lesia Mateshuk-Vatseba[2]

[1] Department of Human Anatomy and Histology, Uzhhorod National University, Medical Faculty, Ukraine

[2] Department of Normal Anatomy, Lviv National Medical University named after Danylo Halytskyi, Ukraine

SUMMARY

The purpose of the study was to study the morphometric and electron microscopic changes of the parenchyma of the mesenteric lymph nodes of rats under the conditions of action of monosodium glutamate and its abolition. The paper presents and analyzes data from an experimental study conducted on 76 albino rats in females and males of reproductive age. Experimental animals are divided into 5 groups. Eight weeks of exposure to monosodium glutamate (MSG) showed a significant decrease in the relative area of the cortical substance in the parenchyma of the mesenteric lymph nodes of albino rats in males and females by 10.3% and 8.3%, respectively, and an increase in the relative area of the medullary substance by 16.1% and 13.2%, respectively with an intact group of animals. Submicroscopically after eight weeks of exposure to monosodium glutamate, as well as after eight weeks of cancellations, in the parenchyma of lymph nodes intercellular spaces are enlarged, lymphocytes have low electron density, karyolysis, organelles at different stages of decay, the number of macrophages increases, cellular detritus and osmiophilic inclusions in the cytoplasm of macrophages and in the intercellular space. The wall of arterioles is thickened, sclerosed, nuclei of large endothelial cells. There are thorough defects in the capillary wall, venous plethora. The hemocapillary lumen is narrowed due to numerous protrusions and microvilli of the cytolema of endothelial cells. Changes appear after two weeks of action of monosodium glutamate and increase by the eighth week of the experiment. Any changes will not return to normal after cancellation of exposure to monosodium glutamate.

Key words: Lymph node – Lymphocytes – Macrophages – Monosodium glutamate

INTRODUCTION

One of the most common food additives not only in Ukraine but also worldwide is monomonosodium glutamate (MSG, C5H8NO4NaH2O). This monosodium salt of glutamic acid, often found in nature, exists as free glutamate, and as bound to other amino acids in protein. This food additive belongs to the group of flavor enhancers used in a wide range of products, such as soups, sauces, puddings, chips, meat products and mixed condiments (Hussein et al., 2017; Rutska et al., 2017). However, despite its widespread prevalence, its effect on the body remains insufficiently studied (Zanfirescu et al., 2018). By

Corresponding author:
Tetiana Harapko, Ph.D. Department of Human Anatomy and Histology, Medical Faculty, Uzhhorod National University, Kapushanska Str., 22, 88000, Uzhhorod, Ukraine. Phone: +380506443548. E-mail: garapkotv@gmail.com

Submitted: July 1, 2020. **Accepted:** September 15, 2020

enhancing the taste of food, monomonosodium glutamate leads to an increase in the amount of food consumed per day, which causes a high-calorie diet (HCD). In studies, the authors describe that HCD leads to metabolic syndrome, insulin resistance, diabetes, splenomegaly, hypertension, heart attack, etc. (Buchan et al., 2018; El-Aziz et al., 2018; Kothari et al., 2017).

The results of a study in experimental animals using this additive showed that the consumption of monomonosodium glutamate leads to an increase in lipid peroxidation, nitric oxide, neurotransmitters, accompanied by the accumulation of ß-amyloid peptides in the animal's body (Hussein et al., 2017). According to other studies, the authors concluded that monomonosodium glutamate leads to obesity (Bautista et al., 2019). It was also found that the addition of monomonosodium glutamate to the diet of rats reduces the excretion of Na, K and water from the body. NaCl retention leads to hypertension, accompanied by renal pathology, intrarenal oxidative stress and decreased nitric oxide secretion (Contini et al., 2017).

An urgent task of modern medicine is to study the effect of dietary supplements, monomonosodium glutamate in particular, on the structure of the parenchyma and the vascular bed of lymphoid (immune) organs. The latter include lymph nodes, which play a role in the body of a kind of biological «filters», whose function is to neutralize antigens, because they themselves are antigen-dependent proliferation and differentiation of T- and B-lymphocytes (Oliveira et al., 2019). Lymphocytes and macrophages are among the major cells involved in the immune response (Arundina et al., 2017; Kusumaningsih et al., 2018). Having studied the features of the structural reorganization of the immune system under the action of monomonosodium glutamate, it becomes possible to study methods for correcting these changes.

The aim of the research was to study the morphometric and electron microscopic changes of the parenchyma of mesenteric lymph nodes of rats under the conditions of action of monosodium glutamate and its abolition.

MATERIALS AND METHODS

The study was conducted on 76 albino rats of male and female reproductive age (2.5-6.5 months) weighing 120-280 g. The microanatomy of the structural components of the mesenteric lymph nodes of albino rats under physiological norms was examined in 10 intact animals. The experimental animals were divided into 5 groups: the first group (10 animals), who had been on a high calorie diet (HCD) for two weeks; the second (10 animals), the third (10 animals), and the fourth group (10 animals), who had been on HCD for four, six, and eight weeks, respectively; the fifth group (10 animals), who had been on a HCD for eight weeks, followed by a standard vivarium diet for eight weeks. Each group had 5 male rats and 5 female rats. HCD was achieved by adding 0.07 g / kg of rat body weight to food monosodium glutamate.

Controls were served by 16 albino rats who received a standard vivarium diet instead of the high-calorie diet.

All experimental animals were kept in the vivarium of Danilo Halytskyi National Medical University. The studies were conducted in accordance with the provisions of the European Convention for the Protection of Vertebrate Animals Used for Experimental and Other Scientific Purposes (Strasbourg, 1986), Council of Europe Directives 86/609 / EEC (1986), Law of Ukraine No. 3447-IV «On the Protection of Animals from Cruelty behavior», the general ethical principles of animal experimentation, approved by the First National Congress of Ukraine on Bioethics (2001).

Before the material was taken, the animals were numbed with anesthesia. The fixation of the mesenteric lymph nodes was performed with a 1.5% solution of osmium tetroxide in 0.2 M monosodium cacodylate solution at pH 7.2 for 2-2.5 hours in the cold. Dehydration in increasing concentrations of ethyl alcohol (50°, 70°, 90° and absolute) for 30 min each and propylene oxide for 10 min. The material was poured into a mixture of epoxy resins and polymerized for 24 h in a thermostat at 60°C. The sections were made on a UMTP-6M ultramicrotome using a diamond knife (DIATOM) and double Reynolds and uranyl acetate were contrasted. Sections of lymph nodes

were examined using a TEM - 100 transmission electron microscope. Photo material was documented using a SONY - H9 digital camera.

Morphometric studies were performed at specific times on histological specimens stained with hematoxylin and eosin using VideoTest-5.0, CAARA Image Base, Stepanizer, and Microsoft Exel on a personal computer.

Statistical processing of digital data was performed using Excel software and STATISTICA 6.0 using the parametric method. The numerical values of the parameters are represented by sample averages (M), standard deviation (σ), standard error of the mean (m), Student's t test (t). The results of the calculations were presented in graphical form in histograms using Microsoft Office, indicating confidence intervals at 95% confidence level (p = 0.95).

RESULTS

In animals of intact and control groups, according to our histological studies, the structure of the mesenteric lymph nodes was consistent with the species norm. Externally, the lymph nodes are covered by a connective tissue capsule from which numerous cortical and medullary trabeculae depart deep into the parenchyma of the node. On the cramped part of the node are hila The parenchyma of the lymph node consists of located on the periphery of the cortical substance, and closer to the hilum of the medullary substance. Electron microscopically found that small, medium and large lymphocytes have a typical structure. Small lymphocytes have a diameter of about 6-7 μm, contain a large nucleus and a thin section of the cytoplasm with numerous ribosomes. Medium lymphocytes with a diameter of about 7-9 μm contain a more rounded nucleus with a distinct nucleolus. The cytoplasm contains ribosomes, a granular endoplasmic reticulum and mitochondria (Fig. 1). The large lymphocytes (lymphoblast) have a diameter of about 10 μm, the nucleus is filled with euchromatin, the karyolema is flat. The cytoplasm contains mitochondria and ribosomes. Macrophages have a different nucleus shape, with primary and secondary lysosomes in their cytoplasm.

Two weeks after HCD submicroscopic structure of small and medium lymphocytes is typical. Nuclei are of rounded shape, cytoplasm contains organelles (mitochondria, granular endoplasmic reticulum). However, the contours of the nuclear membrane are not equal, the cytoplasmic membrane loses clarity in some areas (Fig. 2). Among unmodified lymphocytes, there are destructively altered cells whose nuclei have pycnosis signs, and mitochondria contain damaged mitochondrial ridges. *Reticulo*-endothelial cells contain enlarged nuclei and thickened processes. The number of organelles in the cytoplasm is small, the latter partially changed. The vessels of the hemomicrocirculatory bed are somewhat enlarged, full-blooded.

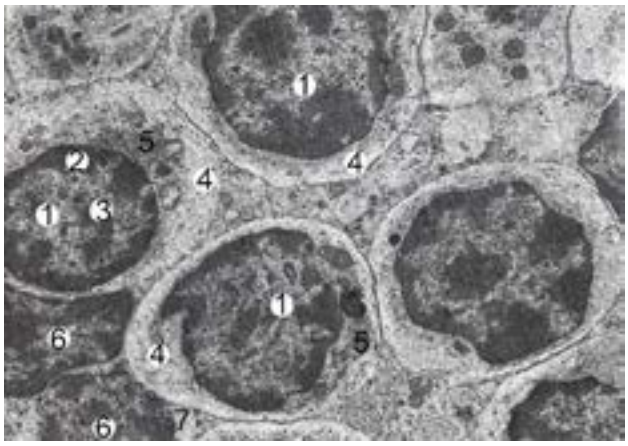

Fig. 1.- Electron-microscopic organization of the cortical substance of the mesenteric lymph node of the albino rat-female intact group. Electronic micrograph. Approx. × 6000. Designation: euchromatin (1), heterochromatin (2) and nucleolus (3) in the nucleus of the middle lymphocyte; the cytoplasm (4) contains ribosomes (5); nucleus (6) and cytoplasm (7) of small lymphocyte.

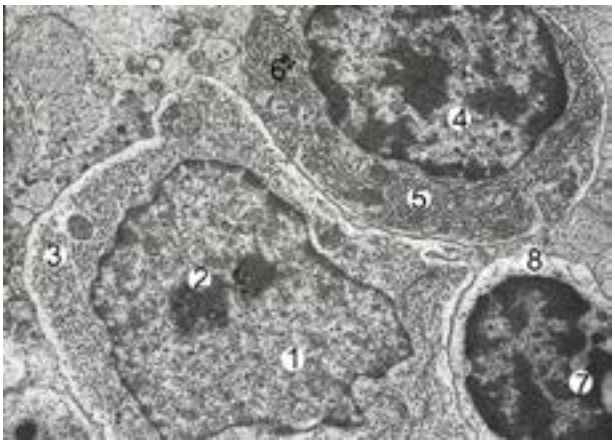

Fig. 2.- Electron microscopic organization of cortical substance of mesenteric lymph node of albino rat female after two weeks of HCD. Electronic micrograph. Approx. × 6000. Designation: Euchromatin (1) and nucleolus (2) in lymphoblast nucleus, 3 – cytoplasm; nucleus (4) and cytoplasm (5) of middle B-lymphocyte, 6 – osmiophilic inclusions; nucleus (7) and cytoplasm (8) of small B lymphocyte.

Submicroscopically, after four weeks of HCD, nuclei with apoptosis phenomena were detected in part of the lymphocytes of all populations.

Preferably they are in the state of karyorexis or karyolysis. In the cytoplasm are lighted areas, mitochondria are hypertrophied with light matrix. The lumen of the arteries and arterioles is slightly expanded. In relation to the cytoplasm of endothelial cells, their nuclei occupy a large part. On the luminal surface of endothelial cells in the wall of hemocapillaries, the number of microvilli grows, the cariolem forms protrusions. Organelles in the cytoplasm of endothelial cells lose the clarity of the contours. The lumen of the veins and venules is somewhat increased (Fig. 3).

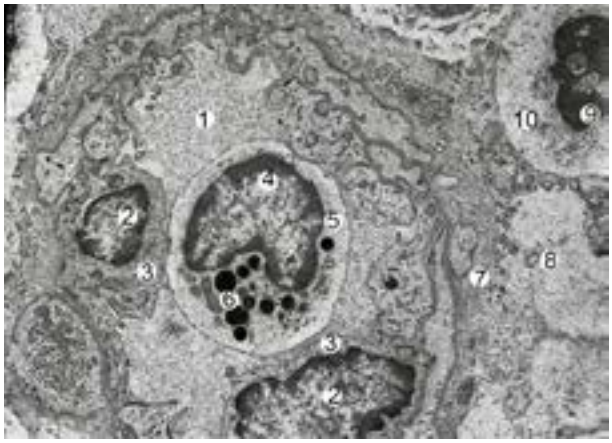

Fig. 3.- Electron microscopic organization of a fragment of a mesenteric lymph node of a albino rat male in four weeks of HCD. Electronic micrograph. Approx. × 6000. Designation: 1 - lumen of the venula; nucleus (2) and cytoplasm (3) of endothelial cells; nucleus (4) and cytoplasm (5) of basophilic leukocyte; 6 – granule; 7 – swollen and thickened basement membrane; 8 – vascular edema; nucleus (9) with signs of apoptosis and cytoplasm (10) of lymphocyte.

Submicroscopically, after six weeks of HCD, the number of macrophages with a large number of phagosomes increases in the cytoplasm, fragments of damaged lymphocytes and other osmiophilic inclusions. *Reticulo*-endothelial cells nuclei are enlarged, deformed, cytoplasm contains damaged organelles. The number of lymphocytes with signs of apoptosis is increasing (Fig. 4). In the part of lymphocytes in the nucleus there are no nucleolus, cytoplasm is enlightened, organelles are damaged. The mitochondria with the enlightened matrix, the tubules of the granular endoplasmic reticulum are swollen, dilated. In the lumen and in the wall of the postcapillary venules with high endothelium, a large number of lymphocytes may indicate an increase in the processes of lymphocyte migration into the parenchyma of the lymph node from the blood.

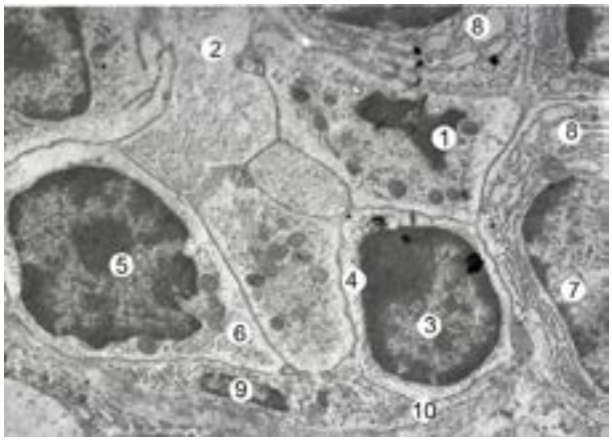

Fig. 4.- Electron-microscopic organization of the cortical substance of the mesenteric lymph node of the albino rat female after six weeks of HCD. Electronic micrograph. Approx. × 6000. Designation: 1 – lymphocyte karyolysis; 2 – destructive area; nucleus (3) and cytoplasm (4) of small B-lymphocyte; nucleus (5) and cytoplasm (6) of middle B lymphocyte; nucleus (7) and cytoplasm (8) of the lymphoblast; 8 – vacuolated cytoplasm of lymphocytes; deformed nucleus (9) and thinned processes of the *reticulo*-endothelial cells.

Submicroscopically after eight weeks of HCD, as well as after eight weeks of cancellation, the changes in the parenchyma of the lymph nodes of both male rats and females intercellular spaces are expanded, lymphocytes have low electron density, there is karyolysis, organelles at different stages. The number of macrophages increased, in whose cytoplasm and extracellular spaces a large number of cellular detritus and osmiophilic inclusions are seen. The latter indicates the growth of the process of cell death. The proportion of collagen fibers and microfibrils in the parenchyma of the node increased. The wall of arterioles is thickened, sclerosed, nuclei of large endothelial cells. There are thorough defects in the capillary wall, venous plethora. The hemocapillary lumen is narrowed due to numerous protrusions and microvilli of the cytolema of endothelial cells, in cross section it has a star-shaped shape. Some areas of the hemocapillaries are so narrow that they do not pass blood cells (Fig. 5).

The dynamics of changes in the relative area of cortical and medullary substances and cortical-medullar index (CMI) of lymph nodes of albino male rats in control and experimental groups are expressed in Table 1. Two weeks after HCD, a significant increase in the relative area of cortical substance was shown in the parenchyma of lymph nodes of albino rats of females by 7.6%, compared with the intact group of animals. Accordingly,

the relative area of the medullary substance decreases and is 12.0% less than the parameters of the intact group of animals. CMI decreases in female rats by 22.2%.

Fig. 5.- Electron microscopic organization of a fragment of a mesenteric lymph node of a albino rat female of reproductive age after eight weeks of HCD. Electronic micrograph. Approx. × 8000. Designation: 1 - deformed endothelial cell nucleus; 2 - cytoplasm of endothelial cells; 3 - narrowed lumen of the hemocapillary; 4 - stratified and swollen basal membrane of the hemocapillary; 5 - vascular edema; 6 – shoots of cytolemy on its luminal surface.

Four weeks after HCD, a decrease in the relative area of cortical substance was revealed in the parenchyma of lymph nodes of albino rats of females by 11.0%, compared to the previous group of animals, and there were 4.2% less indicators of intact group of animals. Accordingly, the relative area of the medullary substance increases by 21.3% compared to the previous group of animals, and is 6.7% more than the parameters of the intact group of animals. CMI decreases in female rats by 26.4%.

Six weeks after HCD, a decrease in the relative area of the cortical substance was revealed in the parenchyma of lymph nodes of albino rats of females by 5.3%, compared to the previous group of animals, and there were 9.3% less indicators of intact group of animals. Accordingly, the relative area of the medullary substance increases by 7.5% compared to the previous group of animals, and is 14.7% more than the parameters of the intact group of animals. CMI decreases in female rats by 12.0%.

Eight weeks after HCD, an increase in the relative area of the cortical substance was revealed in the parenchyma of lymph nodes of albino rats of females by 1.1%, compared to the previous group of animals, which means 8.3% less parameters of intact group of animals. Accordingly, the relative area of the medullary substance decreases by 1.3% compared to the previous group of animals, and is 13.2% more than the parameters of the intact group of animals. CMI in female rats was 19.0% less than in the intact group of animals.

Eight weeks after HCD, after which 8 weeks of standard vivarium food ration succeeded, a relative decrease in the cortical area was revealed in the parenchyma of lymph nodes of albino rats in females by 1.2%, compared to the previous group of animals, and by 9.4% less than the parameters of the intact group of animals. Accordingly, the relative area of

Table 1. Dynamics of changes in the relative area of cortical and medullary substances and cortical-medullar index (CMI) of lymph nodes of albino male rats in control and experimental groups (M ± m).

Group name	$S_{cortic.subst.}$, %	$S_{medul.subst.}$, %	CMI
Intact animals	61.23±1.7	38.77±0.76	1.58±0.11
I group – 2 weeks HCD	65.9±1.34*	34.1±0.56*	1.93±0.21*
II group – 4 weeks HCD	58.65±1.43	41.35±0.63	1.42±0.18*
III group – 6 weeks HCD	55.53±1.29*	44.47±0.71*	1.25±0.2*
IV group – 8 weeks HCD	56.12±1.65*	43.88±0.78*	1.28±0.12*
V group – 8 weeks HCD after what 8 weeks of cancellation	55.46±1.28*	44.54±0.69*	1.25±0.13*

* - values that are statistically significantly different from those of the intact animal group ($p < 0.05$).

the medullary substance increases by 1.5% compared to the previous group of animals, and is 14.9% more than the parameters of the intact group of animals. CMI in female rats was 20.9% less than in the intact animal group.

DISCUSSION

From studies described in the literature, it is known that the introduction of monomonosodium glutamate at a dose of 30 mg / kg body weight leads to the accumulation in the body of excessive amounts of low and medium molecular weight and reduced ability of the kidneys to excrete toxic products. The shift of markers of intoxication syndrome towards catabolic substances is revealed. One week after the experiment, the results correspond to the phase of partial compensation, which is characterized by an increased concentration of low and medium molecular weight substances in erythrocytes and blood plasma. After two weeks and up to one month of the experiment, catabolic markers of endogenous intoxication predominate, which continue to accumulate in erythrocytes and plasma, indicating a transition to the phase of partial decompensation of all systems and organs involved in detoxification (Krynytska et al., 2019). Based on these results, the organs of the immune system are also affected by intoxication of the body as a side effect of monomonosodium glutamate.

The results of a study conducted on eight-week-old rats on a high-calorie diet showed an increase in blood levels of triglycerides, total cholesterol, low-density lipoproteins, weight gain (De Farias et al., 2019). These are all signs of obesity, which also affects negatively the organs of the immune system.

Similar results are obtained in a study where obesity caused by a high-calorie diet leads to cell death and activation of macrophages in the lymph nodes. The authors concluded that obesity-related inflammation induces lymph node fibrosis and is likely to increase the lumen of the sinuses and subsequently reduce the interaction of immune cells. The resulting effects of immune regulation are likely to contribute to the suppression of immunosuppression and lymphatic dysfunction during obesity (Foster et al., 2017).

The results of a study in which experimental animals received a high-calorie diet that included 20% protein, 20% carbohydrates and 60% fat for two weeks, indicate that the parenchyma of lymph nodes increases the proportion of macrophages and stromal cells that contain lipid inclusions. For comparison, we used a group of animals that received a low-calorie diet that included 20% protein, 70% carbohydrates and 10% fat for two weeks. The authors proved that stromal cells express a large number of genes associated with lipid metabolism, which indicates that lymph nodes are involved in lipid metabolism (Streich et al., 2020).

The novelty of the results described by us is the use of electron microscopic research methods, which gave new data at the ultrastructural level on the structure of lymph nodes under the action of monomonosodium glutamate.

Prospects for further development are related to the study of morphometric and electron microscopic changes in the structural components of rats lymph nodes under conditions of correction of the action of monosodium glutamate.

Conclusions

As a result of a study in rats males and females, we found:

1. After eight weeks of action of monosodium glutamate a significant decrease in the relative area of the cortical substance in the parenchyma of lymph nodes of albino rats of males and females respectively, and an increase in the relative area of the medullary substance in comparison with an intact group of animals.
2. Electron microscopic changes appear after two weeks of action of monosodium glutamate and increase by the eighth week of the experiment. Any changes detected after eight weeks of exposure to monosodium glutamate will not return to normal after cancellation.

ACKNOWLEDGEMENTS

The authors thank all members of Faculty of Medicine, Uzhhorod National University, Lviv

National Medical University named after Danylo Halytskyi, Ukraine for their kind cooperation.

REFERENCES

ARUNDINA I, DIYATRI I, BUDHY TI, JIT FY (2017) The effect of brotowali stem extract (*Tinospora crispa*) towards increasing number of lymphocytes in the healing process of traumatic ulcer on diabetic Wistar rat. J Int Dental Med Res, 10(3): 975-980.

BAUTISTA RJH, MAHMOUD AM, KONIGSBERG M, GUERRERO NELD (2019) Obesity: pathophysiology, monomonosodium glutamate-induced model and anti-obesity medicinal plants. Biomed Pharmacother, 111: 503-516.

BUCHAN L, CHAHEYLA R, FISHER A, HELLINGS A, CASTRO M, AL-NAKKASH L, et al. (2018) High-fat, high-sugar diet induces splenomegaly that is ameliorated with exercise and genistein treatment. BMC Res Notes, 11: 752.

CONTINI MC, FABRO A, MILLEN N, BENMELEJ A, MAHIEU S (2017) Adverse effects in kidney function, antioxidant systems and histopathology in rats receiving monomonosodium glutamate diet. Exp Toxicol Pathol, 69(7): 547-556.

DE FARIAS TSM, CRUZ MM, DE SA RCC, SEVERI I, PERUGINI J, SENZACQUA M, CERUTTI SM, GIORDANO A, CINTI S, ALONSO-VALE MIC (2019) Melatonin supplementation decreases hypertrophic obesity and inflammation induced by high-fat diet in mice. Front Endocrinol, 10: 750.

EL-AZIZ R, NAGUIB M, RASHEDB L (2018) Spleen size in patients with metabolic syndrome and its relation to metabolic and inflammatory parameters. Egyptian J Int Med, 30: 78-82.

FOSTER M, VANDERPOOL K (2017) Transmission electron microscopy analysis of visceral and subcutaneous lymph nodes: high fat diet-induced morphological changes. FASEB J, https://www.fasebj.org/doi/abs/10.1096/fasebj.31.1_supplement.lb515.

HUSSEIN U, HASSAN N, ELHALWAGY M, ZAKI A, ABUBAKR H, NAGULAPALLI VK, JANG KY, BISHAYEE A (2017) Ginger and propolis exert neuroprotective effects against monomonosodium glutamate-induced neurotoxicity in rats. Molecules, 22(11): 1928.

KOTHARI V, LUO Y, TORNABENE T, O'NEILL AM, GREENE MW, GEETHA T, BABU JR (2017) High fat diet induces brain insulin resistance and cognitive impairment in mice. Biochim Biophys Acta, 1863: 499-508.

KRYNYTSKA I, MARUSHCHAK M, NAUMOVA L, MAZUR L (2019) The toxic impact of monomonosodium glutamate in rats. J Med J, 53(2): 91-101.

KUSUMANINGSIH T, LUTHFI M, MOFFAN MDB (2018) *Macrophages analysis on gingival tissue of diabetic rats after insulin leaf extract administration.* J Int Dental Med Res, 11(1): 308-311.

OLIVEIRA E, CASTRO S, AYUPE CM, AMBROSIO MGE, DE SOUZA VP, MACEDO GC, FERREIRA AP (2019) Obesity affects peripheral lymphoid organs immune response in murine asthma model. Immunology, 157(3): 268-279.

RUTSKA AV, GETSKO NV, KRYNYTSKA IY (2017) Toxic impact of monosodium glutamate on a living organism. Med Clin Chemistry, (1): 119-127.

STREICH K, SMOCZEK M, HEGERMANN J, DITTRICH-BREIHOLZ O, BORNEMANN M, SIEBERT A, BLEICH A, BUETTNER M (2020) Dietary lipids accumulate in macrophages and stromal cells and change the microarchitecture of mesenteric lymph nodes. J Adv Res, 24: 291-300.

ZANFIRESCU A, CRISTEA AN, NITULESCU GM, VELESCU BS, GRADINARU D (2018) Chronic monomonosodium glutamate administration induced hyperalgesia in mice. Nutrients, 10: 1.

The morphology of the pterion and asterion sutures in Iranian population

Hossein Jafari Marandi [1], Jaber Gharehdaghi [2], Forouzan Fars [3], Masoud Zeinali [1], Hosein Safari [1]

[1] Ahvaz Jundishapur University of Medical Sciences, Ahvaz, Iran
[2] Iran Legal Medicine Organization, Tehran, Iran
[3] Iran University of Medical Sciences, Tehran, Iran

SUMMARY

The pterion and asterion are at the outer surface of the skull. The pterion is the region where the frontal, sphenoid, parietal and temporal bones join together, and the asterion is the intersection of parietal, temporal and occipital bones. The sutural pattern of both are different in the various population and races. This study examines the patterns of suture of the pterion and asterion in 210 semi-skulls of 146 males and 64 females cadaver. Four main types of anatomical patterns were found: sphenoparital 84.2%, frontotemporal 8.1%, star shaped 3.5% and epipteric 2.4%. In the study of asterion, in 14.7%, type I, and 86.3% type II was observed. In the first study of the sutural pattern of the pterion and asterion in Iranian population, similarity to the other studies of the Indian and Middle Eastern regions was observed.

Key words: Morphology – Pterion –Asterion – Surface anatomy

INTRODUCTION

The pterion is adjacent to the temporal cavity and the binding site of the frontal, parietal, temporal, and sphenoid bone, and is located in the anterolateral part of the skull, which is differing among primates. In the asterion, the connection between the parietal, temporal and occipital bones is created (Fig. 1). The variation in the pattern of the pterion has a surgical importance to deep-seated structures. The stability of sutures in animals in a particular species raises the genetic basis (Williams et al., 1998).

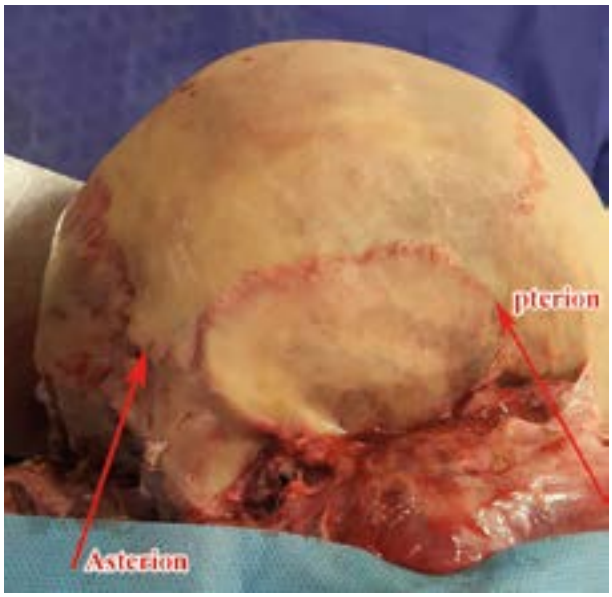

Fig. 1.- Pterion and asterion.

In 1956, Murphy and coworkers described four types of pterion (Murphy, 1956). Based on this classification, the sphenoid bone is connected to the parietal bone, and the suture is of sphenoparital type, and this prevents the attachment of frontal and parietal bones to each other. In the type

Corresponding author:
Hosein Safari. Department of Neurosurgery, Ahvaz Jundishapur University of Medical Sciences, Ahvaz, Iran. P.O. Box: 61357-33118. Phone and Fax: 0098-61-33743019. Mobil Phone: 0098-918-337-6058. E-mail: Hoseinsafari1382@gmail.com

Submitted: August 28, 2020. **Accepted:** September 9, 2020

of fronto-temporal, frontal and temporal bones contact each other and prevent the attachment of frontal and parietal bones (Kumar and Mahajan, 2014). In the star-shaped type, the irregular shape of the sutures are similar to the letter K, and the bones meet at one point. It should be noted that in the area of the pterion region there is also the possibility of developing a sutural bone (epipteric type) (Kumar and Mahajan, 2014) (Fig. 2).

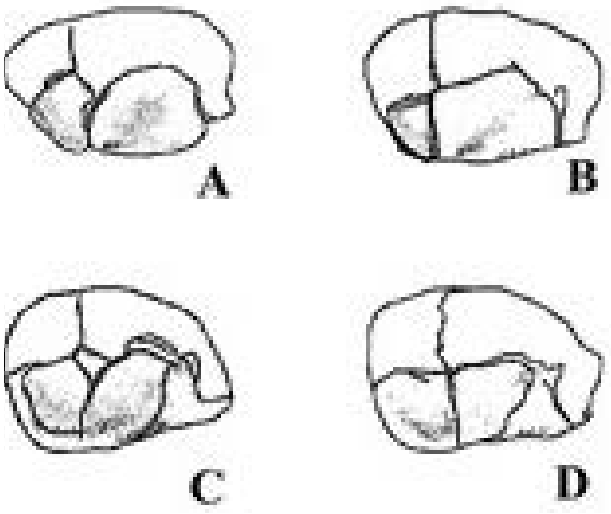

Fig. 2.- Pterion variations: A) Sphenopatietal. B) Frontotemporal. C) Epipteric. D) Stellate.

Occasionally, bone formation may also occur in the vicinity of the septum of another bony building (sutural bone). Although the authors believe that the sutural bone is a natural and gene-controlled process, studies also emphasize the role of pathologies such as hydrocephalus, as well as studies focusing on the role of ethnic and racial differences in the incidence of sutures forms (Havaldar et al., 2015). The shape of the asterion and pterion sutures are important in the neurosurgical approaches to the cranial cavity (Ersoy et al., 2003; Ucerler and Govsa, 2006; Galindo de León et al., 2013; Havaldar et al., 2015; Natekar et al., 2018).The current study examines the forms of sutures of the pterion and asterion point in the Iranian population.

MATERIALS AND METHODS

After obtaining the necessary authorization, 210 adult semi-skulls, including 69.5% males and 30.5% females, were examined. In this study, asterion sutures were classified into 2 types: type I which had a sutural bone and type II without sutural bone (Fig. 3).

Fig. 3.- Asterion types. Type I which had a sutural bone (A) and type II without sutural bone (B).

Each suture point of the pterion was divided into sphenoparital, fronto-temporal, stellar and epipteric (sutural). In each sample, soft tissue was removed from the suture points using appropriate tools and then the sutures were examined. In this research, descriptive statistics (frequency, mean, variance, standard deviation) were used to analyze the data. To analyze the demographic characteristics of the research, statistical analysis with SPSS software was used.

RESULTS

Asterion

Regarding the results of the study, 210 semi-skull specimens were categorized in 181 specimens (85.3% of type II) and 29 specimens (14.7% of type I) asterions.

Among the females, type I of asterion (14.8%) was slightly more common than in men (13.7%). However, there was no significant difference between the two sexes. Among the tested specimens, asterion type II was more common in men with 86.3% than women with 85.2%. However, there was no significant difference between the two sexes (Tables 1-2 and 5, and Diagrams 1-2).

Table 1. Frequency of asterion in Genders.

Sex	Asterion	
	II	I
Male : 146	86.3% (126)	13.7% (20)
Female: 64	85.2% (55)	14.8% (9)
Total: 210 we	85.3% (181)	14/7% (29)

Diagram 1. Frequency of asterion types in gender.

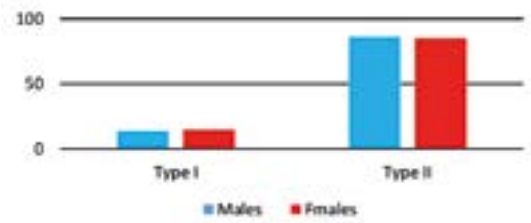

Pterion

According to the results, based on the 210 samples studied, 177 specimens (84.2%) were found to have sphenopariatal, of which 84.4% were male and 84.2% were female respectively. This type was the most common form of the pterion in this study. Also, the epipteric type of the pterion with 2.4% (five samples) was the lowest form of pterion in the studied samples.

Table 2. Frequency of asterion in right and left hemispheres based on gender.

Asterion	Left Hemisphere		Right Hemisphere	
	Female	Male	Female	Male
I	13	26	8	24
II	19	47	24	49

Diagram 2. Frequency of asterion in the right and left hemispheres based on gender.

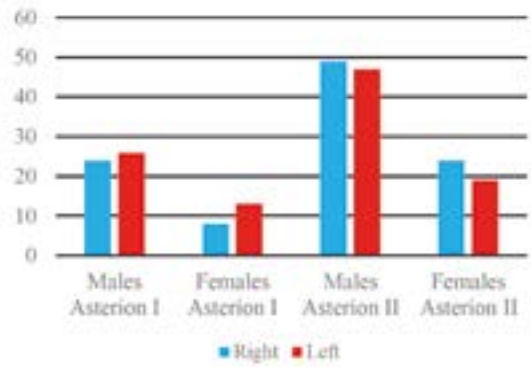

Sexual difference in pterion types was not observed between the studied samples, although the star-shaped type of pterion in females was 5.8%, more than that of the male, 4.7% (Tables 3-4 and 6 and Diagrams 3-4).

According to the results of 210 semi-skulls of pterions in the right and left hemispheres, the frontotemporal type in the right semi-skull hemisphere was more common in females than in males. Also, the star-shaped pterion in the right hemisphere of males is more common than in females. However, there is no significant difference between the two types of sex and semi-skull of epipteric and star shaped of pterions.

Table 3. The prevalence of pterion between sexes by their type.

Sex	Pterion			
	ST	EP	FT	SP
Male: 146	4.7% (7)	2.7% (3)	8.2% (12)	84.4% (123)
Female: 64	5.8% (4)	2.5% (2)	7.5% (5)	84.2% (54)
Total: 210 we	5.3% (11)	2.4% (5)	8.1% (17)	84.2% (177)

Diagram 3. The prevalence of the pterions among the sexes in terms of their type.

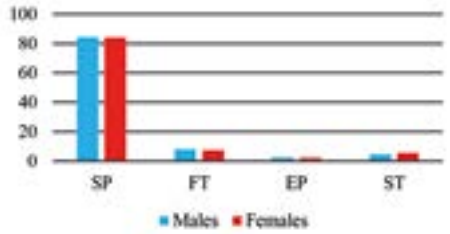

Table 4. The prevalence of different types of pterions in the right and left of the examined samples.

Type of pterions	Left: 105		Right: 105	
	Female	Male	Female	Male
SP	32	57	32	56
FT	2	6	3	6
EP	1	2	1	1
ST	2	3	2	4

Diagram 4. The prevalence of different types of pterions in the right and left of the examined samples.

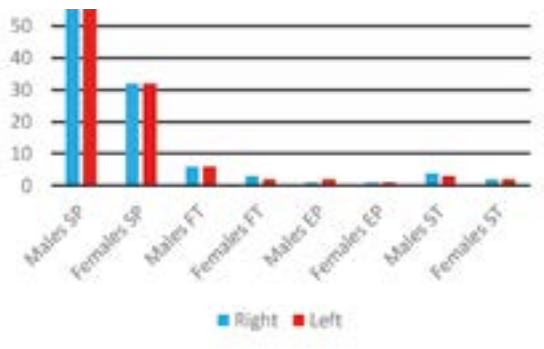

Table 5. Prevalence of Asterion types in different populations.

Study	Country	Year	Number of Sample	Asterion type	
				I	II
Berry and Berry	British Columbia	1967	50	12.0	88.0
Berry and Berry	Peru	1967	53	7.5	92.5
Berry and Berry	Egypt	1967	250	14.4	85.6
Berry and Berry	Berme	1967	51	14.7	85.3
Berry and Berry	Panjab	1967	53	16.9	83.1
Kellock & Parsons	Australia Aborigines	1970	-	19.8	80.2
Gumusburun et al.	Turkey	1977	302	9.92	90.08
Mwachaka et al.	Kenia	2009	79	20.0	80.0
Present study	Iran	2018	210	14.7	85.0

DISCUSSION

The findings of this study are in line with previous studies, although some differences are evident. Ashley's study on the subject of pterion from an anthropological perspective points to the higher percentage of epipteric sutures in the human societies (Ashley-Montagu, 1933). In this study, the findings were in the period between 1772 and 1930, which contains important points in the pattern of the pterion in humans. He identified sixteen general patterns of pterion.

Murphy (1956) studied four main patterns of pterion and five basic patterns for epipteric sutures. Wang et al. (2006), studying the skull sutures between the monkeys and observing the pattern of family gathering, suggested that this diversity was inherited. Liu et al. (1995), in a study on mice, emphasizes the role of temporal rotation in the development of sutures and the adaptation of skull growth.

Liu et al. (1999), showed that increased activity of the MSX2 gene plays a direct role in the morphogenesis of skull bones. In other words, according to the results of morphological and genetic studies, the pattern of suture formation is influenced by ethnic and environmental factors.

In the current study, the prevalence of type I asterion was 14.7%, which is equivalent with the study by Berry and Berry (1967) in Egyptian and Indian populations. However, in the study of Mwachaka et al. (2009), asterion type 1 was reported in 20% of cases. In the recent study, the sample of asterion type 1 was lower in women, with no difference in men on the right and left side of the skull. Singh (2012), in a study on 55 skull cases, reported an asterion type I occurrence of 16.36% in samples. In this study, type I asterion in the left side was lower in men than in women.

Havaldar et al. (2015), in a study on the morphology of asterion sutures in India, which were performed on 250 skulls, asterion type I was seen in 18% of men and 20% of women, and also the type II in 82% of men and 80% of women was seen. There was no difference in the asterion morphology in the Indian population compared to other populations. In the study of Galindo-de León et al. (2013), asterion type I was seen in 74.4% of the cases.

The study of Deepak and Dakshayani (2015), which was designed on 50 skulls of both genders to assess the type of asterion, and the importance of bony landmarks in relation to adjacent venous sinus structures, type II (lack of sutural bone) with 73% was more common than type I. In the present study, 85.3% of the cases were asterion type II specimens. This review is consistent with previous studies.

In the Murphy (1956) study, which was conducted among native Australians, 75% of the specimens were sphenoparietal sutures. Saxena et al. (1988) and Asala and Mbajiorgu (1996), in the Nigerian, Southern and Northern Indian populations, reported prevalence of sphenoparietal suture between 82.1 and 93.5%, respectively. In studies by Zalawadia et al. (2010), Mwachaka et al. (2009), Hussain et al. (2011) and Ukoha et al. (2013) that were conducted in populations in Kenya, India and Nigeria, the sphenoparietal sutures values was reported between 66 to 91.7%.

The studies of Ersoy et al. (2003) and Ogouz et al. (2004), which were performed on the Turkish population, reported sphenoparietal sutures values between 87.35% and 88%. The highest levels of sphenoparietal sutures were reported

by Saxena et al. (1988) with 95.3% in the Indian population, and the lowest in 66% of cases in the study of Mwachacka et al. (2009) in Kenya. According to the results of this study, we can say that sphenoparietal suture has been observed in 84.2% of cases, which is in accordance with previous studies.

Ersoy et al. (2003) performed a study on 490 adult mature skulls. In this study, 9% of cases (44 out of 490 cases) were of epipteric bone. They concluded that there is a higher possibility of unwanted entry into the orbital cavity in epipteric skulls with anterior position. The highest rates of epipteric sutures reported by Lee et al. (2001) that was 40.3%. In the current study, an amount of 2.4% was obtained for epipteric sutures.

In the study of fronto-temporal sutures, the highest prevalence (15%) was reported in the study by Mwachaka et al. (2009) and in Lee et al. (2001) studying the Korean population, in which no fronto-temporal sutures were seen. In this study, the incidence of fronto-temporal sutures was found to be 8.1% among the studied population.

In the study of the Matsumura et al. (1991), the star-shaped sutures, 17.7%, reported the highest prevalence rates among the populations. In the studies of Asala and Mbajiorgu (1996), and Lee et al. (2001), on Nigerian and Korean populations, the star-shaped sutures were not seen.

In the study of epipteric sutures, a large dispersion has been reported. In Lee et al. (2001), epipteric sutures were reported as 40.3%, which was the highest percentage reported among different populations. Also, in the studies of Saxena et al. (2003) and Oguz et al. (2004), this gap was not seen in the population of South India and Turkey. In the current study, epipteric suture was observed with 2.4% in the studied population.

Conclusion

The shape of the pterion and asterion sutures in the Iranian population is in line with other populations. Since both major sutures are under investigation, important landmarks are in the surgical approach. The prevalence of sutural bones (type I in asterion and the epipteric in the pterion) may affect the surgical approach.

REFERENCES

ASALA SA, MBAJIORGU FE (1996) Epigenetic variations in the Nigerian skull: sutural pattern at the pterion. East African Med J, 73(7): 484-486.

ASHLEY-MONTAGU MF (1933) The anthropological significance of the pterion in the primates. Am J Phys Anthropol, Vol. XVIII, no. 2.

BERRY CA, BERRY RJ (1967) Epigenetic variation in the human cranium. J Anat, 101(2): 361-379.

CHARULATA S, ABHILASHA W (2015) To study the morphology of pterion in dry human skull in Vidarbha Region. Int J Sci Res (IJSR), 4(1).

DEEPAK S, DAKSHAYANI KR (2015) Morphometric features of asterion in adult human skulls. Int J Res Med Sci, 3(6): 1325-1328.

ERSOY M, EVLIYAOGLU C, BOZKURT MC, KONUKSAN B, TEKDEMIR I, KESKIL IS (2003) Epipteric bones in the pterion may be surgical pitfall. Minim Invasive Neurosurg, 46: 364-365.

GALINDO-DE LEÓN S, HERNÁNDEZ-RODRÍGUEZ AN, MORALES-ÁVALOS R, THERIOT-GIRÓN MC, ELIZONDO-OMAÑA RE, GUZMÁN-LÓPEZ S (2013) Morphometric characteristics of the asterion and the posterolateral surface of the skull: relationship with dural venous sinuses and neurosurgical importance. Cir Cir, 81: 269-273.

GUMUSBURUN E, SEVIM A, KATKICI U, ADIGUZEL E, GULEC E (1997) A study of sutural bones in Anatolian-Ottoman skulls. Int J Anthropol, 12(2): 43-48.

HAVALDAR PP, SHRUTHI BN, SAHEB SH, HENJARAPPA KS (2015) Morphological study on types of asterion. Int J Intg Med Sci, 2(10): 167-69.

HUSSAIN SS, MAVISHETTER GF, THOMAS ST, PRASANNA LC, MURALIDHAR P (2011) A study of sutural morphology of the pterion and asterion among human Indian skulls. Biomed Res, 22: 73-75.

KELLOCK WL, PARSONS PA (1970) A comparison of the incidenceof minor nonmetrical cranial variants in Australian Aborigines with those of Melanesia and Polynesia. Am J Phys Anthropol, 33(2): 235-239.

KUMAR S, MAHAJAN A (2014) Pterion formation in North Indian Population: An anatomico-clinical study. Int J Morphol, 32(4): 1444.

LEE UY, PARK DK, KWON SO, PAIK DJ, HAN SH (2001) Morphological analysis of the pterion in Korean. Korean J Phys Anthropol, 14: 281-289.

LIU YH, KUNDU R, WU L, LUO W, IGNELZI JR MA, SNEAD ML, MAXSON JR ME (1995) Premature suture closure and ectopic cranial bone in mice expressing Msx2 transgenes in the developing skull. Proc Natl Acad Sci USA, 92: 6137-6141.

LIU YH, TANG Z, KUNDU RK, WU L, LUO W, ZHU D, SANGIORGI F, SNEAD ML, MAXSON RE (1999) Msx2 gene dosage influences the number of proliferative osteogenic cells in growth centers of the developing murine skull: a possible mechanism for MSX2-mediated craniosynostosis in humans. Develop Biol, 205: 260-274.

MANJUNATH KY, THOMAS IM (1993) Pterion variants and epiptericossicles in South Indian skulls. J Anat Soc India, 42: 85-94.

MATSUMARA G, KIDA K, ICHIKAWA R, KODAMA G (1991) Pterion and epipteric bones in Japanese adults and fetuses with special reference to their reference to their formation and variations. Acta Anat Nippon, 66: 462-471.

MURPHY T (1956) The pterion in Australian Aborigine. Am J Phys Anthropol, 14(2): 225-244.

MWACHAKA PM, HASSANALI J, ODULA P (2009) Sutural morphology of the pterion and asterion among adult Kenyans. Braz J Morphol Sci, 26(1): 4-7.

NATEKAR PE, DESOUZA FM, NATEKAR SP (2018) Pterion: An anatomical variation and surgical landmark. www: indianjotol.org (Accesed on April 26) IP: 178.131.81.57.

OGUZ O, SANLI SG, BOZKIR MG, SOAMES RW (2004) The pterion in Turkish male skulls. Surg Radiol Anat, 26: 220-224.

SAXENA SK, JAIN SP, CHOWDHARY DS (1988) A comparative study of pterion formation and its variations in the skulls of Nigerians and Indians. Anthropol Anz, 46: 75-82.

SAXENA RC, BILODI AKS, MANE SS, KUMAR A (2003) Study of pterion in skulls of awadh area-in and around Lucknow. Kathmandu Univ Med J, 1: 32-33.

SINGH R (2012) Incidence of sutural bones at asterion in adults indian skulls. Int J Morphol, 30(3): 1182-1186.

SUDHA R, SRIDEVI C, EZHILARASI M (2013) Anatomical variation in the formation of pterion and asterion in south Indian population. Int J Curr Res Rev, 5(9): 93-98.

UCERLER H, GOVSA F (2006) Asterion as a surgical landmark for lateral cranial base approaches. J Cranio-Maxillofac Surg 34: 415-420.

UKOHA U, ORANUSI CK, OKAFOR JI, UDEMEZUE OO, ANYABOLU AE, NWAMARACHI TC (2013) Anatomic study of the pterion in Nigerian dry human skulls. Nigerian J Clin Pract, 16(3): 9.

WANG Q, OPPERMAN LA, HAVILL LM, CARLSON DS, DECHOW PC (2006) Inheritance of sutural pattern at the pterion in rhesus monkey skulls. Anat Rec A Discov Mol Cell Evol Biol, 288(10): 1042-1049.

WILLIAMS L, BANNISTER L, BERRY M, COLLINS P, DYSON M, DUSSEK E (1998) Gray's Anatomy. 38th ed. Churchill Livingstone, London, npp 568-595.

ZALAWADIA A, VADGAMA J, RUPARELIA S, PATEL S, RATHOD SP, PATEL SV (2010) Morphometric study of pterion in dry skull Gujarat Region. Njirm, 1: 25-29.

Scimitar syndrome: A case report

Zehra S. Kasar[1], E. Ertekin[2]

[1] Aydın Adnan Menderes University, Faculty of Medicine, Department of Anatomy, Aydın, Turkiye
[2] Aydın Adnan Menderes University, Faculty of Medicine, Department of Radiology, Aydın, Turkiye

SUMMARY

Partial abnormal pulmonary venous return syndromes are rare congenital anomalies, in which some or all of the vena pulmonalis drains into the atrium dexter or systemic circulation. Scimitar syndrome, one of the abnormal venous return syndromes, is characterized by right vena pulmonalis draining into the vena cava inferior or atrium dexter. In this article, we presented the multislice computed tomography angiography findings of a 59-year-old female with Scimitar syndrome.

Key words: Scimitar syndrome – Pulmonary venous return anomalies – Computed Tomography

INTRODUCTION

Scimitar syndrome is a congenital anomaly characterized by a partially abnormal connection of the pulmonary veins. In this abnormal pulmonary venous return syndrome, vena (v.) pulmonalis dexter drains into vena cava inferior (VCI), atrium dexter, sinus coronarius, v. azygos, v. portaeor v. hepatica (Ho et al., 2009). In the literature, the first publication that reported the v. pulmonalis dexter drained into VCI was made by George Cooper in 1836. As a result of the autopsy examination of a 10-month-old child, he stated hypoplasia of right pulmonalis dexter and lung, abnormal arterial feeding of the right lung, displacement of heart to the right side (dextrocardia), and partial abnormal connection of v. pulmonalis dexter with VCI (Cooper, 1836). In the definition of the syndrome, the term "Scimitar" was first used by Neill et al in 1960 (Neil et al., 1960). In 1949, Dotter et al. published the angiogram images of three Scimitar syndrome patients for the first time (Dotter et al., 1949).

On chest X-ray, v. pulmonalis dexter occurs as a convex abnormal vein in the lower lung, which runs parallel to the right heart margin and extends towards the diaphragm (Dupuis et al, 1992). This appearance is compared to a curved-tip Turkish sword (scimitar) and is therefore called 'Scimitar syndrome'. Scimitar syndrome has rarely been described in v. pulmonalis sinistra (D'cruz et al., 1964). In this syndrome, the risk of developing right ventricular failure increases as v. pulmonalis dexter drains into the VCI (Kamler et al., 2003).

The etiology of scimitar syndrome is not exactly understood currently, but it is probably attributable to an embryological error of the fundamental development of the lung bud in early embryogenesis (Cicek et al., 2014). In the lung bud, the endodermal tissue that forms the pulmonary veins does not grow into the mesodermal tissue that meets the pulmonary vein outflows in the common atrium. As a result, venous blood of the right lung drains into the systemic circulation.

CASE REPORT

A 59-year-old female patient was admitted to the Cardiology outpatient clinic with complaints of fa-

Corresponding author:
Zehra Seznur Kasar. Adnan Menderes University, Faculty of Medicine, Department of Anatomy, Aydın, Turkey. Phone: +90 533 6130381.
E-mail: zehra.kasar@adu.edu.tr
Orcid number: 0000-0001-9226-0659.

Submitted: May 11, 2020. **Accepted:** August 31, 2020

tigue and shortness of breath. She never smoked and had no chronic disease in her history. In the physical examination, her general condition was good and vital signs were normal. The patient did not have clubbing and cyanosis. The effort test performed in the outer center was negative. In the echocardiography examination performed in our institution, the left ventricle (LV) diameter and wall movements were normal, ejection fraction (EF) was 60%. Minimal mitral regurgitation, 1-2 degrees of aortic regurgitation and 1-2 degrees of tricuspid regurgitation were detected. Pulmonary artery pressure (PAP) was measured as 35 mmHg, tricuspid annular plane systolic excursion (TAPSE) as 1.9 cm, right ventricle (RV) as 35 mm, right atrium (RA) as 46 mm. No transition was observed in the interatrial septum (IAS). VCI was collapsing more than 50%.

The patient who had a high PAP value was referred to the chest diseases outpatient clinic. The patient without a history of lung disease had an irregular breathing problem at night. She had an effort dyspnea and the modified Medical Research Council (MMRC) dyspnea scale is 2. Complete Blood Count (CBC) and biochemistry values were normal. Spirometric evaluation results were found to be borderline in terms of obstructive pathology [vital capasity (VC) max: 1.95 L (%84), forced vital capacity (FVC): 1.91 L (%85), forced expiratory volume in first second (FEV1) % 70.58L].

On the posterior-anterior (PA) chest radiograph, the right heart contour became evident due to enlargement of the right atrium. In addition, a tubular opacity was noted in the right lung lower zone (Fig. 1). There was no obvious pathology in the lung parenchyma. To evaluate the tubular opacity, Thoracic Computed Tomography (CT) and CT Angiography (CTA) were performed with Multislice CT device. Multiplanar reformat images were created in axial, sagittal and coronal planes with a thickness of 3 mm from the 0.5 mm thick raw data obtained. It was observed in CT that the right superior and inferior pulmonary veins were trending towards the inferior in the neighborhood of the heart, merging immediately above the diaphragm and drained into the VCI (Fig. 2). Left pulmonary veins were normally drained into the left atrium. Truncus pulmonalis was measured 36 mm in diameter and was wide (pulmonary hypertension). Right and left pulmonary artery diameters were within normal limits (26.2 and 26.5 mm). Right heart compartments were larger than expected. As a result of the examinations, Scimitar syndrome was diagnosed with abnormal pulmonary venous return anomaly in right pulmonary veins and pulmonary hypertension. Medical and surgical treatment was not considered, and the case was followed up.

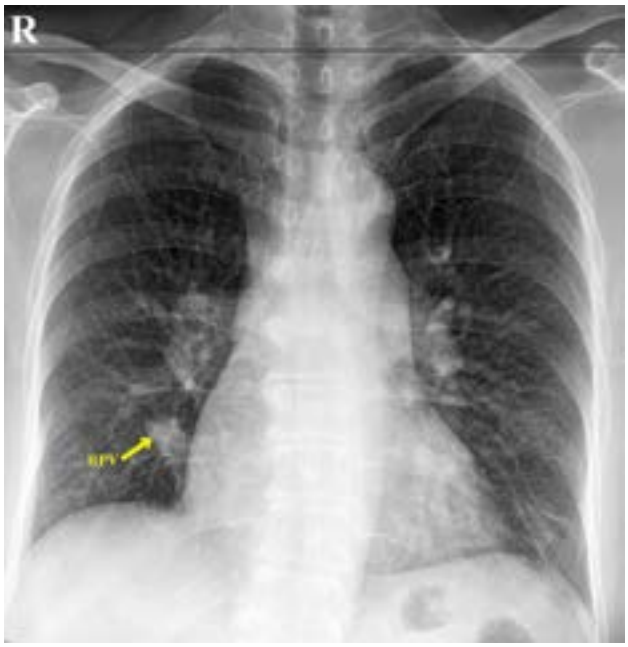

Fig. 1.- On the posterior-anterior chest radiogram, an opacity is observed in the lower zone of the right lung, parallel to the heart contour formed by the right pulmonary vein (RPV) (called as scimitar sign).

COMMENTS

Scimitar syndrome is a rare congenital cardiovascular defect. Although it is stated that this syndrome is found in approximately 1-3 cases in 100 thousand live births, it is thought that the incidence is higher due to asymptomatic cases as in our case (Cooper, 1836). Scimitar syndrome constitutes 3-5% of all partial abnormal pulmonary venous return syndrome (Neill et al., 1960). This syndrome is most common in right v. pulmonalis, and can be partial or total (D'cruz et al., 1964).

It is generally asymptomatic in the adult period, but may present with recurrent lung infections or exertional dyspnea. Although cases with pulmonary artery and lung hypoplasia are detected in early childhood due to the development of pulmonary hypertension (HT) and heart failure, it

can be said that the development of pulmonary HT and right heart failure is also rarely seen in adult patients (Diaz-Friaset al., 2020). Miller et al. (1995) reported that cases where less than half of the oxygenated blood from the lungs participate in the systemic circulation are asymptomatic. In our case, it was observed that the right superior and inferior vena pulmonalis were totally drained to VCI. It is noteworthy that no symptoms were observed until adulthood in the case in which no significant hypoplasia was observed in the right lung. In addition, our case states that there is shortness of breath at night instead of effort dyspnea. This can be explained by the fact that the patient lives a sedentary life. Nighttime shortness of breath was thought to be related to borderline obstructive pathology observed in respiratory function test.

Fig. 2.- Intravenous contrast-enhanced computed tomography shows bilateral pulmonary arteries and veins. On the coronal reformat images, right pulmonary veins (RPV) are drained into the inferior vena cava by showing a downward course towards the diafragma in the neighborhood of the right atrium (**a**), and the left pulmonary veins (LPV) drain into the left atrium with a normal course (**b**). The dreinage of the right pulmonary veins into the vena cava inferior (VCI) was also seen in axial images (**c** and **d**). Right and left pulmonary arteries (RPA and LPA) are observed in normal course and diameter on axial images (**e**). TP = pulmonary trunk.

Imaging methods play a major role in the diagnosis of Scimitar syndrome. In particular, it is diagnostic to see the shadow of the pulmonary vein in the chest x-ray that descends towards the diaphragm near-by the right atriumand resembles a short curved (Turkish sword = Scimitar). Conventional Angiography or CT / MR Angiography are modalities that can be used for diagnosis in patients without typical chest x-ray. Our case who applied to hospital with an atypical symptom did not have a typical Scimitar sign or accompanying lung hypoplasia and dextrocardia on chest x-ray. In the CTA examination performed for further evaluation, it was observed that the right-lung superior pulmonary vein extends inferiorly in the right heart border, whereas the inferior pulmonary vein extends slightly towards the cardiophrenic sinus, and these two veins merge above the diaphragm and drain into VCI. Due to the distant course of the two pulmonary veins, the typical scimitar shade could not be visualized on x-ray.

Conclusion

As a result, knowing the clinical and radiological findings of Scimitar syndrome, which is a special form of partial abnormal right pulmonary venous return anomaly, is very important for early diagnosis and treatment.

REFERENCES

COOPER G (1836) Case of malformation of the thoracic viscera consisting of imperfect development of the right lung and transposition of the heart. London Med Gazette, 18: 600-601.

CICEK S, ARSLAN AH, UGURLUCAN M, YILDIZ Y, AY S (2014) Scimitar syndrome: the curved Turkish sabre. Semin Thorac Cardiovasc Surg Pediatr Card Surg Annu, 17(1): 56-61.

D'CRUZ IA, ARCILLA RA (1964) Anomalous venous drainage of the left lung into the inferior vena cava: a case report. Am Heart J, 67: 539-544.

DIAZ-FRIAS J, WIDRICH J (2020). Scimitar Syndrome. In: StatPearls [Internet]. Treasure Island (FL): StatPearls Publishing; Available from: https://www.ncbi.nlm.nih.gov/books/NBK546602/

DOTTER CT, HARDISTY NM, STEINBERG I (1949) Anomalous right pulmonary vein entering the inferior vena cava; two cases diagnosed during life by angiocardiography and cardiac catheterization. Am J Med Sci, 218(1): 31-36.

DUPUIS C, CHARAF LA, BREVİÈRE GM, ABOU P, RÉMY-JARDIN M, HELMIUS G (1992) The “adult” form of the scimitar syndrome. Am J Cardiol, 70(4): 502-507.

HO LM, BHALLA S, BİERHALS A, GUTİERREZ F (2009) MDCT of partial anomalous pulmonary venous return (PAPVR) in adults. J Thoracic Imaging, 24(2): 89-95.

KAMLER M, KERKHOFF G, BUDDE T, JAKOB H (2003) Scimitar syndrome in an adult: diagnosis and surgical treatment. Interact Cardiovascular Thoracic Surg, 2(3): 350-351.

MILLER S, WALTMAN A (1995) The pulmonary circulation. In: Tavares JM, Ferrucci JT (eds). *Radiology: Diagnosis-Imaging Intervention*. JB Lippincott, Philadelphia, pp 1-19.

NEILL CA, FERENCAZ C, SABİSTON DC, SHELDON H (1960) The familial occurrence of hypoplastic right lung with systemic arterial supply and venous return, “scimitar syndrome”. Bull Johns Hopkins Hosp, 107: 1-21.

Impact of multimodality integrated anatomy teaching approach towards teaching effectiveness, student engagement, and social interaction

Fauzia Nausheen[1,2], Frank Scali[2], Sherif S. Hassan[2, 3]

[1] Department of Biomedical Education, California Health Science University-COM, Clovis, CA, USA

[2] Department of Medical Education, California University of Science and Medicine, School of Medicine, San Bernardino, CA, USA

[3] Department of Anatomy, Faculty of Medicine, Cairo University, Cairo, Egypt

SUMMARY

Medical schools are substituting anatomy dissection with various supplemental learning techniques such as virtual and augmented reality. Most studies focus on the knowledge of anatomy content as an outcome measure without evidence of clinical anatomical conceptual knowledge, engagement in group learning, or social development. Despite having no absolute standard method of learning or teaching anatomy, especially considering today's modern era of disruptive medical innovations and technology, there have been reports of successful teaching using problem-based learning. In our medical school, we present the anatomy lab experience in a balanced multimodal integrated approach using plastinated cadaveric materials supported by clinical cases, quizzes, virtual reality, imaging, ultrasound (US) experience, and dissection videos, all presented in a team-based learning environment.

During the "Structural Integrity of Human Body" (MSK) course, six anatomy lab sessions were created consisting of clinically integrated topics. Students were divided into three groups, each consisting of four students. Each lab session contained multiple stations utilizing a different form of a learning experience. Students' perceptions and comments about these learning experiences were collected during the end of course evaluations and an exclusive anatomy lab survey.

More than 90% of students agreed that the integrated anatomy labs enhanced their learning experience. However, the exclusive imaging experience was rated lower. 64% of students agreed that hands-on ultrasound had improved their learning experience. The dissection video watching station was rated very low. The students' perception survey revealed that students learned more while working in teams than being led by the faculty. Data on the students' work-life balance was favorable and within the national standards. The students' engagement and effectiveness were assessed by their lab quizzes, lab attendance, and grades in the lab practical exam.

Multimodal clinical teaching in anatomy lab provided students with conceptual knowledge of integrated disciplines and elaborated their understating of contextual clinical-anatomical concepts. The relaxed, active learning lab

Corresponding author:
Fauzia Nausheen MD. Biomedical Education, California Health Sciences University, College of Osteopathic Medicine, 2500 Alluvial Avenue, Clovis, CA 93611, USA. Phone: 586-339-5341. E-mail: fnausheen@chsu.edu.

Submitted: June 1, 2020. **Accepted:** August 27, 2020

environment helped students to work efficiently within their teams and improve their social interaction.

Key words: Integrated anatomy – Multimodal approach – Student engagement – Anatomy lab clinical applications

INTRODUCTION

Many medical schools are substituting anatomy dissection with supplemental learning techniques that include digital learning such as virtual reality, augmented reality (AR), or mixed reality headset display (MR). Although the effectiveness of these techniques has been reported, data also suggest that digital learning may pose interference with learning (Nicholson et al., 2008; Nilsson et al., 2007; Qayumi et al., 2004; Devitt and Palmer, 1999). Most studies also focus on the knowledge of anatomy content as an outcome measure without any evidence of engagement, group learning, or social development during the anatomy lab experience (Hopkins et al., 2011). Virtual reality has recently become a popular modality for teaching anatomy because of its unique visualization capabilities; that is, virtual reality can place the user within the system or organ being studied. Another technical modality, MR, has the capability of simulating sensations while the user is immersed in a virtual environment (Izard et al., 2017). These modern methodologies have been a practical supplemental teaching resource, but their impact on assessment scores requires validation. Additionally, the participants complained of headaches, dizziness, or blurred vision while using the AR or virtual reality tools (Moro et al., 2017).

There have been reports of successful efforts to teach integrated anatomy by problem-based learning or case-based learning; however, the available data on the approach used for integrating clinical cases during anatomy teaching is scarce (Bains and Kaliski, 2019). There is no standard method of learning or teaching anatomy. This is especially true considering advancements in medical innovations and technologies. Our medical school uses a flipped-classroom method incorporated with a modified team-based approach. Traditionally, the flipped-classroom model means the students take charge of their learning by actively engaging in the class. The instructors facilitate the students' teaching and learning by using multiple blended strategies mainly focused on student preferences and difficulty level.

At our institution, we provide students with an online recording of lectures, and valuable learning resources focused on their USMLE steps preparation. In class, the instructor chooses the strategies of student preferences to discuss the problems in teams and let them work through to find the correct answers. In addition to classes, we present the anatomy lab experience in a balanced multimodal integrated approach focusing on combining cadaveric prosections with advanced technology. Towards this attempt, we integrated the use of plastinated cadaveric materials with clinical cases, quizzes, virtual reality, Imaging, ultrasound experience (US), and prosection videos in anatomy labs in a team-based learning environment (Bains and Kaliski, 2012; Johnson et al., 2012).

This study assesses the impact of a multimodal approach using virtual technology, integrated clinical cases, plastinated prosections, and ultrasonography in integrated team-based learning in anatomy lab teaching. The hypothesis of this study is that teaching anatomy lab in a low-pressure active learning environment while using multiple integrated modalities could improve the medical students' engagement within their teams. This team collaboration could eventually improve the effectiveness of learning anatomy and the social interactions between students.

METHODS

Our medical school runs a 4-year program where Years 1 and 2 mainly address the basic sciences integrated with clinical sciences, while in Years 3 and 4 the students rotate in clinical clerkships at the hospitals. Year 1 begins at the end of July and runs through the end of May (a total of 10 months). Year 2 begins in July and ends in March. The overall length of time for students to study the basic sciences is 18 months.

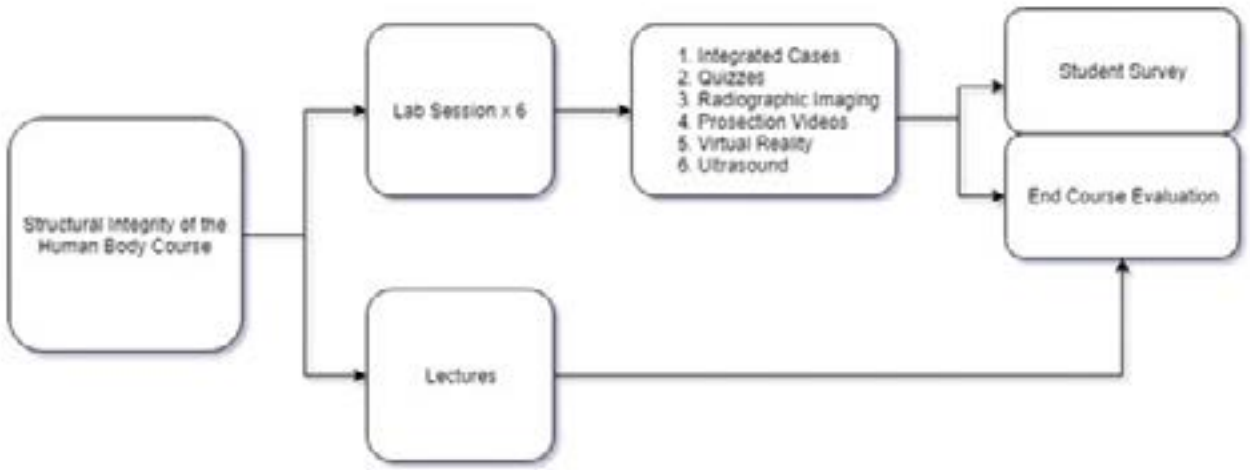

Fig. 1.- Flow chart to show the teaching methods among teams in the anatomy lab and lectures during the MSK course.

During the "Structural Integrity of Human Body" (MSK) course, the second course in Year 1, six anatomy lab sessions were created. Each session consisted of clinically integrated topics lasting four hours. Currently, the total number of medical students in a single class is 130. The students are divided randomly into groups of 10 that are called "colleges." Each college is further divided into two teams of five students. The five students work in these teams during their basic science training, and most of the curriculum is delivered using a modified team-based learning format. Students review online recorded lectures, after which they attend in-person 30-minute flipped classroom sessions. Each flipped classroom session starts with individual and team readiness assurance tests (I-RATS and T-RATS).

During the laboratory sessions, students worked within their groups along with their teammates. The anatomy faculty served as facilitators during the lab sessions. The histology labs were conducted in separate sections, but the content was integrated with pathology, and gross anatomy was found relevant. Each anatomy lab session contained multiple stations, lasting thirty-minutes per station (Fig. 1). Each station contained a different form of learning experience integrated with clinical thematic teaching of anatomy and the relevant clinical case of that week. These anatomy lab stations were: 1) the integrated clinical case studies on anatomy specimens, 2) embedded quizzes, 3) radiographic imaging, 4) prosection videos, 5) virtual reality, and 6) ultrasound. The quizzes consisted of checking the basic concepts of applied anatomy. The ultrasound station had handheld wireless probes connected online with the i-Pads. The Acland's and faculty-recorded videos were made available at the video station. Students' perceptions and comments about these experiences were collected during the end of course evaluations and an exclusive anatomy lab survey. The survey questions addressed the experience, engagement, achievement of learning outcomes, and integration between the basic science and clinical sciences.

The study protocol was approved by the Institutional Review Board of the medical school.

RESULTS

All survey studies and students' end-of-course evaluations are collected and analyzed by the office of the assessment and evaluation and the office of continuous quality improvement. Data were collected and analyzed regarding the percent of participating students (n=88/total class n=100), who endorsed strongly disagree, disagree, neutral, agree, and strongly agree. The mode for all questions was five or "strongly agree." The questionnaire was delivered to students by email, and the office of assessment and evaluations collected all results.

The end of the course evaluations revealed that 91% of students felt the MSK course was well organized, the learning outcomes were presented (96%), and basic sciences were well integrated

with clinical sciences (94%). 88% of students perceived improvement in problem-solving skills. Flipped classroom sessions enhanced their learning of clinical concepts (67%). 89% of students reported that anatomy labs enhanced their learning experience (Table 1).

Table 1. End of the course evaluation comments class of 2023.

No.	Survey questions	Agree	Disagree
1	The course was well organized.	91%	9%
2	The learning outcomes were clearly presented.	96%	4%
3	The basic science I learned was integrated with clinical sciences.	94%	6%
4	I received meaningful narrative feedback during the course.	77%	23%
5	I acquired/improved my problem-solving skills.	87%	13%
6	My learning experience was enhanced by the Laboratories	89%	11%
7	My learning experience was enhanced by the iRAT/tRAT (question added after 5200)	92%	8%
8	My learning experience was enhanced by: Flipped classroom discussion (question added after 5200)	67%	33%
9	My learning experience was enhanced by the Clinical skills sessions (question added after 5200)	98%	2%
10	My learning experience was enhanced by the College colloquium (question added after 5200)	48%	52%

In a second survey, students were asked to compare and rate the different teaching modalities concerning the learning of anatomy in labs. 92% of students reported that application questions on anatomical specimens created the most practical anatomy learning experience. They were provided with images of CT scan, X- Rays, and MRIs combined with recall recognition and identification questions. This imaging experience was rated lower than the application question on specimens (62% vs 92%). The one-on-one faculty sessions were appreciated by many students (70%), but according to students' perception survey about their learning, there seemed a trend that students learned more while working in groups. 64% of students agreed that the hands-on US improved their learning experience of anatomy, but the student in the US interest group was more inclined to perform the ultrasound. The dissection video watching station was rated very low in ranking; only 7% thought they were helpful to enhance the learning experience (Table 2).

The students considered watching videos during lab hours as "a waste of time." They suggested that videos be utilized for pre-lab preparation instead. Students commented very positively on the effectiveness of anatomy lab teaching using second-order and application questions as clinical correlates. They liked the high-yield concepts integrated within the clinical cases associated with the tagged cadaveric specimens during these lab sessions. Students liked the freedom to move around different stations and collaborate with their peers in teams (Table 3). Students also provided valuable suggestions such as inviting radiologists to these lab sessions, providing narratives to the imaging slides, adding more ultrasound lab sessions, increasing the number of integrated clinical cases at each station, facilitating interaction between teams in the lab by using technology incorporating Audience Response System clickers or online turning points.

Table 2. Students perception about the structural integrity of the human body course (MSK) Course: anatomy lab teaching survey results.

No.	The following enhanced my learning of Anatomy in Lab			
	The following teaching modalities enhanced my learning of anatomy in laboratories	Agree	Neutral	Disagree
1	Application questions on specimens	92%	5%	3%
2	One on one sessions with faculty	70%	15%	15%
3	Imaging questions on radiographs, CT scans and MRI	62%	27%	9%
4	Hands on Ultrasonography	64%	19%	6%
5	Videos	7%	23%	50%

The end of course data on student's work-life balance revealed that the average number of hours that students spent per day on sleep were seven, on exercise and support was one, on educational activities were ten, time spent with friends and family was four, and on other activities were two hours (Fig. 2). Students' engagement was assessed by their participation in quizzes before the flipped classroom sessions via I-RATS and T-RATS. Students' participation approached 100%, and their interest in completion of the course, faculty, and peer evaluations was 97% (Fig. 3). Bias may be considered with these figures due to the grade associated with student participation.

Table 3. Students anatomy lab teaching comments about the best lab experience.

NO.	Comments
1	Anatomy lab where it was mostly second order questions and required both the identification of the muscle or nerve as well as it is function and clinical correlation.
2	I also liked the histology lab where we looked at different histology slides and magnification to determine the clinical problem for the patient but I would have like for it to include the other groups in all the slides so that everybody is paying attention, maybe use a clicker system or ttpoll for it.
3	Practice questions/quizzes and posted answers to those questions were the best source of info to study with. Examining cadavers that had been pinned was also very helpful to guide studying.
4	The session where different stations were created, and students had the freedom to roam around the lab and collaborate with other students and professors.
5	The variety of ways the material is presented, from observing tagged specimens to answering questions imaging studies helped me understand the material better.
6	There was no timer or set area and you could go where you needed the most review, was perfect. Best lab to date.

Faculty perceived using a multimodal approach of anatomy teaching in a team-based environment, the anatomy lab became more engaging for students. The integrated clinical cases helped students understand the clinical concept within the context of anatomy. The hands-on ultrasound experience enhanced the students' interest and understating of anatomy. Students worked in high-performance teams with high energy and enthusiasm in a relaxed and active learning lab environment that helped improve social interaction.

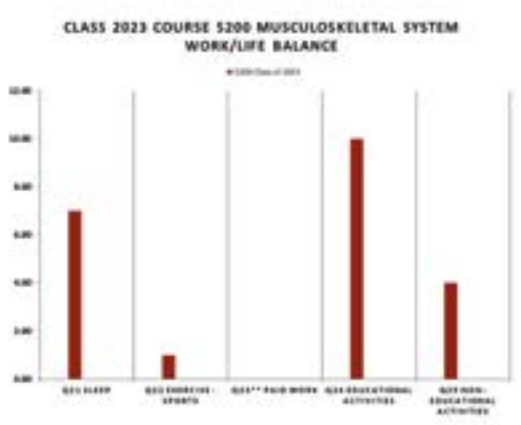

Fig. 2.- Data on work life balance of students: sleep, work, study, friends and family and exercise.

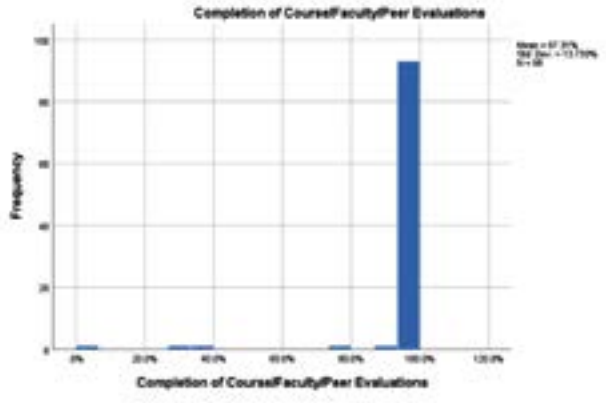

Fig. 3.- Students contribution in completing the faculty, course and peer evaluation.

DISCUSSION

Anatomy education is typically linked with cadavers, smelly dissection halls, and didactic lectures completed as a discipline by first-year medical students. While keeping some of the traditional teaching anatomy elements, most schools are approaching integrated system-based curricula (Drake, 2013). This paradigm shift takes the directions of a multimodal teaching approach, which is thought to achieve the best learning outcome as it caters to multiple learning styles (Drake and Pawlina, 2014). Instead of spending long hours in dissection and sitting in didactic lectures, the active learning pedagogies are implemented in these new curricula. Most of these teaching modalities encourage interactive learning to instruct anatomy via the team, problem, and case-based approaches (Green et al., 2014). Recent advancement in learning pedagogy is the use of a flipped-classroom approach; that is, students

viewing prerecorded lectures before their in-class activities. There is strong evidence that a flipped classroom teaching approach has a significant influence on student learning compared to traditional teaching (Hew and Lo, 2018).

Our curriculum is created based on a similar philosophy of active learning using a flipped classroom, a team-based approach that was supported by the recorded lectures and classroom activities. Weekly activities include clinical presentation driven sessions with all disciplines integrated around a chosen theme per week. Flipped classroom activities are mainly focused on competency-based content delivery to promote contextual learning where students are given a reason to learn and understand concepts (Rizzolo et al., 2010). All of these factors contributed to our successful delivery of musculoskeletal system course. Students strongly agreed that learning outcomes were clearly presented, and the basic sciences were well integrated with the clinical sciences. This successful delivery was achieved because of a change in the teaching pedagogy, and faculty created flipped classroom activities to encourage student's participation in solving the clinical problems in a team-based environment.

To enhance the learning of anatomy in a laboratory setting, the multimodal teaching approach helped the faculty succeed in achieving the learning outcome. The efficacy of an anatomy lab was improved by using the integrated clinical approach. Clinical application questions, which integrated concepts in pathology, physiology, and biochemistry, were asked while presented with anatomical specimens. Students were encouraged to work individually and then in teams to solve those clinical problems in a stepwise approach. The first part of each question was always to identify the structures and look for its location and relations. The second part of the question was to recall the neurovasculature and surrounding components in the structure of interest. The last part was to combine all the aforementioned concepts and correlate them with their clinical context. The logistics of using clinical application questions linked to the cadaveric specimens in this manner enhanced the integrated learning experience. Students were engaged and interested to pursue the next step to solve the problem. Literature suggests and supports improved student confidence when integrating anatomy knowledge clinical methods (Bradley et al., 2015).

The anatomy team also wanted to incorporate the element of integrated learning self-learning and self-assessment through formative quizzes. There is evidence that supports the positive impact of self-leaning and self-assessment that improves the knowledge, performance, and lifelong learning (Duffy and Holmboe, 2006). The answers to practice problems on specimens were discussed and uploaded to the school's Learning Management System. There has been considerable emphasis on imaging exposure during the foundation years of medical students, but there remains controversy among anatomy faculty about the methods to teach imaging in anatomy laboratories. The question is that whether-or-not structure identification is sufficient to interpret images the way it is done in clinical practice (Marsland et al., 2018). We believed that future physicians should learn imaging in the clinical context. The labs that the anatomy team devised contained a hybrid of identification and application questions seen on most relevant medical images taken by different imaging modalities like X-Rays, Computerized Tomography (CT) scans, Magnetic resonance images (MRI), and the US. The results of the current study revealed that students appreciated incorporating radiographs in the lab with concerns about the explanation and interpretation of images. Literature supports the importance of imaging in the modern curriculum, but at the same time these sessions are required to be well planned with the collaboration of the content experts (Nwachukwu, 2014).

Functional living anatomy teaching with the US has become an important modality that has incorporated the modern curriculum to supplement the traditional cadaver-based and cross-sectional anatomy (Hoppmann et al., 2015). To enhance integrated learning, the US has been shown to promote the understanding of physiology, pathophysiology, and anatomy (Garcia de Casasola et al., 2015). Some medical schools incorporate the Point-of-Care US in their curricula to improve

medical students' diagnostic and clinical skills (Vasileios et al., 2013).

The students had hands-on ultrasonography sessions to perform the US with cordless scanners that display images on I-pads and cell phones. The required lab outcome was to identify the structures in their clinical context. Students felt very strongly about having more US sessions as they perceived it as an excellent learning resource to integrate their clinical skills and anatomy. This data is consistent with studies conducted at other established and renowned medical schools. The results of most of these studies were inclined towards creating a four-year integrated US program with more exposure in years one and two (Bahner et al., 2014). Our students believed the US sessions helped improve their perception of anatomy, which is similar to the findings in previous studies (Smith et al., 2018).

Overall the integrated labs were perceived very positively by the students. Additionally, they created a culture of improved social interaction among them. The students were actively engaged in learning by their peers who have benefited both the peer teachers and the learners (Benè and Bergus, 2014). The anatomy team plans to implement high-tech anatomy labs with state-of-the-art equipment to augment the integrated learning of anatomy.

Regarding the work-life balance, our students slept on an average of seven per 24 hours. These findings were consistent with the average requirement of sleep by a healthy adult. According to the sleep foundation, the daily sleep time averages about seven to eight hours for an adult with little variation due to the lifestyle (Sleepfoundation.org., 2020). Many studies supported increased performance, improved alertness, and mood after attaining required sleep time (Belenky et al., 2003). One study revealed a performance decrease when subjects were exposed to 13 hours of sleep or more (Taub et al., 1977). Studies have shown that sleep restriction of four hours a night can cause a significant effect on normal health, such as an increase in the heart rate or blood pressure, inflammation, obesity, or glucose tolerance. There was evidence of increase mortality in subjects who reported short sleep hours (less than seven) and long sleep hours (more than nine) (Tochikubo et al., 1996; Meier-Ewert et al., 2004; Spiegel et al., 1999; Spiegel et al., 2004; Knutson et al., 2009). Based on all these studies, we strongly encouraged our students to get enough sleep regularly and balance their studies, work, and life.

Conclusions

Integrated clinical teaching in anatomy lab provided students with a conceptual knowledge of integrated anatomy, pathology, and physiology that will prepare them for the high-stake exams and clerkship years. The integration of clinical cases with the cadaveric specimens and hands-on ultrasound elaborated the understating of contextual clinical-anatomical concepts essential for future physicians. During the anatomy lab, the relaxed, active learning environment helped students to work efficiently within their teams and improve their social interaction.

Author relevant Credit roles:

FN: Conceptualization; Data collection and analysis; original idea, study design, original draft, review and editing. FS: Conceptualization, Important intellectual contribution, data collection, critical review, data analysis. SH: Conceptualization, critical review and editing. Important intellectual contribution, data collection, and analysis.

REFERENCES

BENÈ KL, BERGUS G (2014) When learners become teachers: a review of peer teaching in medical student education. Fam Med, 46(10): 783-787.

BAHNER DP, GOLDMAN E, WAY D, et al. (2014) The State of Ultrasound Education in U.S. Medical Schools: Results of a National Survey. Acad Med, 89: 1681-1686.

BELENKY G, WESENSTEN NJ, THORNE DR, THOMAS ML, SING HC, REDMOND DP, et al. (2003) Patterns of performance degradation and restoration during sleep restriction and subsequent recovery: a sleep dose-response study. J Sleep Res, 12(1): 1-12.

BAINS M, KALISKI DZ (2012) An anatomy workshop for improving anatomy self-efficacy and competency when transitioning into a

problem-based learning, Doctor of Physical Therapy program. Adv Physiol Educ, 44(1): 39-49.

BRADLEY A, KHAN K, MADURSKA M, RIDDELL A, SALDANHA J (2015) From cadavers to clinical practice: the anatomy of lifelong learning. Scott Med J, 60(4): 161-163.

DEVITT P, PALMER E (1999) Computer-aided learning: An overvalued educational resource? Med Educ, 33: 136-139.

DRAKE RL (2013) A retrospective and prospective look at medical education in the United States: Trends shaping anatomical sciences education. J Anat, 224(3): 256-260.

DRAKE RL, PAWLINA W (2014) Multimodal Education in Anatomy: The Perfect Opportunity. Anat Sci Educ, 7: 1-2.

DUFFY D, HOLMBOE S (2006) Self-assessment in lifelong learning and improving performance in practice physician know thyself. JAMA, 296(9): 1137-1139.

GARCIA DE CASASOLA SANCHEZ G, PEINADO DG, GOLLARTE AS, ACEITUNO EM, VAZQUEZ IP, MACHO JT (2015) Teaching of clinical ultrasonography to undergraduates: students as mentors. Rev Clin Esp, 215: 211-216.

GREEN RA, FARCHIONE D, HUGHES DL, CHAN SP (2014) Participation in asynchronous online discussion forums does improve student learning of gross anatomy. Anat Sci Educ, 7: 71-76.

HEW KF, LO CK (2018) Flipped classroom improves student learning in health professions education: a meta-analysis. BMC Med Educ, 18(1): 38.

HOPKINS R, GLENN R, TIMOTHY W (2011) Exploring the changing learning environment of the gross anatomy lab. Acad Med, 67: 883-888.

HOPPMANN RA, RAO VV, BELL F et al. (2015) The evolution of an integrated ultrasound curriculum (iUSC) for medical students: 9-year experience. Crit Ultrasound J, 7: 1-15.

IZARD SG, JUANES MÉNDEZ JA, PALOMERA PR (2017) Virtual reality educational tool for Human Anatomy. J Med Syst, 41(5): 76.

JOHNSON EO, CHARCHANTI AV, TROUPIS TG (2012) Modernization of an anatomy class: From conceptualization to implementation. A case for integrated multimodal-multidisciplinary teaching. Anat Sci Educ, 5(6): 354-366.

KNUTSON KL, VAN CAUTER E, RATHOUZ PJ, YAN LL, HULLEY SB, LIU K, LAUDERDALE DS (2009) Association between sleep and blood pressure in midlife: the CARDIA sleep study. Arch Intern Med, 169(11): 1055-1061.

MARSLAND MJ, TOMIC D, BRIAN PL, LAZARUS MD (2018) Abdominal anatomy tutorial using a medical imaging platform. MedEdPORTAL, 14: 10748. doi: 10.15766/mep_2374-8265.10748.

MEIER-EWERT HK, RIDKER PM, RIFAI N, REGAN MM, PRICE NJ, DINGES DF, et al. (2004) Effect of sleep loss on C-reactive protein, an inflammatory marker of cardiovascular risk. J Am Coll Cardiol, 43: 678-683.

MORO C, ŠTROMBERGA Z, RAIKOS A, STIRLING A (2017) The effectiveness of virtual and augmented reality in health sciences and medical anatomy. Anat Sci Educ, 10(6): 549-559.

NICHOLSON DT, CHALK C, FUNNELL WR, DANIEL SJ (2008) The evidence for virtual reality. Med Educ,. 42: 224.

NILSSON T, HEDMAN L, AHLQVIST J (2007) A randomized trial of simulation-based versus conventional training of dental student skill at interpreting spatial information in radiographs. Simul Healthc, 2: 164-169.

NWACHUKWU CR (2014) Cadaver CT scans a useful adjunct in gross anatomy: The medical student perspective. Anat Sci Educ, 7: 83-84.

QAYUMI AK, KURIHARA Y, IMAI M, et al. (2004) Comparison of computer-assisted instruction (CAI) versus traditional textbook methods for training in abdominal examination (Japanese experience). Med Educ, 38: 1080-1088.

RIZZOLO LJ, RANDO WC, O'BRIEN MK, HAIMS AH, STEWART WB (2010) Design, implementation, and evaluation of an innovative anatomy course. Anat Sci Educ, 3: 109-120.

SAKELLARIOU S, WARD BM, CHARISSIS V, CHANOCK D, ANDERSON P (2009) Design and implementation of augmented reality environment for complex anatomy training: Inguinal canal case

study. In: Shumaker R (ed). *Virtual and Mixed Reality*. Proceedings, 5622: 605-614.

SLEEP FOUNDATION (2020) https://www.sleepfoundation.org/professionals/ whitepapers-and-position-statements/white-paper-how-much-sleep-do-adults-need. Accessed on March, 29, 2020.

SMITH JP, KENDALL JL, ROYER DF (2018) Improved medical student perception of ultrasound using a paired anatomy teaching assistant and clinician teaching model. Am Assoc Anat, 11: 175-184.

SPIEGEL K, LEPROULT R, VAN CAUTER E (1999) Impact of sleep debt on metabolic and endocrine function. Lancet, 354: 1435-1439.

SPIEGEL K, TASALI E, PENEV P, VAN CAUTER E (2004) Sleep curtailment in healthy young men is associated with decreased leptin levels, elevated ghrelin levels, and increased hunger and appetite. Ann Intern Med, 141: 846-850.

TAUB J, GLOBUS G, PHOEBUS E, DRURY R (1977) Extended sleep and performance. Nature, 233: 142-143.

TOCHIKUBO O, IKEDA A, MIYAJIMA E, ISHII M (1996) Effects of insufficient sleep on blood pressure monitored by a new multibiomedical recorder. Hypertension, 27(6): 1318-1324.

VASILEIOS F. PANOULAS, ANNA-LENA DAIGELER, ANURA S.N. MALAWEERA, et al. (2013) Pocket-size hand-held cardiac ultrasound as an adjunct to clinical examination in the hands of medical students and junior doctors. Eur Heart J Cardiovasc Imaging, 14(4): 323-330.

Roles of standardized patients (SPs) in medical education: Students' reflection

Parima Saxena, Laura Varghese, Haider Hilal, Nahidh Al-Jaberi, Tarek Almabrouk, James Coey

St. George's University, School of Medicine, Northumbria University, Drill Hall, Newcastle Upon, UK

SUMMARY

The use of standardized patients (SPs) is becoming increasingly common in medical education. Many advantages exist for the use of SPs in early medical education, justifying the success of their implementation. It provides students with a safe environment to practice clinical skills, feedbacks and exposes the hidden curriculum in medicine such as professionalism. The suggestions that have been offered may be beneficial to all early medical education programs that use SPs in early medical education and OSCE evaluations, and these recommendations may improve these programs for students, faculty, clinical tutors and SPs alike.

Key words: Standardized patients – Hidden curriculum – Medical education – Clinical skills – Professionalism – Implementation

INTRODUCTION

The use of standardized patients (SPs) in medical education is becoming increasingly common, providing first and second-year medical students with the opportunity to practice skills that they will use during their clinical years. Numerous advantages exist for the use of SPs in early medical education, justifying the success of their implementation since 1963 (Wallace, 1997). Firstly, SPs offer medical students a safe environment to practice clinical skills (Barrows, 1993). It is beneficial to students and clinical patients alike, as neither party needs to fear possible worsening of a patient's condition (Shankar and Dwivedi, 2016). Secondly, in their ongoing interaction students usually develop a rapport with SPs, offering students a comfortable environment in which they can improve their clinical skills (barrows, 1993). Thirdly, in many medical education programs SPs provide students with feedback on their technical and communication skills, enabling them to refine their skills in a safe learning environment (McGovern et al., 2006). SPs are also instrumental in the implementation of the hidden curriculum in medicine, which involves learned elements on professionalism and patient care that are not explicitly stated (Lehmann et al., 2018). Lastly, and perhaps most importantly, early medical education involving the use of SPs allows students to begin understanding the physician-patient relationship, which will be a cornerstone of their future profession (Weaver and Erby, 2012).

It has been widely established that SPs have transformed early medical education for the better. This article describes the interactions of students, faculty and clinical tutors with SPs at

Corresponding author:
Tarek Almabrouk, PhD, MSc, MBChB. St. George's International School of Medicine, Northumbria University Drill Hall, Northumberland Road, Newcastle upon Tyne NE1 8ST. Phone: +44 (0)191 227 3654. E-mail: talmabro@sgu.edu.

Submitted: June 12, 2020. **Accepted:** September 15, 2020

the Keith B. Taylor Global Scholars Program of St. George's University in Newcastle Upon Tyne, United Kingdom. By reflecting upon these SP sessions, a significant role of SPs in undergraduate medical education and recommendations for SPs protocols can be made in all institutes.

CLINICAL CASES

St. George's University employs the use of SPs during first- and second-year medical student sessions, during which medical students are introduced to basic physical examination and application of ultrasound as a teaching tool to provide a clinically relevant understanding of basic sciences. These are closely supervised sessions led by clinical tutors and instructors, who are all medically-trained professionals. Prior to any training session, SPs were screened using clinical history questionnaires and full physical examination. In this article, using three different case scenarios, we will attempt to describe the interaction between SPs and students, along with opportunities to learn tools of the hidden curriculum when dealing with SPs.

Case 1

A 55-year-old male SP with no history of hypertension or ischemic heart disease was recruited for an ultrasound imaging lab in which the cubital fossa was to be visualized. No cubital fossa ultrasound imaging was conducted on the SP by students or clinical tutors before the lab. However, during the laboratory teaching session, the SP was found to have a high originating radial artery by participating students. Students were unable to find a brachial artery but rather found two arteries at the cubital fossa in this patient. After a detailed ultrasound of the upper limb of the SP, a high-originating radial artery was confirmed by a clinical tutor. Such incidental findings discovered in SPs during imaging training sessions are common and have potential implications on clinical examination, research design, especially in the areas of informed consent, patient privacy and results disclosure. In our case, the issue of patient privacy had to be considered. Given the unique circumstances of this situation, wherein both clinical tutors and students had been privy to the findings, maintaining patient confidentiality in this more public setting had to be prioritized. Had the patients not been recruited as an SP, they would likely have never known that they had a high-originating radial artery. Such an anatomical variation, however, does have relevance when considering procedures involving the cubital fossa such as trans-radial coronary procedures (Lo et al., 2009). Thus, informing the patient about this anatomical variation during lab and their potential implications had to be balanced with the risk of alarming or causing unnecessary distress to the patient.

Case 2

A 63-year-old male SP with no significant past medical history was recruited for participation in an abdominal ultrasound session. During a pre-session evaluation of the SP by a clinical tutor, the tutor discovered a hyperechoic liver, leading to the suspicion of liver disease. An informal medical interview of the SP was subsequently conducted by faculty. At this time, several factors, including physical symptoms (pain, fever, etc.), lifestyle choices and alcohol consumption, were assessed. This case brings to light ethical considerations involving patient lifestyle choices, and how best to respond to them professionally and respectfully. Chronic alcoholism is negatively perceived in both a medical and social context, often creating a stigma against alcoholic patients. Detailed history has been taken, and the SP presented, was discovered to have a substance abuse problem, which was likely the cause of this incidental finding. Therefore, Students, clinical tutors and faculty have a responsibility to ensure that such patients are free from judgement and decision making about the SPs findings.

Furthermore, given the more public setting of this incidental finding, all parties involved have an ethical obligation to the patient to maintain patient confidentiality.

Case 3

A 70-year-old male asymptomatic SP with a history of arthritis was recruited to participate in an ultrasound session on the abdomen. This particular session involved visualization of

abdominal vessels. Upon ultrasound imaging of the abdominal aorta, students discovered that the SP had an aortic aneurysm. Upon discussion with the patient, clinical tutors learned that the patient was aware of this potentially life-threatening pre-existing condition. This case highlighted the need to establish a standardized protocol for both SP recruitment and incidental findings in simulated laboratories. This case can be used in describing structural pathology to medical students in their early years. However, a proper pre-screening of all SPs should be a part of the medical curriculum.

Case Commentary

Implementation of a standardized protocol may provide medical programs with more control over SP interactions while outlining an approach to communication skills, professionalism and ethical concerns should they arise. The first step towards this goal requires answers to the following questions:

1. Should SPs have medical screening before entry into the program?
2. What are the benefits of using standardized patients from a diverse background, with potentially pre-existing medical conditions?
3. How should students and instructors respond to any findings that are discovered during clinical sessions? What is the appropriate way to react in the situation? Who should notify the patient?
4. How should the patient be accommodated in future sessions?

STANDARDIZED PATIENTS AND MEDICAL SCREENING

In many educational programs, standardized patients are selected based on interviews, acting skills and response towards students (Nestel et al., 2011). The above cases suggest the additional need for medical screening of SPs before their recruitment. Such screening should be comprehensive, including both medical and social history of the patient.

Given that medical screening is integrated into SP recruitment, there are many benefits of using such screening to select only healthy SPs for early medical education programs. Firstly, a healthy population of SPs will allow students to learn normal anatomy. It is especially important for programs that use an ultrasound-based approach for a clinical understanding of anatomy, as students must be able to appreciate and grasp normal anatomy before they can identify deviations and diseases (Swamy and Searle, 2012). Prior medical screening of SPs may also create a more stress-free practice as they will not have to fear potentially harming patients or worsening a pre-existing condition (Nestel et al., 2011; Nie et al., 2011).

In addition to admitting SPs based on pre-screening, there is a benefit of having medically qualified clinical tutors who evaluate patients using physical and ultrasound examination before each SP session—a practice that has been implemented into the Keith B. Taylor Global Scholars Program.

Examination by clinical tutors before each session identifies pre-existing abnormalities or conditions so that both clinical tutors and patients can be aware of any issues that may arise during the session with students. It also allows clinical tutors to prepare students for any pathologies or deviations from textbook anatomy that may be present in SPs. Such practices would enable a conducive learning environment wherein all parties are aware of what will be identified during the laboratory session.

Benefits of using diverse standardized patients

During clinical years, students will more often encounter patients with pre-existing conditions rather than healthy patients. Thus, the potential use of SPs with pre-existing conditions for early supervised medical education offers a more realistic perspective of challenges that students may face in their future careers.

If a certain proportion of SPs with pre-existing conditions are chosen to be used in early medical education programs, it will enable students to apply the knowledge they have gained from didactic lectures in a controlled clinical setting. Studies have demonstrated that the practical application of knowledge in the clinic is a proven

learning approach (Abela, 2009; Mayer, 2010). Perhaps a phased introduction of pathology would be beneficial for student learning, where students are first exposed to standardized patients to appreciate normal anatomy, and they are gradually exposed to patients with pathology. The discussed cases could be ideal learning situations for students to begin to understand disease mechanisms, assess patient histories, and discuss treatment and handling of patients. Thus, the ideal learning environment for medical students may involve a balance between healthy patients and those with pre-existing conditions, allowing them to visualize both normal anatomy and related pathology.

In medical education, one aspect of training is the clinical encounter in which trainee or medical student meets the real patients. Indeed, this clinical encounter allows improving both practical skills such as procedural skills, physical examination and unpractical ones such as communication skills, professionalism (Beigzadeh et al., 2016). However, there are many reasons have determinately affected the use of SPs in medical education. These reasons are continuous changes in the healthcare systems and the reliability of real patients. The latter is very challenging, because, if the education system is planning to use real patients, it is indicated to have control over many variables such as risks, type of diseases, stages of the illnesses and level of the interaction. These variables can be easily controlled in both simulated patients and standardized patients. Another aspect of concerns can be related to the paucity of suitable educational cases in early medical education. Of course, the availability of standardized patients depends on the type of departments and facilities available in every educational institution. Moreover, the ethical considerations are different between the two types of patients. Indeed, the ethical consideration regarding the use of SPs is more complicated, and sometimes are difficult (Bergin and Fors, 2003).

It is worth noting that the used SPs can be easily accomplished by training them on a variety of clinical scenarios in which we control their response to medical students' questions and examinations. The use of SPs allows strict control over the learning objectives and content and the presentation or the clinical scenarios (Beigzadeh et al., 2016). The use of standardized patients in medical education allows a fair evaluation of students' strengths and weaknesses in a supportive way. Indeed, additionally, positive feedbacks will increase the level of students' confidence and reduces the level of anxiety (Lane and Rollnick, 2007).

Indeed, all previously discussed aspects require careful planning regarding the use of standardized patients and simulated patients in medical education. Furthermore, most suitable and well-trained healthcare providers should be responsible for delivering such an approach to avoid any unwanted complications.

Response to incidental findings

The cases presented above further stress the importance of implementing a protocol to respond to any incidental findings that may occur during SP physical exam and ultrasound sessions (Beigzadeh et al., 2016). Incorporating such a standardized protocol into the pre-laboratory training of students, clinical tutors and faculty will allow for a respectful and appropriate response to unexpected situations from all involved.

On the other hand, the lack of professionalism and confidentiality with standardized patients might lead to an inappropriate response. Information disclosure and associated patients' response should be considered. SPs may experience fear, shock, or embarrassment in the same manner as we would appreciate the feelings of a patient in a real medical setting (Marsick and Watkins, 2001). As such, a comprehensive protocol should stress the importance of professionalism and clear, respectful communication when providing guidelines for incidental findings. Besides, a hierarchy of responsibility should exist as in any educational setting. Faculty and clinical tutors should be informed of incidental findings discovered by students before notifying patients. It allows for more experienced medical professionals to confirm the findings and convey them to the patient accurately and appropriately while maintaining patient confidentiality. With

patient and faculty consent, students may then be able to use this opportunity to learn about the pathology and how to deliver diagnoses to patients appropriately (Ziv et al., 2003; Rosenbaum et al., 2004).

Patient accommodation for future sessions

After the discovery of an incidental finding, the question arises as to whether or not the patient should continue to participate in future sessions. If the system decided to recruit real patients as SPs, special accommodations should be implemented to prioritize their health and safety. It raises questions as to how best to accommodate patients with pre-existing conditions without detriment to student learning.

As stated previously, patients with pre-existing conditions can be viewed as an excellent learning opportunity for students. In order to maximize student learning and patient comfort, students should be made aware, with patient consent, of these pre-existing conditions and how to manage patients accordingly without causing harm. Additionally, the SP should be educated on their condition and be made aware of potential risks involved with participation in supervised sessions.

Conclusions

This article offers insight into ethical considerations that may need to be made with the use of standardized patients in medical education. This article has attempted to outline suggestions that may be beneficial to all early medical education programs that use SPs in early medical education and OSCE evaluations. These recommendations may improve these programs for students, faculty, clinical tutors and SPs alike.

SPs are instrumental to student learning, student development and implementation of the hidden curriculum. Continued use of SPs in medical education is paramount for students in their preclinical years. It should evolve to consider (1) the impact of using only healthy SPs, (2) implications of using SPs with pre-existing conditions, (3) response to adverse events which may occur during SP sessions, (4) ethical responsibility for patient disclosure, and (5) how best to optimize student learning alongside patient comfort and well-being.

ACKNOWLEDGEMENTS

We thank St. George's staff for assistance, and authors' comments that significantly improved the manuscript.

REFERENCES

ABELA J (2009). Adult learning theories and medical education: A review. Malta Med J, 21: 11-8.

BARROWS HS (1993) An overview of the uses of standardized patients for teaching and evaluating clinical skills. AAMC. Acad Med, 68(6): 443-451.

BEIGZADEH A, BAHMANBIJRI B, SHARIFPOOR E, RAHIMI M (2016) Standardized patients versus simulated patients in medical education: are they the same or different. J Emerg Pract Trauma, 2(1): 25-28. doi: 10.15171/jept.2015.05.

BERGIN RA, FORS UG (2003) Interactive simulated patient – an advanced tool for student-activated learning in medicine and healthcare. Computers Educ, 40(4): 361-376.

LANE C, ROLLNICK S (2007) The use of simulated patients and role-play in communication skills training: a review of the literature to August 2005. Patient Educ Counseling, 67(1-2): 13-20.

LEHMANN LS, SULMASY LS, DESAI S (2018) Hidden Curricula, Ethics, and Professionalism: Optimising clinical learning environments in becoming and being a physician: a position paper of the American College of Physicians. Ann Int Med, 168(7): 506-508.

LO TS, NOLAN J, FOUNTZOPOULOS E, et al. (2009) Radial artery anomaly and its influence on trans-radial coronary procedural outcome. Heart (British Cardiac Society), 95(5): 410-415.

MARSICK VJ, WATKINS KE. Informal and Incidental Learning. New Directions for Adult and Continuing Education.2001(89):25-34.DOI: 10.1002/ace.5MAYER RE (2010) Applying the science of learning to medical education. Med Educ, 44(6): 543-549.

MCGOVERN MM, JOHNSTON M, BROWN K, ZINBERG R, COHEN D (2006) Use of standardized pa-

tients in undergraduate medical genetics education. Teaching Learning Med, 18(3): 203-207.

NESTEL D, TABAK D, TIERNEY T, LAYAT-BURN C, ROBB A, CLARK S, MORRISON T, JONES N, ELLIS R, SMITH C, MCNAUGHTON N, KNICKLE K, HIGHAM J, KNEEBONE R (2011) Key challenges in simulated patient programs: An international comparative case study. BMC Med Educ, 11(1): 69.

NIE Y, LI L, DUAN Y, CHEN P, BARRACLOUGH BH, ZHANG M, LI J (2011) Patient safety education for undergraduate medical students: a systematic review. BMC Med Educ, 11(1): 33.

ROSENBAUM ME, FERGUSON KJ, LOBAS JG (2004) Teaching medical students and residents skills for delivering bad news: a review of strategies. Acad Med, 79(2): 107-117.

SHANKAR PR, DWIVEDI NR (2016) Standardized patient's views about their role in the teaching learning process of undergraduate basic science medical students. J Clin Diagn Res, 10(6): JC01-JC05.

SWAMY M, SEARLE RF (2012) Anatomy teaching with portable ultrasound to medical students. BMC Med Educ, 12: 99.

WALLACE P (1997) Following the threads of an innovation: the history of standardized patients in medical education. Caduceus (Springfield, Ill.), 13(2): 5-28.

WEAVER M, ERBY L (2012) Standardized patients: a promising tool for health education and health promotion. Health Promotion Practice, 13(2): 169-174.

ZIV A, WOLPE PR, SMALL SD, GLICK S (2003) Simulation-based medical education: an ethical imperative. Acad Med, 78(8): 783-788.

European Journal of Anatomy